Surrogate Models for Improved Performance in Structural Safety Performance Assessment

Bibek Rana Magar
Bachelor of Engineering (Honours) (Civil Engineering)

Thesis submitted for the fulfilment of the requirements for the degree of Doctor of Philosophy

Victoria University, Australia
Institute for Sustainable Industries and Liveable Cities

October 2025

Abstract

This thesis is concerned with a model surrogation framework whereby the performance in certain structural safety assessment processes can be improved. In particular, the study aims to develop suitable surrogate models to reduce the time spent on numerical or laboratory simulation components in the process of Monte Carlo simulation-based reliability and safety assessment. A comprehensive review of structural safety assessment methodologies was conducted to establish the need for surrogate modelling. The review highlighted those conventional approaches, including Monte Carlo simulation, Bayesian methods, and time-marching algorithms, often require thousands of simulations runs and substantial computational resources, limiting their practical application in engineering design and assessment. It is important to replace these time-consuming components with suitably constructed surrogate models.

To fulfill the scope of the study, a numerical study was conducted to examine a two-storey nonlinear frame structure subjected to strong wind loads. The fragility analysis of the structure was assessed using the inter-storey displacement as the primary performance. Due to the highly variable and dynamic nature of wind loads, structural response analysis can be computationally demanding Therefore, force time histories and storey stiffness parameters were used as input variables to develop a neural network-based surrogate model capable of predicting inter-storey displacements. It was demonstrated that well-constructed surrogate models can accurately reproduce the simulation results of classical time-marching algorithms while substantially improving computational efficiency and significantly reducing computational cost.

The framework was subsequently extended to the fragility assessment of a three-storey building subjected to earthquake actions. Nonlinear structural analyses were performed using industry-standard design software to account for material failure under seismic actions. Variations in material properties were incorporated to generate datasets containing inter-storey and horizontal displacement responses. These datasets were used to train neural network based surrogate models that effectively reproduced the results of the nonlinear simulations, providing a computationally efficient alternative to conventional analysis procedures.

The research further examined the development of surrogate models for analytical and laboratory-based simulations involving storage silos and backfilled mine stopes. Understanding stress development in these systems is essential for ensuring structural safety and operational reliability. An initial pilot study based on published experimental data facilitated the development of a preliminary surrogate model for silo structures. This was followed by laboratory experiments on a silo prototype and backfilled mine stope systems. Vertical stresses at the silo base and shear stresses along the silo wall were measured under varying filling materials, fill heights, and wall roughness conditions. Experimental data were subsequently used to train neural network surrogate models capable of accurately predicting stress distributions in both silos and backfilled mine stopes.

The accuracy of the developed neural-network based surrogate models was evaluated by comparing their predictions against results derived from the traditional method (numerical simulation/ experimental method). In all cases, the surrogate models produced results within acceptable error limits, demonstrating their reliability as replacements for more computationally demanding assessment methods.

Finally, the applicability of the developed surrogate models within complete structural safety assessment frameworks was investigated. The earthquake and silo surrogate models were integrated into reliability analysis to estimate the probability of failure of representative structures under prescribed loading conditions. Failure criteria were defined using threshold values of inter-storey displacement and stress, respectively. Monte Carlo simulations involving thousands of simulation runs were performed using the surrogate models, enabling rapid estimation of failure probabilities with substantially reduced computational time. The findings confirm that neural network-based surrogate modelling provides an effective and efficient approach in reducing the time consumed by classical analysis techniques while maintaining acceptable levels of accuracy The study also identifies opportunities for future improvements through the incorporation of more advanced input variables and modelling strategies, enabling the application of surrogate modelling to increasingly complex real-world engineering problems.

Declaration of Authenticity

"I, Bibek Rana Magar, declare that the PhD thesis entitled "**Surrogate Models for Improved Performance in Structural Safety Performance Assessment"** is no more than 80,000 words in length, including quotes and exclusive of tables, figures, appendices, bibliography, references, and footnotes. This thesis contains no material that has been submitted previously, in whole or in part, for the award of any other academic degree or diploma. Except where otherwise indicated, this thesis is my own work".

"I have conducted my research in alignment with the Australian Code for the Responsible Conduct of Research and Victoria University's Higher Degree by Research Policy and Procedures."

"This thesis has been edited for clarity of expression, punctuation and grammar using Grammarly and AI. This use complies with VU guidelines on use of editors in HDR theses and overall VU policy on use of AI in research."

Signature: 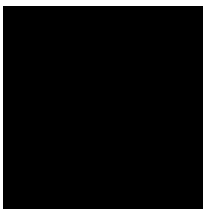

Date: 23/10/2025

Acknowledgement

I would like to thank the following people, without whom this research would not have been completed. First, I would like to thank my principal supervisor Dr. Vincent Wang, whose insight and knowledge into the subject matter helped me to walk this journey. I would also like to extend my thanks to my co-supervisor, Dr. Rudi Van Staden, for the continuous support during my PhD research. I would like to extend my sincere thanks to my previous co-supervisor, Prof. Sam Fragomeni, for helping me to successfully defend my candidature.

I would also like to thank all the lab technicians, Mr. Nitesh Gunoory, Mr. Donald Ermel, and Mr. Joseph Angelone, for helping me conduct my experimental studies, as well as the academic staff at Victoria University who supported me during my research. I am also thankful to Victoria University for providing me with a scholarship for my research. I am also grateful to Dr. Nipun Shrestha for his assistance with my PhD application. I also appreciate Dr. Rajnesh Gautam, Dr. Dinesh Pandey, and Foad Ghasemi for their support during my studies.

Finally, I would like to thank my family, especially my mother, Shree Maya Rana; my father, Dr. Eak Rana; and my sister, Binuja Rana Magar, for their unwavering support throughout my PhD journey. They have been a pillar of strength and my greatest source of motivation during difficult times. Additionally, I would also like to thank all my PhD colleagues and friends for their continuous motivation throughout this journey.

Table of Contents

Abstract i
Declaration of Authenticity iii
Acknowledgement iv
List of Figures vii
List of Tables xi
List of Abbreviations xiii
Chapter 1.0 Introduction 1
Chapter 2.0 Literature Review 5
Chapter 2.1: Reliability analysis of civil structures 5
Chapter 2.2: Model surrogation involving numerical analysis and/or experimental testing. 8
Chapter 2.2.1 Model Surrogation involving Reliability analysis. 8
Chapter 2.2.2 Model Surrogation Involving Monte Carlo Simulation 9
Chapter 2.3 Identification of the research gap. 10
Chapter 2.4 Objective and scope of the study 12
Chapter 3: Model surrogation for fragility analysis of nonlinear frame structures subjected to strong wind loads. 13
Chapter 3.1: Performance of structures under strong wind loads 15
Chapter 3.2: Model setup for Nonlinear hysteretic two-storey shear frame subjected to strong wind loads. 17
Chapter 3.3: Model Implementation 19
Chapter 3.4: Results and analysis 24
Chapter 4: Model surrogation for fragility analysis of nonlinear structures subjected to seismic actions 28
Chapter 4.1: Performance of structures under seismic actions 28
Chapter 4.2: Model setup for Nonlinear hysteretic three-storey buildings subjected to seismic load. 30
Chapter 4.3: Model Implementation 39
Chapter 4.4: Results and analysis 51
Chapter 5: Model surrogation for the safety assessment of silo structures. 55
Chapter 5.1: Performance of silo structures 57
Chapter 5.2: Pilot study based on data in relevant literature review 59

Chapter 5.3: Parametric study 66
Chapter 5.4: Laboratory setup for silo structures 86
Chapter 5.5: Laboratory testing implementation 89
Chapter 5.5.1: Defining layers for the testing 90
Chapter 5.5.2: Required input data for the experiments 90
Chapter 5.5.3: Targeted output variables from the experiments 91
Chapter 5.5.4 Implementation of the laboratory procedures 92
Chapter 5.6: Results and Analysis 97
Chapter 6: Model surrogation for the safety assessment of backfilling mine stopes 115
Chapter 6.1: Performance of backfilled mine stopes 116
Chapter 6.2: Laboratory setup for backfilled mine stopes 118
Chapter 6.3: Laboratory testing implementation 120
Chapter 6.3.1: Defining layers for the testing 121
Chapter 6.3.2: Required input data for the experiments 121
Chapter 6.3.3: Targeted output variables from the experiments 123
Chapter 6.3.4 Implementation of the laboratory procedures 124
Chapter 6.4: Results and Analysis 125
Chapter 7: Application of surrogate model to structural safety assessment 139
Chapter 7.1: Applications of constructed surrogate model in relation to data collected from numerical studies (wind load and seismic actions) 140
Chapter 7.2: Applications of constructed surrogate model in relation to experimental studies (silo structures and backfilled mine stopes) 143
Chapter 8: Summary, Conclusion, Recommendations for future work 148
References 155

List of Figures

Figure 1: A flowchart demonstrating the process carried out during the nonlinear study 18
Figure 2: Force recorded against time for the 1st level of the building 20
Figure 3: Force recorded against time for the 2nd level of the building 20
Figure 4: u vs tt for the 1st level of the building 21
Figure 5: u vs tt for the 2nd level of the building 21
Figure 6: udot vs tt for the 1st level of the building 22
Figure 7: udot vs tt for the 2nd level of the building 22
Figure 8: Neural network performance of the trained surrogate model 24
Figure 9: Regression line to validate the trained surrogate model 25
Figure 10: Comparing target and output from the surrogate model 26
Figure 11: Plan view of the structure in ETABS model 32
Figure 12: Three-dimensional view of the structure in ETABS model 33
Figure 13: Neural network performance of the surrogate model for horizontal displacement when 30 GPa 39
Figure 14: Regression values for the trained surrogate model 40
Figure 15: Neural network performance for vertical displacement in the 3rd storey when 30 GPa 41
Figure 16: Regression values of the trained surrogate model 42
Figure 17: Neural network performance for horizontal displacement when 40 GPa. 43
Figure 18: Regression values of the trained surrogate model 44
Figure 19: Neural network performance for vertical displacement when 40 GPa 45
Figure 20: Regression values for the trained surrogate model 46
Figure 21: Neural network performance of the surrogate model for horizontal displacement for 50 GPa 47
Figure 22: Regression values for the trained surrogate model 48
Figure 23: Neural network performance of the surrogate model for vertical displacement of 50 GPa 49
Figure 24: Regression values for the trained neural network 50
Figure 25: Comparing target and output for horizontal displacement 52
Figure 26: Comparing target and output for vertical displacement 53

Figure 27: A prototype for the laboratory testing of the silo (Widisinghe et. al, 2014) 56
Figure 28: Performance of the trained surrogate model for vertical stress prediction 62
Figure 29: Regression analysis for vertical stress surrogate model 62
Figure 30: Comparison of target boundaries and surrogate model outputs (vertical stress) 63
Figure 31: Performance of the trained surrogate model for shear stress prediction 64
Figure 32: Regression analysis for shear stress surrogate model 65
Figure 33: Comparison of target boundaries and surrogate model outputs (shear stress) 65
Figure 34: Performance of the trained surrogate model for vertical stress prediction with the number of neurons set to 5 68
Figure 35: Regression analysis for vertical stress surrogate model with the number of neurons set to 5 69
Figure 36: Comparison of target boundaries and surrogate model outputs (vertical stress) 69
Figure 37: Performance of the trained surrogate model for vertical stress prediction with the number of neurons set to 15 70
Figure 38: Regression analysis for vertical stress surrogate model with the number of neurons set to 15 71
Figure 39: Comparison of target boundaries and surrogate model outputs (vertical stress) 71
Figure 40: Performance of the trained surrogate model for vertical stress prediction with the number of neurons set to 20 72
Figure 41: Regression analysis for vertical stress surrogate model with the number of neurons set to 20 73
Figure 42: Comparison of target boundaries and surrogate model outputs (vertical stress) 73
Figure 43: Performance of the trained surrogate model for vertical stress prediction with the number of neurons set to 25 74
Figure 44: Regression analysis for vertical stress surrogate model with the number of neurons set to 25 75

Figure 45: Comparison of target boundaries and surrogate model outputs (vertical stress) 75
Figure 46: Performance of the trained surrogate model for shear stress prediction with the number of neurons set to 5 77
Figure 47: Regression analysis for shear stress surrogate model with the number of neurons set to 5 78
Figure 48: Comparison of target boundaries and surrogate model outputs (shear stress) 78
Figure 49: Performance of the trained surrogate model for shear stress prediction with the number of neurons set to 15 79
Figure 50: Regression analysis for shear stress surrogate model with the number of neurons set to 15 80
Figure 51: Comparison of target boundaries and surrogate model outputs (shear stress) 80
Figure 52: Performance of the trained surrogate model for shear stress prediction with the number of neurons set to 20 81
Figure 53: Regression analysis for shear stress surrogate model with the number of neurons set to 20 82
Figure 54: Comparison of target boundaries and surrogate model outputs (shear stress) 83
Figure 55: Performance of the trained surrogate model for shear stress prediction with the number of neurons set to 25 84
Figure 56: Regression analysis for shear stress surrogate model with the number of neurons set to 25 84
Figure 57: Comparison of target boundaries and surrogate model outputs (shear stress) 85
Figure 58: Cylinder used for the prototype 87
Figure 59: Base (weighing scale) to measure the mass 88
Figure 60: Load cell to capture the load transferred to the wall of the tube 88
Figure 61: Laboratory setup used for conducting the laboratory-based experiment. 93
Figure 62: Fine sand used as the filling material in the experiment 94
Figure 63: Crusher dust used as the filling material in the experiment 94
Figure 64: River sand used as the filling material in the experiment 95
Figure 65: Regression plot of the neural network trained using fine sand data. 100

Figure 66: Validation performance of the trained neural network for fine sand 101
Figure 67: Comparison of the target and the output data from the lab and the surrogate model respectively 103
Figure 68: Regression plot of the neural network trained using river sand data..... 106
Figure 69: Validation performance curve for the river sand surrogate model 107
Figure 70: Figure representing the comparison of the output through lab-based experiment and the MATLAB surrogate model 108
Figure 71: Regression plot of the neural network trained using crusher dust data. 111
Figure 72: Validation performance curve for the crusher dust surrogate model 112
Figure 73: Comparison of the data (output and target data) for crusher dust..... 113
Figure 74: Laboratory setup for the experimental simulation of backfilled mine stopes 120
Figure 75: Coarse sand used as the experimental backfill material 122
Figure 76: Crushed stone used as the experimental backfill material 123
Figure 77: Regression plot of the neural network trained using coarse sand data. 128
Figure 78: Validation performance of the trained neural network for coarse sand . 129
Figure 79: Comparison of the target and the output from the lab data and the surrogate model respectively for coarse sand..... 131
Figure 80: Validation performance of the trained neural network for stone 134
Figure 81: Regression plot of the neural network trained using stone data..... 135
Figure 82: Comparison of the output and the target data for stone 137
Figure 83: A general framework of model surrogation for other application purposes 149
Figure 84: Relationship between chapters 4, 5 and 6 151

List of Tables

Table 1: Output for rounds of simulation 23
Table 2: Data generated from ETABS when Young's Modulus is 30 GPa 35
Table 3: Data derived from ETABS when Young's Modulus is 40 GPa 36
Table 4: Data derived from ETABS when Young's Modulus is 50 GPa 37
Table 5: MSE values of each surrogate model..... 51
Table 6: Regression values of each surrogate model 51
Table 7: Experimental data adapted from Widisinghe (2014)..... 60
Table 8: Comparing the performance of the vertical stress surrogate models 76
Table 9: Comparison of the performance of the shear stress surrogate models 85
Table 10: Experimental data obtained for fine sand 98
Table 11: Comparison between laboratory measurements and surrogate model predictions for fine sand 102
Table 12 Experimental data obtained for river sand 104
Table 13: Comparison between laboratory measurements and surrogate model predictions for river sand 107
Table 14: Experimental data obtained for crusher dust 109
Table 15: Comparison between laboratory measurements and surrogate model predictions for crusher dust 112
Table 16: Experimental data obtained for coarse sand 126
Table 17: Comparison between laboratory measurements and surrogate model predictions for coarse sand 130
Table 18: Experimental data obtained for stone 132
Table 19: Comparison between laboratory measurements and surrogate model predictions for stone 136
Table 20: Simulation time spent for analysing the probability of failure of the structure in relation to horizontal displacement 141
Table 21: Simulation time spent for analysing the probability of failure of the structure in relation to vertical displacement 142
Table 22: Simulation time spent for analysing the probability of failure of silo in relation to fine sand 144
Table 23: Simulation time spent for analysing the probability of failure of silo in relation to river sand 144

Table 24: Simulation time spent for analysing the probability of failure of silo in relation to crusher dust..... 145

List of Abbreviations

ACI	American Concrete Institute
AKMCMC	Adaptive Kriging and Markov Chain Monte Carlo
EM	Expectation Maximization
DEM	Discrete Element Method
FEM	Finite Element Method
FFM	Fixed Funnel Method
FORM	First Order Reliability Method
FOSM	First Order Second Moment
FPB	Friction Pendulum Bearing
GP	Genetic Programming
HDMR	High Dimensional Model Representation
MCS	Monte Carlo Simulation
MNN	Modular Neural Network
MOGA	Multi-Objective Genetic Algorithm
MSE	Mean Squared Error
RC	Reinforced concrete
REIF	Reliability-based Expected Improvement Function
SCC	Steel Concrete Composite
SCR-RC	Steel Reinforced Concrete – Reinforced Concrete
SFA	Seismic Fragility Analysis
SFSI	Soil Foundation Structure Interaction
SORM	Second-Order Reliability Method
SSMRs	Standing Seam Metal Roofs
SVMr	Support Vector Machine Regression
TLBO	Teaching Learning Based Optimization

Chapter 1.0 Introduction

Structural safety is a fundamental consideration in civil engineering, as it directly influences the reliability, serviceability, and resilience of infrastructure systems. Reliability analysis of a civil structure is used as a method to assess the safety performance of the structure by quantifying the risk of failure under uncertain conditions. Through consideration of factors such as loading conditions, material properties, environmental influences, and modelling uncertainties, reliability analysis evaluates the probability that the structure will function without failure and perform its intended function throughout its design life. It is therefore necessary for understanding the safety assessment of a structure. Therefore, reliability assessment has become an essential component of modern structural engineering practice and risk-informed decision-making.

Reliability analysis of a structure is generally carried out in two ways: analytical derivation and numerical simulation. Analytical derivation involves using mathematical functions or equations to replicate and model the behaviour of the structure and evaluate its reliability based on these equations. Methods such as the First-Order Reliability Method (FORM) or the Second-Order Reliability Method (SORM) are widely used in the analytical derivation method for the purpose of reliability analysis. While these methods can provide efficient reliability estimates for relatively simple systems, their application becomes increasingly challenging when dealing with highly nonlinear structural behaviour, complex loading conditions, or multiple sources of uncertainty.

Numerical simulation involves computational techniques to mimic and model the behaviour of the complex structure based on numerous factors and analyse its reliability based on these simulations. It involves using the Finite Element Method (FEM) to simulate the behaviour of the structure under various conditions. Among these methods, Monte Carlo Simulation (MCS) is widely used to assess the reliability of a structure through repeated simulations of the structural behaviour by randomly varying the input parameters. Although this approach can provide highly accurate reliability estimates, it often requires an exceptionally large number of simulations to achieve statistical convergence, resulting in substantial computational demands.

Recent advances in computational intelligence and machine learning have created new opportunities for improving the efficiency of structural reliability analysis. Researchers have increasingly combined Monte Carlo Simulation method with machine learning-based approaches. This has helped to develop efficient and accurate Monte Carlo Simulations for complex scenarios with non-linear performance function, thereby improving computational techniques. Recent years have shown significant progress in the development of Monte Carlo Simulation technique through various approaches, including hybrid methods, Bayesian techniques, and the integration of machine-based learning methods with traditional Monte Carlo simulation techniques. These advances have highlighted the potential of surrogate modelling as an effective strategy for reducing computational costs associated with traditional simulation-based methods.

A suitable numerical or experimental simulation model is needed to assess the safety performance of a civil structure under normal or extreme circumstances. The model should replicate the behaviour of the structure. Various simulation models have been widely developed in the field of civil engineering for the reliability analysis of civil structures. In a typical Monte Carlo simulation-based reliability analysis, a numerical or experimental simulation model is run thousands of times before a reasonably accurate result can be obtained, adding to the computational complexity of the model. As an example, Dhar and Datta (2009) reported a 30-day run time on a 2.4 GHZ Oeptron AMD machine with 4 GB of RAM to find optimal solutions for a linked simulation-optimization model applied to a small aquifer system. In a context as such, reducing the time needed to run the simulation model not only relates to efficiency but also affects the practical viability of the analysis on many occasions.

Surrogate modelling has emerged as a promising solution to this challenge. A surrogate model is a computationally efficient approximation of a numerical or experimental model. By understanding the relationships between input variables and structural responses, surrogate models can reproduce the behaviour of complex systems with significantly reduced computational effort. Neural network-based surrogate models are particularly attractive because of their ability to capture highly nonlinear relationships and generalise complex structural behaviours from available

data. When properly trained, such models can replace computationally intensive simulation procedures while maintaining satisfactory levels of predictive accuracy.

The motivation for this research arises from the need to improve the efficiency of structural safety assessment procedures without compromising analytical accuracy. Although considerable progress has been made in the development of simulation-based reliability analysis methods, opportunities remain for improving computational performance through the integration of advanced surrogate modelling techniques. Existing studies have demonstrated the potential of machine learning approaches in selected applications; however, the development of a unified framework capable of supporting safety assessment across a range of civil engineering structures and loading conditions remains limited. This gap presents a significant research opportunity with practical implications for structural design, risk assessment, and infrastructure management.

This research has practical implications because it is based on real-life issues. The outputs of the study will be useful to policymakers, decision-makers, government agencies, and researchers. This study will be centred on enhancing safety assessment procedures for civil engineering structures for the present and the future. Findings and recommendations of this research, by implementing the innovative surrogate model technique, will be significant to structural designers and civil builders as the safety performance of relevant civil structures can be quantified with improved efficiency. Furthermore, the research contributes to the growing body of knowledge on surrogate modelling and its application within structural engineering.

The main contribution to the knowledge from the proposed research will be to derive a surrogate model for the assessment of the safety performance of selected civil structures under normal or extreme circumstances. The research investigates the ability of surrogate models to replace computationally intensive numerical and experimental simulation procedures while preserving the accuracy required for reliability analysis. By reducing the number of simulations runs, the proposed approach aims to improve computational efficiency and enable more practical implementation of Monte Carlo simulation-based safety assessments.

The thesis is organized as follows. Chapter 2 presents a comprehensive review of the relevant literature and identifies the research gaps that motivate the study. Chapter 2 also presents the scope of the proposed study. Chapter 3 investigates surrogate modelling for the fragility analysis of nonlinear frame structures subjected to strong wind loads. Chapter 4 extends the framework to structures exposed to seismic actions. Chapter 5 presents an experimentally validated surrogate modelling approach for reinforced concrete silos, demonstrating the integration of numerical and laboratory-based simulation data.

Chapter 6 focuses on the development of surrogate models for backfilled mine stopes. Chapter 7 evaluates the application of the developed surrogate models within a broader structural safety assessment framework, including wind-loaded structures, earthquake-resistant structures, silo systems, and backfilled mine stopes. Finally, Chapter 8 summarises the major findings of the research, discusses the broader implications of the proposed framework, and provides recommendations for future research directions.

Chapter 2.0 Literature Review

Structural reliability analysis is a vital tool used in safety engineering and structural assessment. It provides an analytical framework for evaluating the probability of the failure of a structural system to fulfill specified performance requirements when subjected to uncertain loading conditions and material properties. Therefore, reliability analysis has become an essential part of the design, evaluation, maintenance, and management of civil infrastructure. Over the course of decades, significant advances have been made in analytical, numerical, probabilistic, and data-driven approaches for reliability assessment. This chapter reviews the literature relevant to structural reliability analysis and surrogate modelling techniques, with particular emphasis on their application in civil engineering. The chapter also identifies existing research gaps and outlines the objectives and scope of the research.

Chapter 2.1: Reliability analysis of civil structures

Reliability analysis has been commonly used to assess the safety and performance of civil engineering structures under various uncertain actions or loading conditions. Recent studies have explored different analytical and computational approaches for assessing structural reliability and probability of failure of a structural system. Sufyan et al. (2023) developed three hybrid Random Forest (RF)-based models for the reliability analysis of portal frame structures. During the study, structural response was measured in terms of the displacement subjected to lateral forces on the portal frames. The results demonstrated the potential of machine learning techniques to improve the efficiency of reliability analysis assessments while maintaining satisfactory predictive accuracy.

Similarly, Tsai et al. (2022) investigated the vulnerability of a traffic signal structure in the USA subjected to strong wind loads. The methodology combined fatigue damage accumulation models with local wind speed probability distributions to estimate the fatigue life and structural reliability. The study highlighted the importance of incorporating environmental uncertainties into reliability analysis assessments of infrastructure exposed to extreme weather conditions.

Reliability analysis has also been applied to more complex structural systems. Benyahi et al. (2018) performed a non-linear and reliability analysis of metallic truss structures using the Hasofer–Lind reliability method. The study focused on estimating the reliability indices, evaluating various loading scenarios, and determining the probability of failure. Likewise, Ni et al. (2023) proposed a reliability analysis method for civil structures with incomplete data using Bayesian inference method. The methodology was validated through numerical investigations involving a two-span, two-storey reinforced concrete building and a five-span bridge structures, as well as experimental studies on an eight-storey steel frame structure to estimate structural failure probabilities.

The assessment of structural reliability over time has attracted increasing attention because of deterioration and ageing of the structure. Woju et al. (2023) evaluated a Time-dependent reliability (TDR) of structures by generating functions of input variables and output quantities that incorporate fuzziness over time. This approach enabled the assessment of evolving safety indices and time-variant performance levels for different failure modes. Similarly, Yang et al. (2024) investigated the long-term response of a long span concrete-filled steel tube (CFST) structures using a time-dependent reliability methodology. Fang et al. (2024) further advanced the field by performing structural reliability analysis of a structure using a hybrid reliability analysis framework that accounts for the coupled effect of randomness and fuzziness, using a fuzzy Bayesian interval estimation strategy.

Machine learning approaches have increasingly been integrated into reliability-related studies. Mustafa et al. (2023) developed several high-performance machine learning models for predicting the allowable load-carrying capacity of pile foundations using geotechnical parameters as input variables. Findings demonstrated the capability of data-driven methods to achieve high prediction accuracy while reducing computational effort. Roy et al. (2024) proposed an adaptive sparse Bayesian regression-based direct metamodeling approach for seismic reliability analysis (SRA) and employed active learning-based algorithm strategies for adaptive training of meta models to efficiently approximate nonlinear seismic structural responses.

Monte Carlo Simulation (MCS) remains one of the most widely adopted methods for reliability assessment because of its flexibility and robustness. Moghaddasi et al. (2011) applied MCS to investigate the influence of soil–foundation–structure interaction (SFSI) on seismic structural responses. A wide range of realistic SFS systems and earthquake input motions were considered in time-history analysis, demonstrating the ability of MCS to represent complex uncertainties. Similarly, Shen and Deodatis (2022) employed MCS to validate a variability response function developed for statically indeterminate beam structures with uncertain material properties represented as random fields.

The effectiveness of MCS has also been demonstrated in collapse and fire reliability analysis. Gordini et al. (2018) used nonlinear analysis combined with MCS to investigate the collapse behaviour of double-layer space structures and assess the effects of initial curvature imperfection on the load-carrying capacity. Likewise, Shi et al. (2013) conducted reliability analysis of structures exposed to fire by considering uncertainties associated with fire development, thermal responses, and structural model parameters.

Reliability-based design optimisation has also benefited from probabilistic approaches. Nguyen et al. (2022) proposed a reliability-based design optimisation algorithm framework for steel–concrete composite (SCC) beams, while Kar and Roy (2022) compared the performance of Monte Carlo Simulation (MCS), First Order Reliability Method (FORM), and First Order Second Moment (FOSM) methods for conducting reliability analysis of a finite cohesive soil slope and concluded that MCS provided superior accuracy. Mohammed and Al-Zaidee (2022) similarly compared FORM and MCS in assessing the serviceability reliability of the Al-Awsej composite bridge in Diyala, Iraq. Additionally, Agarwal et al. (2020) used FORM to conduct computational reliability analysis of reinforced soil-retaining structures (RSRS) under seismic conditions to identify two different failure modes of the structures.

Recent research has focused on improving the computational efficiency of reliability analysis. Ghosh et al. (2021) demonstrated the advantages of the adaptive nature of the Kriging approach for improving seismic fragility analysis (SFA) of structures, with the analysis conducted based on Monte Carlo simulations. Nguyen et al. (2022)

combined subset simulation with deep learning-based surrogate modelling to improve the efficiency of seismic reliability analysis. The methodology was validated using three case studies of increasing complexity. Additionally, Cho (2023) proposed an efficient method for estimating fragility curves of water-retaining structures while minimizing the number of Monte Carlo simulation runs required.

Overall, the literature demonstrates substantial progress in structural reliability analysis through the integration of probabilistic methods, simulation techniques, machine learning algorithms, and surrogate modelling approaches. However, computational efficiency remains a significant challenge, particularly for nonlinear and high-dimensional engineering systems.

Chapter 2.2: Model surrogation involving numerical analysis and/or experimental testing.

Building upon the developments in reliability analysis, researchers have increasingly explored surrogate modelling techniques to overcome the computational limitations associated with conventional simulation methods. Surrogate models are simplified representations of complex systems that approximate the relationship between input parameters and output responses. By replacing computationally expensive simulations with efficient predictive models, surrogate modelling has emerged as an effective strategy for improving computational efficiency in engineering analysis.

Chapter 2.2.1 Model Surrogation involving Reliability analysis.

Numerous studies have investigated the reliability and safety performance of structures exposed to natural hazards such as windstorms and earthquakes. Research by Ellingwood and Kinali (2009), Goode and van de Lindt (2013), Sadan et al. (2013), Stewart et al. (2016), Salman and Li (2017), and Gavanski and Kopp (2017) collectively highlights the importance of probabilistic methods in evaluating structural safety under uncertain loading conditions.

To reduce computational demands associated with reliability assessment, surrogate models have increasingly been incorporated into probabilistic frameworks. Wang et al.

(2016) developed an expectation–maximization (EM) algorithm embedded statistical damage prognosis paradigm for in-service civil structures exposed to natural hazards. By integrating damage diagnosis information into a probabilistic model, the approach enabled efficient prediction of future structural performance and safety of existing structures.

The application of surrogate modelling extends beyond structural engineering. Sreekanth and Datta (2010) developed surrogate models based on genetic programming (GP) and modular neural networks (MNN) coupled with multi-objective genetic algorithm (MOGA) to optimise groundwater pumping strategies in coastal aquifer management. Similarly, Lal and Datta (2018) employed support vector machine regression (SVMr) to predict groundwater pumping-induced saltwater intrusion in coastal aquifers and demonstrated improved predictive performance relative to alternative surrogate approaches such as genetic programming (GP) based surrogate models. These studies illustrate the versatility and effectiveness of surrogate models in capturing complex nonlinear relationships while significantly reducing computational requirements.

Chapter 2.2.2 Model Surrogation Involving Monte Carlo Simulation.

Even though Monte Carlo Simulation remains one of the most reliable probabilistic methods available, its computational cost can become irrational when large numbers of simulations are required. As a result, surrogate-assisted Monte Carlo approaches have become an important area of research.

Wang and Ginger (2014) integrated expectation–maximization (EM) algorithms and Bayesian techniques to estimate wind-induced fragilities of existing civil structures. Their surrogate model successfully approximated nonlinear structural responses and significantly reduced computational effort in fragility assessment. Sivakugan et al. (2014) demonstrated the value of combining numerical simulations and laboratory testing to investigate vertical stress distributions within underground mine stopes necessary for designing the barricades that block the drives during lifting, illustrating the potential for experimentally based surrogate modelling.

Analytical surrogate models have also been proposed. Mostaghel and Byrd (2000) developed a physically based model for bilinear hysteretic systems capable of representing complex multi-degree-of-freedom structural behaviour with reduced computational complexity.

More advanced developments have emerged in recent years. Zhang et al. (2019) introduced a reliability-based expected improvement function (REIF) within a Kriging surrogate model framework to enhance structural reliability analysis. Song et al. (2019) proposed an adaptive kriging combined with Markov chain Monte Carlo (AK-MCMC) simulation method, demonstrating high efficiency in problems involving small failure probabilities and complex nonlinear performance, while Wu et al. (2019) developed a surrogate-based optimization framework integrating high-dimensional model representation (HDMR)-based modelling technique with a teaching-learning-based optimization (TLBO) algorithm, targeting high-dimensional engineering problems.

Regardless of these advances, challenges remain in maintaining surrogate model accuracy for highly nonlinear systems, addressing high-dimensional problems, and integrating numerical and experimental information within a unified framework. These gaps motivate further investigation, which will be discussed in the subsequent section.

Chapter 2.3 Identification of the research gap.

Reliability analysis remains one of the most important tools for assessing the safety and performance of civil engineering structures. Among available approaches, Monte Carlo Simulation (MCS) is widely recognised for its robustness and accuracy. However, their application is often limited by the substantial computational cost associated with large numbers of simulations, particularly for nonlinear and high-dimensional structural systems.

Although continuous advancements in computational hardware have partially eased these challenges, the computational demand of MCS remains excessive for many practical engineering applications to address this limitation, researchers have increasingly adopted surrogate modelling techniques. Methods based on Kriging, support vector machines, neural networks, Bayesian inference, and adaptive learning

have demonstrated considerable potential for reducing computational demands while maintaining acceptable levels of predictive accuracy.

Recent studies have demonstrated the successful application of surrogate modelling techniques such as kriging, support vector machines, and neural networks in various engineering fields, including hydrology and groundwater systems. However, despite these advancements, several limitations remain when applying surrogate models to civil structural reliability problems. These include challenges in handling nonlinear structural responses, ensuring accuracy in estimating small failure probabilities, and effectively integrating numerical simulations with experimental or field data.

However, several limitations remain. Many surrogate models have been developed for specific applications, limiting their transferability to different structural systems and loading conditions. In addition, accurately estimating rare failure events remains challenging because of limited failure data and highly nonlinear performance functions. Existing studies also tend to rely heavily on numerical simulations, with comparatively limited emphasis on experimental validation. Furthermore, there remains a lack of comprehensive frameworks that systematically guide the development, validation, and implementation of surrogate models for structural reliability analysis.

Thus, there is a need for a robust and generalised surrogate modelling framework capable of reducing computational effort while maintaining reliability assessment accuracy across a range of civil engineering applications. This research seeks to address these challenges through the development and evaluation of surrogate modelling approaches for selected civil structures and systems.

Chapter 2.4 Objective and scope of the study

The primary objective of this research is to establish a surrogate modelling framework capable of significantly reducing the time and computational resources required for numerical and experimental simulations used in structural reliability analysis and the safety assessment of selected civil structures.

The specific objectives of the study are:

a) to demonstrate the necessity and feasibility of replacing computationally intensive simulation procedures commonly employed in structural reliability analysis with surrogate modelling techniques;
b) to develop a surrogate model in place of the classical time-marching schemes for improved computational efficiency in the fragility analysis of nonlinear multi-storey steel frame structures subjected to strong wind loads, illustrating numerical simulation-based model surrogation;
c) to suggest and construct a numerical simulation-based surrogate model in relation to the fragility analysis of nonlinear multi-storey steel frame structures subjected to seismic actions for improving the computational efficiency;
d) to propose an experimentally validated, structural design practice based surrogate model for silos and backfilled mine stopes, exemplifying combined numerical and experimental simulation-based model surrogation;
e) to extrapolate the surrogate models developed in selected civil structures, and (b), (c) and (d) to form a more generic framework with wider applications.

The scope of this research encompasses both numerical and experimentally informed surrogate modelling methodologies. The findings are expected to contribute to the development of practical, efficient, and reliable tools for structural safety assessment and reliability-based decision-making in civil engineering.

Chapter 3: Model surrogation for fragility analysis of nonlinear frame structures subjected to strong wind loads.

This chapter describes the general process of creating a surrogate model to improve computational efficiency. Conventional simulation can take an enormous amount of time in real-world situations, which can make standard procedures like design optimization, finding appropriate design solutions, and sensitivity analysis harder to achieve because they require huge numbers like thousands or even millions of simulation evaluations.

Preparing the surrogate model is one of the various ways of diminishing this workload. A surrogate model needs to mimic the true simulation model behaviour as closely as possible to evaluate the problem. Nonetheless, it should be computationally cheaper. A data-driven, bottom-up approach is used to construct surrogate models. While preparing the surrogate model, the input-output behaviour pattern is a key factor rather than the basic detail fundamentals of the simulation code, which are not even supposed to be known. The response of the simulator to a specific number of chosen samples can be modelled to construct a surrogate model. It is called behavioural modelling or black-box modelling. The process will be shown in the pilot study section. The curve fitting process usually involves a single design variable. The use of surrogate models is preferable in experiments and numerical simulations in engineering design; however, it is also used in various areas of science where there are expensive experiments and/or function evaluations.

The challenge in preparing the surrogate model is the creation of a surrogate that is just as precise, perfect, valid, and accurate as possible by making use of as few simulation evaluations as possible. The surrogate modelling process generally consists of three major steps, which may be applied iteratively depending on model performance:

a) Selection of representative samples for model training
b) Construction of the surrogate model, including optimization of the model parameters
c) Validation and assessment of model accuracy

The reliability of the surrogate model is therefore directly dependent on the quality and distribution of the training dataset. Poor sampling strategies or insufficient data can lead to inaccurate predictions and unreliable structural assessment outcomes. An improper surrogate model can be a cause of errors in the outcome.

This chapter is primarily focused on the development of a pilot study, which forms the methodological foundation for the subsequent research presented in Chapter 4. Both the pilot study and Chapter 4 rely on numerical simulation-based investigations. Numerical or experimental simulation needs to be run multiple times for reliability analysis (e.g., Sudret et al. 2005, Koduru and Haukaas 2010, and Szafran et al. 2019), which can often be unrealistic on many occasions.

The surrogate model needs to be run many times. However, the time spent on the surrogate model will be a fraction of the time spent on the time-marching procedure. As an example of the satisfaction of the reliability analysis, the numerical or experimental simulation needs to be run multiple times, up to 10,000 times. Large data sets were achieved through the process. However, it consumed a larger amount of time. If a surrogate model is developed using these data sets, surrogate modelling still needs to be run multiple times for the analysis purpose to train the surrogate model and validate it by comparing it with the previous data sets generated from numerical or experimental simulation. In this case, numerical/ experimental simulation may be run 1000 times, and surrogate modelling may be run 9000 times. However, the time spent on analysis through surrogate modelling will be a fraction of the time consumed by conventional numerical or experimental simulation methods.

The objective is to develop a surrogate model for improving computational efficiency associated with the safety assessment of structures. Numerical/ experimental results are to be used as a tool to prepare the surrogate model by partially replacing experimental studies. The research aims to partially replace the numerical or experimental simulation via surrogate modelling.

Within this research framework, the term safety refers to both serviceability limit state (SLS) and ultimate limit state (ULS) performance conditions. Therefore, a surrogate model is used to reduce the time spent on reliability analysis to improve computational

efficiency. Feed-forward neural network (FFNN) is used as neural network structure to create surrogate model. It will learn and understand complex input-output relationship to produce accurate results. Dataset required for constructing the surrogate model depends on limitations of experimental conditions/ numerical simulations or objectives of the study. For example, it might be possible to generate around 100 datasets some laboratory experiments since it might not be possible to derive thousands of results from thousands of laboratory experiments. Therefore, the research aims to combine laboratory-based experiments with numerical simulations to create surrogate model in chapter 5 and 6, whereas the dataset required to create surrogate models in chapter 3 and 4 would be derived from numerical simulations.

Chapter 3.1: Performance of structures under strong wind loads

The structural response of a typical civil structure under various loading conditions forms the basis for the design of the structural members of the structure. Structural performance is typically evaluated through key response parameters such as bending moments, stresses, strains, displacements, etc, which can occur within the structures. In particular, the effects of strong wind loads have been widely investigated due to their significant impact on structural safety and serviceability.

Several studies have been examined the influence of wind loads on different types of structures and components. Ginger et al. (2015) examined the vulnerability of hot-rolled steel industrial buildings against wind load by analysing the critical load effects used in the structural design of the structure, highlighting that the dominant windward wall can significantly make the structure vulnerable by increasing the design load effects. Similarly, Chou et al. (2023) experimentally studied reinforced concrete (RC) coupling beams under different loading protocols, including wind loading, and observed minor cracking behaviour, suggesting their applicability in performance-based wind design.

Recent research has also explored innovative structural components and configurations. Yoo et al. (2024) assessed the performance of kerf panels used in façade systems under wind loads through static and dynamic analyses, using stress and strain responses to evaluate their load-carrying capacity. In addition, Li et al.

(2024) analysed wind-induced vibrations in inter-storey isolated tall buildings equipped with friction pendulum bearings, using nonlinear time-domain analysis and statistical linearization methods to capture complex structural responses.

From a methodological perspective, Song et al. (2024) proposed analytical approaches based on Green's function and Schwarz–Christoffel formulations to estimate strong wind loads in high-rise buildings. While these methods provide rigorous mathematical frameworks, they can be computationally intensive when applied to complex structures. Complementing this, Zhao et al. (2023) reviewed wind-Induced nonlinear effects across various wind-sensitive structures, including tall buildings, high-rise structures, flexible bridges, and transmission lines, emphasizing the importance of capturing nonlinear behaviour in wind engineering analyses. Also, Kwon et al. (2024) further demonstrated the use of finite element method (FEM) modelling validated against experimental wind resistance tests to evaluate the performance of standing seam metal roofs in industrial structures.

These studies provide an important theoretical and experimental foundation for understanding the wind load-induced structural performance. However, existing research has predominantly focused on specific structural components, such as roofs and cladding systems, with comparatively less emphasis on walls and other exposed structural elements – particularly in the context of modern high-rise construction.

Moreover, although advanced analytical and numerical methods have been developed to estimate wind effects, many of these approaches remain computationally demanding and time-intensive, limiting their practical applicability in large-scale reliability or fragility assessments.

Given these limitations, there is a need for efficient computational approaches that can accurately capture wind-induced structural responses while reducing analysis time. So, the following subchapter focuses on surrogate modelling techniques for fragility analysis of structures subjected to wind loads, aiming to bridge the gap between computational efficiency and predictive accuracy.

Chapter 3.2: Model setup for Nonlinear hysteretic two-storey shear frame subjected to strong wind loads.

This subchapter discusses the construction of a surrogate model to predict the excitation force history caused due to wind load. Nonlinear multi-storey steel frames, under wind loads, has been selected as a specific civil structure for the purpose of the study. The study comprises a simulation model and a developed surrogate model that mimics the true simulation model behaviour as closely as possible.

MATLAB, a programming and numerical computing platform, has been used in establishing the surrogate model for fragility analysis caused due to wind load. A 2-storey building has been assumed as part of the study. The maximum inter-storey displacement of the building is assumed as the milestone to predict the fragility analysis of the building. It is known that wind load is a dynamic load, where the force applied due to wind changes with time at each point of the building.

A flowchart illustrating the overall computational procedure is presented in Figure 1. The figure summarises the input variables, governing relationships, numerical solution strategy, and resulting structural response quantities. These components form the basis of the simulation–surrogate modelling framework developed in this study.

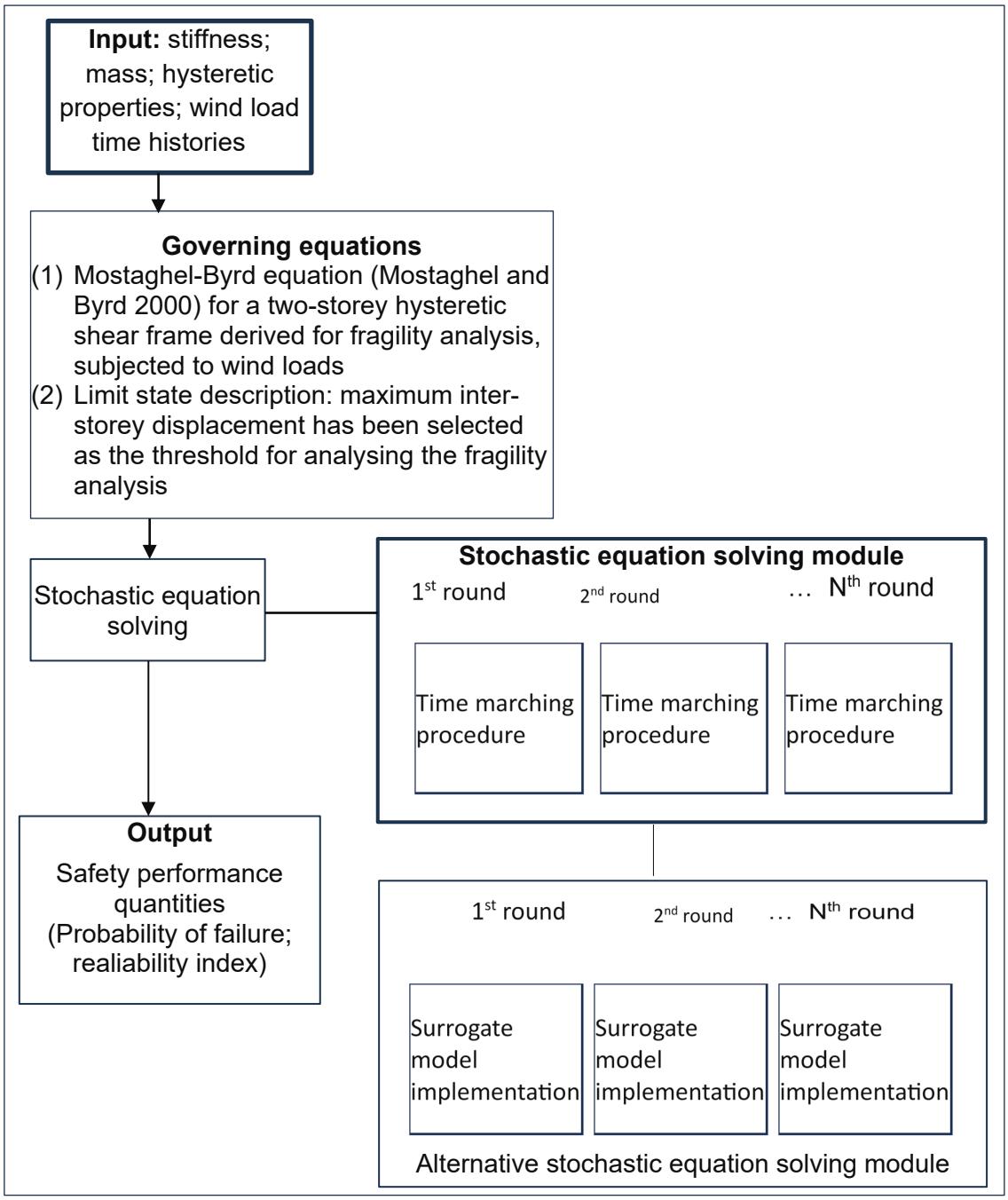

Figure 1: A flowchart demonstrating the process carried out during the nonlinear study

Chapter 3.3: Model Implementation

The simulation model is implemented using a MATLAB-based two-stage computational procedure. The first stage involves the generation of wind-induced excitation force–time histories, while the second stage computes the corresponding structural response in terms of displacement and velocity.

The first part of the MATLAB function derives the excitation force-time histories. Different input variables were used in part 1 of the MATLAB simulation function to create excitation force-time histories. These variables include air density, mean wind speed at 10 m, surface area normal to the direction of the longitudinal wind, heights of the storeys, drag coefficient, storey mass, and storey stiffness. Some of the variables are in scalar quantity, whereas some variables are presented in column vector form when using the MATLAB function. The value of air density is 1.225 kg/m^3, and the mean wind speed at 10 m is assumed to be 60 m/s. The surface area normal to the direction of the longitudinal wind is also assumed to be 10 m^2. The heights of the storeys are assumed to be 7 m and 14 m for the first storey and the second storey, respectively. The drag coefficient is 1.5 with the storey mass assumed as 1,250,000 kg and 1,125,000 kg for the two storeys, respectively. Additionally, storey stiffness is assumed to be 1e7 and 0.9e7 for the storeys.

Since wind is a random variable load, the value of the excitation force-time histories changes with time for two different storey levels. Excitation force is denoted by ‘F’, and the time required for the simulation is denoted by ‘t.’ The excitation force-time histories created from the first iterated evaluation of part 1 of MATLAB can be seen in Figures 2 and 3. Figures 2 and 3 demonstrate the random nature of the wind loads subjected to the point in time at which it was recorded. It can also be observed that the wind load is very strong, with a strength of up to 50 kN.

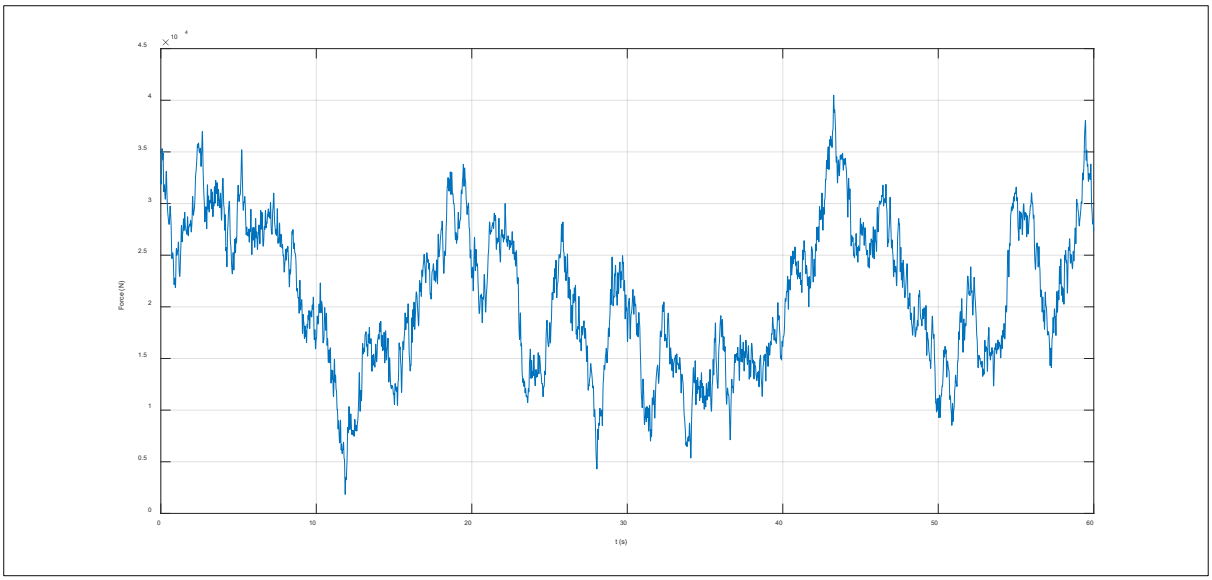

Figure 2: Force recorded against time for the 1st level of the building

Forces plotted in Figures 2 and 3 are wind pressure derived forces from recorded pressures.

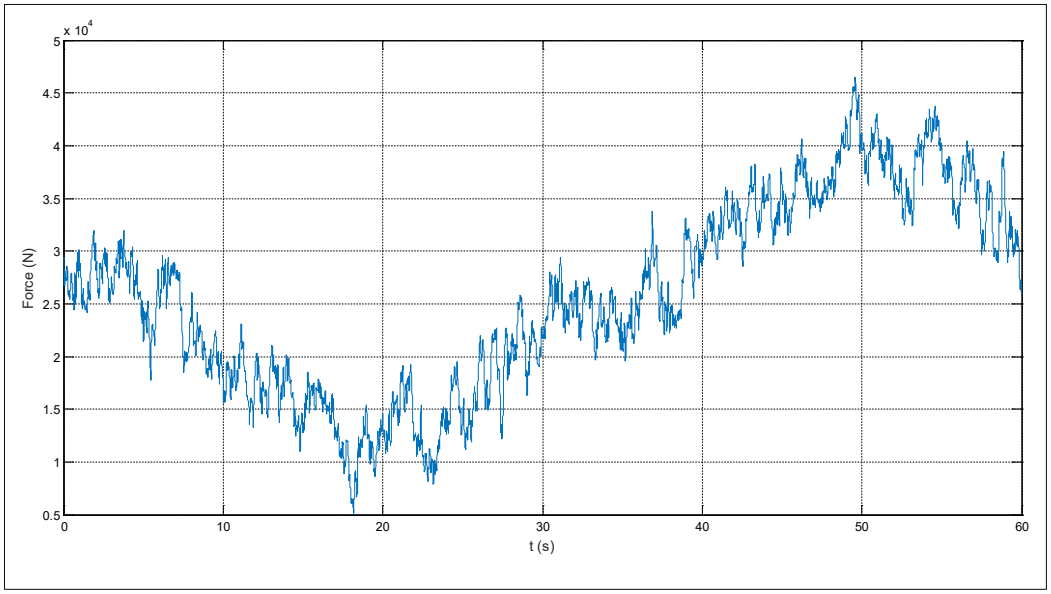

Figure 3: Force recorded against time for the 2nd level of the building

The second part of the MATLAB simulation function aims to generate the response time histories of displacement and velocity. Displacement is denoted by ‘u’, whereas velocity is denoted by ‘udot’. The response time histories created from the first iterated evaluation of part 2 of MATLAB can be seen in Figures 4 to 7. Since figures 4, 5, 6, and 7 are the result of the data acquired from figures 1 and 2, the data suggest that

displacement and velocity are also random variables. It is obvious from these figures that large wind loads have resulted in larger displacements and velocities at the recorded time.

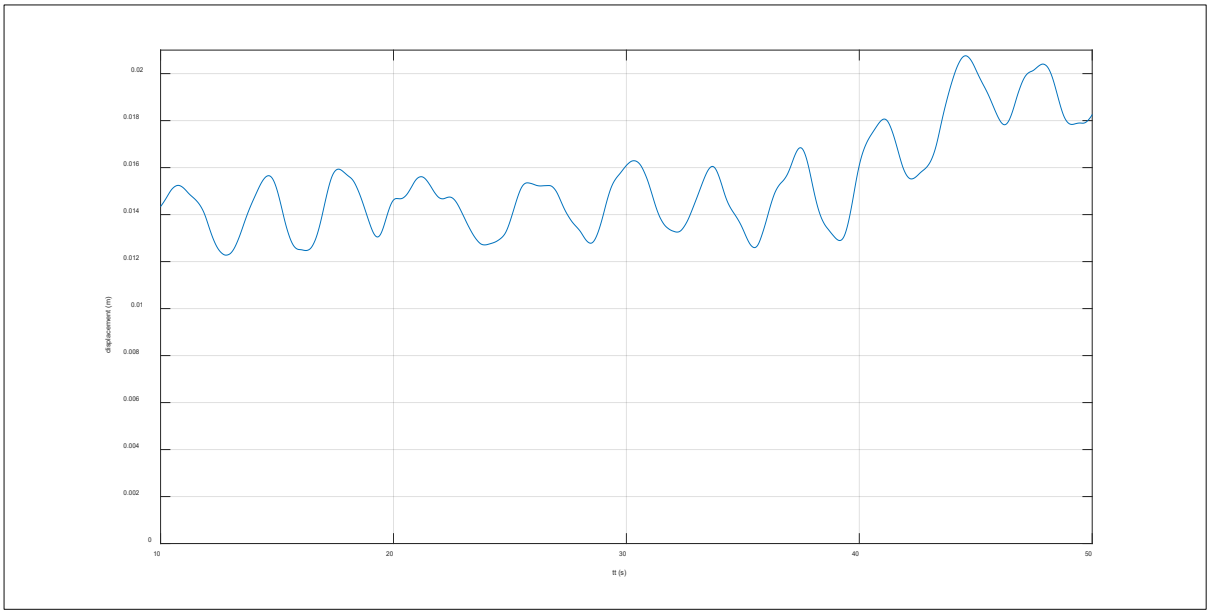

Figure 4: u vs tt for the 1st level of the building

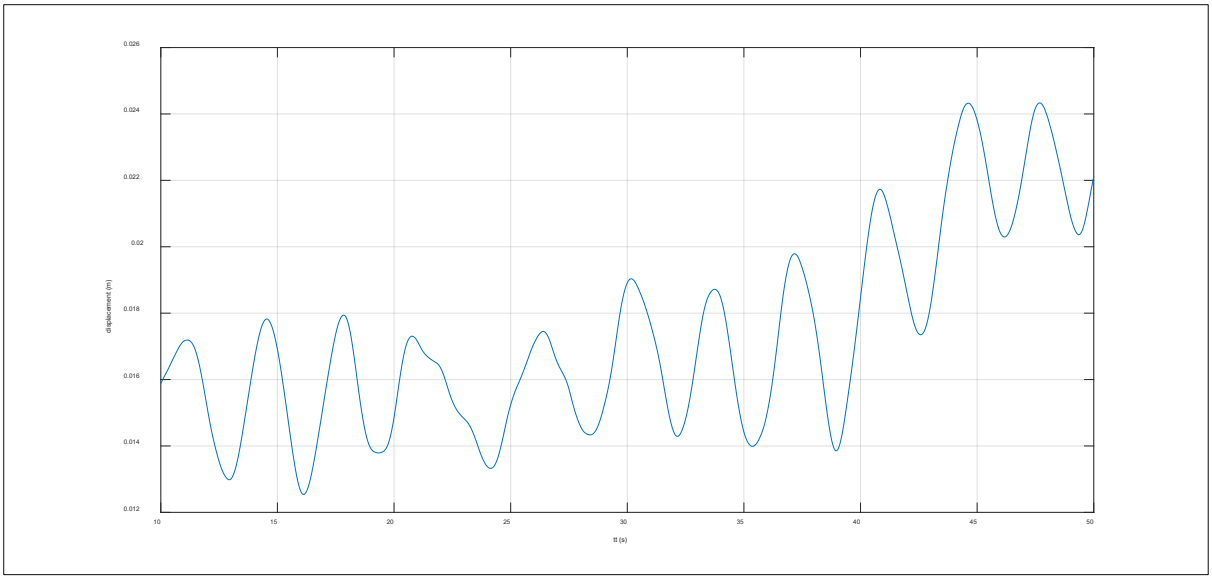

Figure 5: u vs tt for the 2nd level of the building

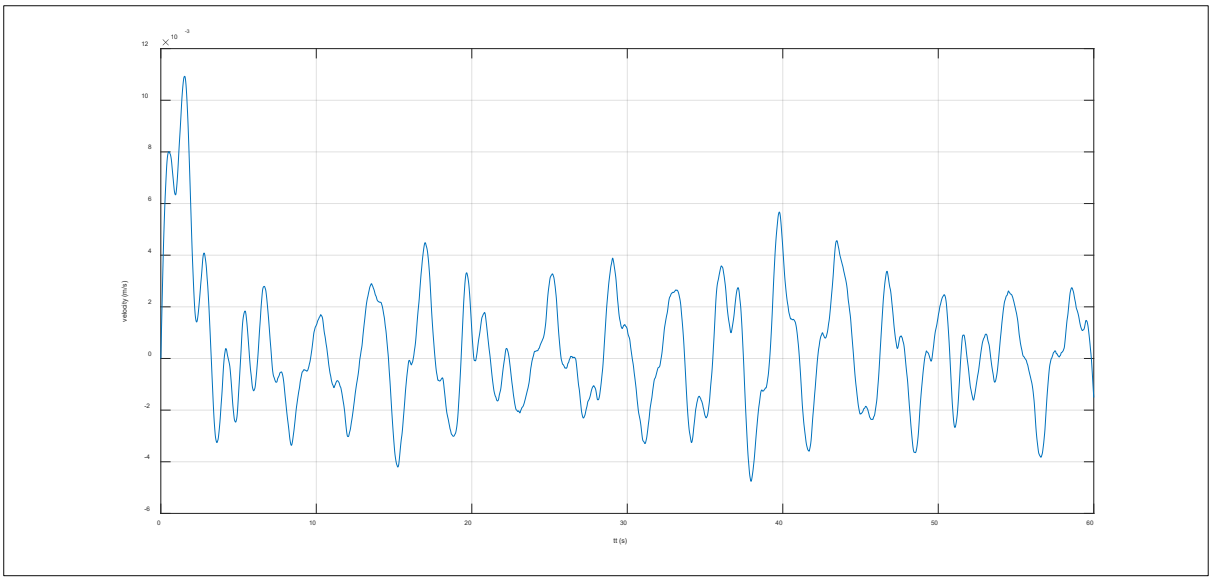

Figure 6: udot vs tt for the 1st level of the building

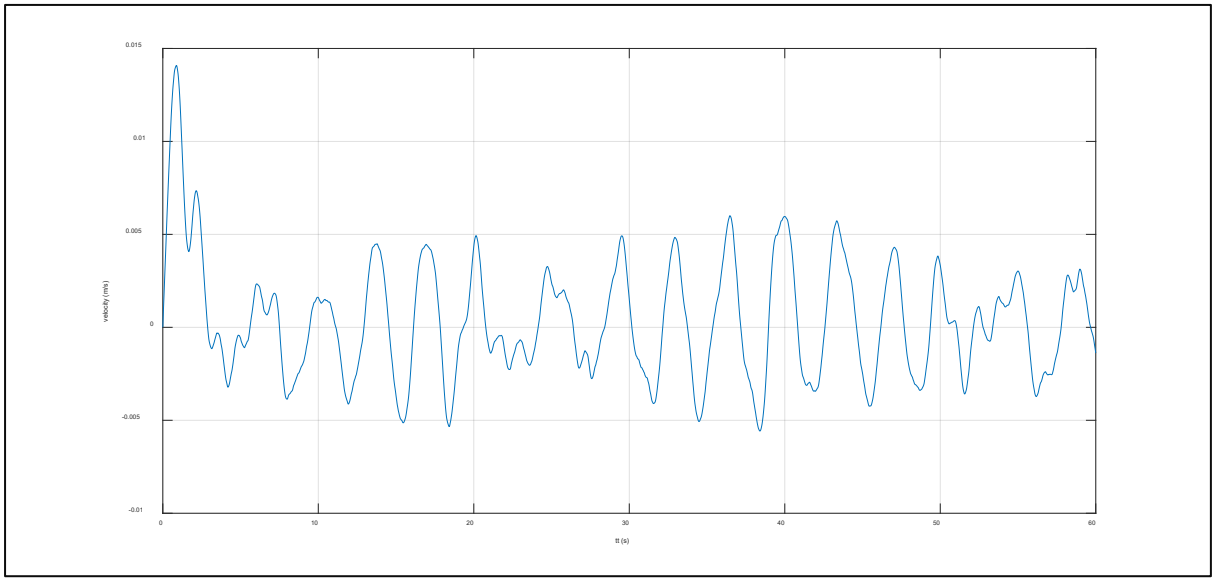

Figure 7: udot vs tt for the 2nd level of the building

The number of rounds can be changed by changing the value of N in the MATLAB function to collect more sample data for increasing the accuracy of the data. The output result for 10 rounds has been derived in the form of the maximum inter-storey displacement happening in the frame. The data has been presented in Table 1. For the time-marching procedure, 10 sets of data have been recorded, which will be used as the threshold for the fragility analysis of the building. However, large sets of data were required for more accuracy. This can require more time, and hence it was not feasible to run the same process over thousands of times. Therefore, a surrogate

model, which is another part of the pilot study, was appropriate for this kind of situation, where a simulation need to be run thousands of times.

Table 1: Output for rounds of simulation

Round	Maximum inter-storey displacement between 2nd level and 1st level (m)	Maximum inter-storey displacement between the 1st level and the ground level (m)	Maximum inter-storey displacement happening in the frame (m)
1	0.0051	0.0158	0.0158
2	0.0043	0.0208	0.0208
3	0.0103	0.0232	0.0232
4	0.0040	0.0162	0.0162
5	0.0045	0.0236	0.0236
6	0.0047	0.0064	0.0064
7	0.0066	0.0163	0.0163
8	0.0067	0.0425	0.0425
9	0.0043	0.0276	0.0276
10	0.0066	0.0199	0.0199

Now, a surrogate model is developed to replicate the behaviour of the simulation model as closely as possible. It was noticed during the simulation model that excitation force wind F and storey stiffness are the only changing variables in the process. Therefore, the surrogate model needs to understand the behaviour pattern of the output based on these two changing variables. Two MATLAB functions are required to complete the process of creating the surrogate model. Part 1 of the MATLAB function will generate the sample data that will be used for modelling purposes. The sample data will consist of excitation force wind F, storey stiffness, and displacement u. Sample data will be fetched and imported into part 2 of MATLAB functions to train the function to understand the behaviour of the input-output pattern. It will develop into what is called a trained neural network surrogate model.

Chapter 3.4: Results and analysis

The performance of the trained surrogate model is evaluated using standard validation metrics. Figure 8 presents the neural network performance plot, showing consistent agreement between training, validation, and testing datasets, indicating stable model convergence and appropriate generalisation capability.

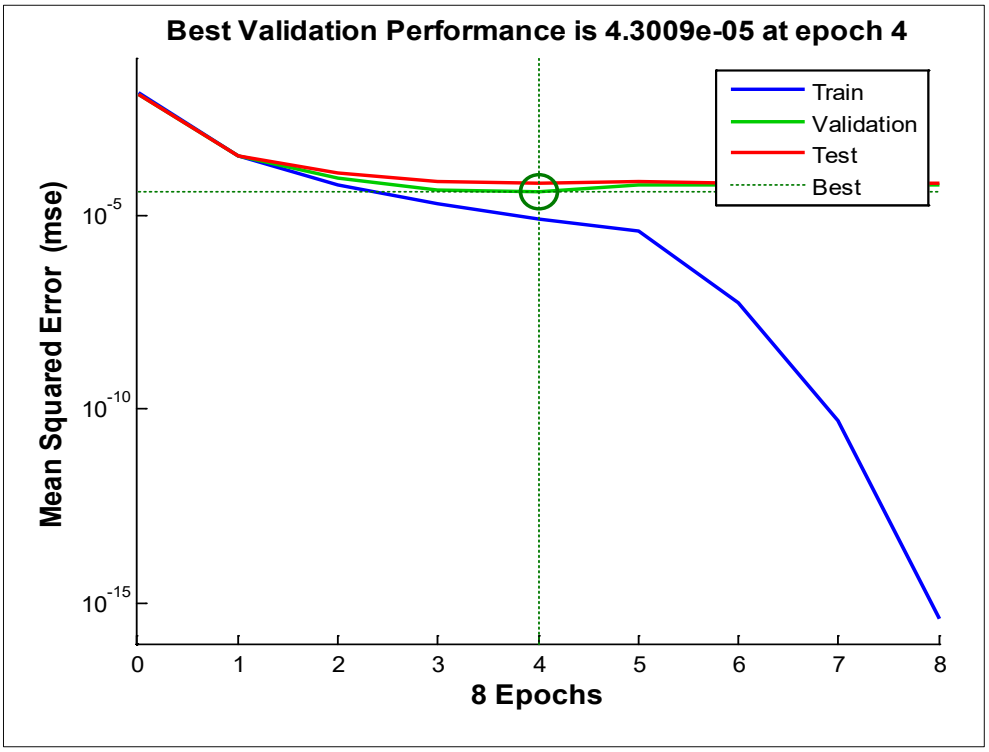

Figure 8: Neural network performance of the trained surrogate model

Similarly, to validate the trained surrogate model, Figure 9 shows the regression line with R as 0.88766.

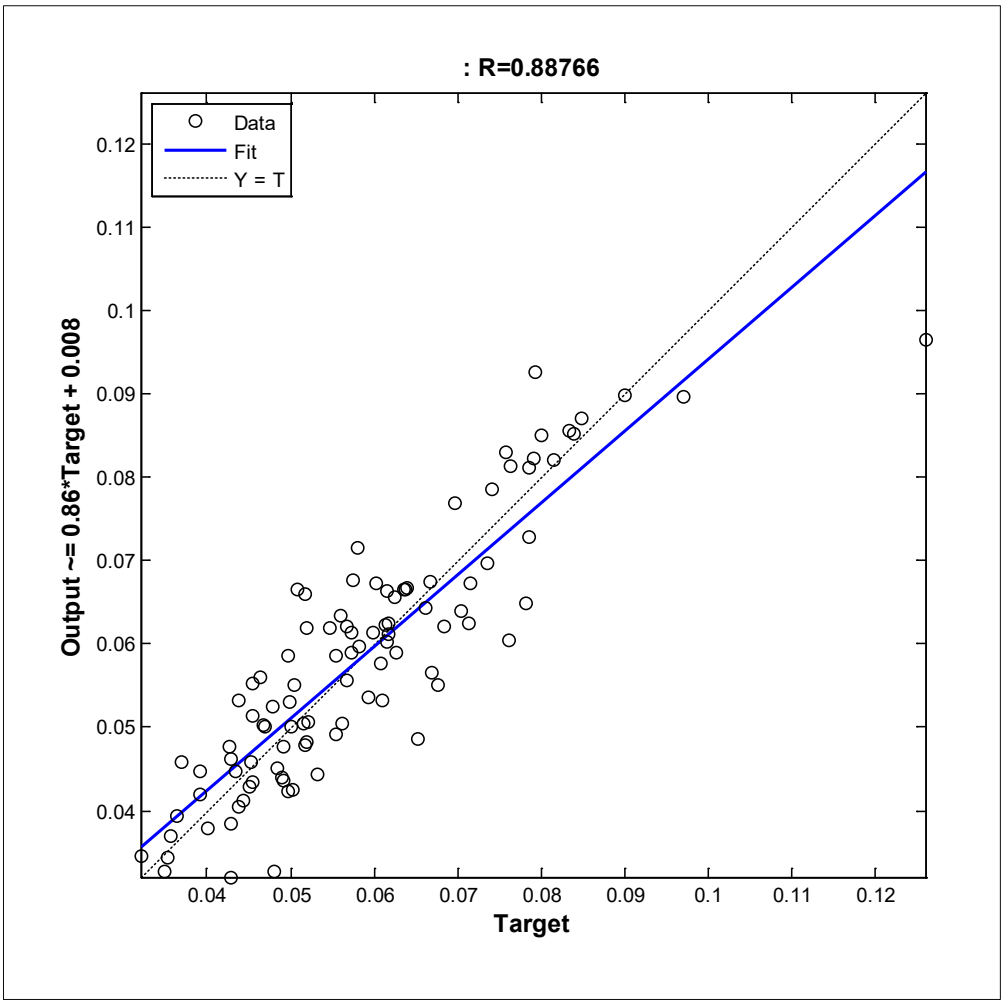

Figure 9: Regression line to validate the trained surrogate model

There are several methods to demonstrate the validation of the trained surrogate model. However, the regression line has been used in the pilot study to validate the trained surrogate model. The regression line shows the relationship between output and target values in Figure 9. The value of R is 0.88766. Output and target values seem to be consistent with each other, as indicated by the 45-degree linear line in Figure 9. Thus, a surrogate model is created to enhance the performance of the simulation, as it was practically impossible to carry out thousands of rounds in a real-life situation.

An additional validation check is performed by comparing surrogate model predictions with target simulation outputs within predefined tolerance limits. Specifically, a ±10% acceptance criterion (i.e., 90%–110% of target values) is adopted to assess predictive reliability. As illustrated in Figure 10, most predicted values fall within these bounds,

confirming that the surrogate model provides sufficiently accurate approximations of the underlying nonlinear system response.

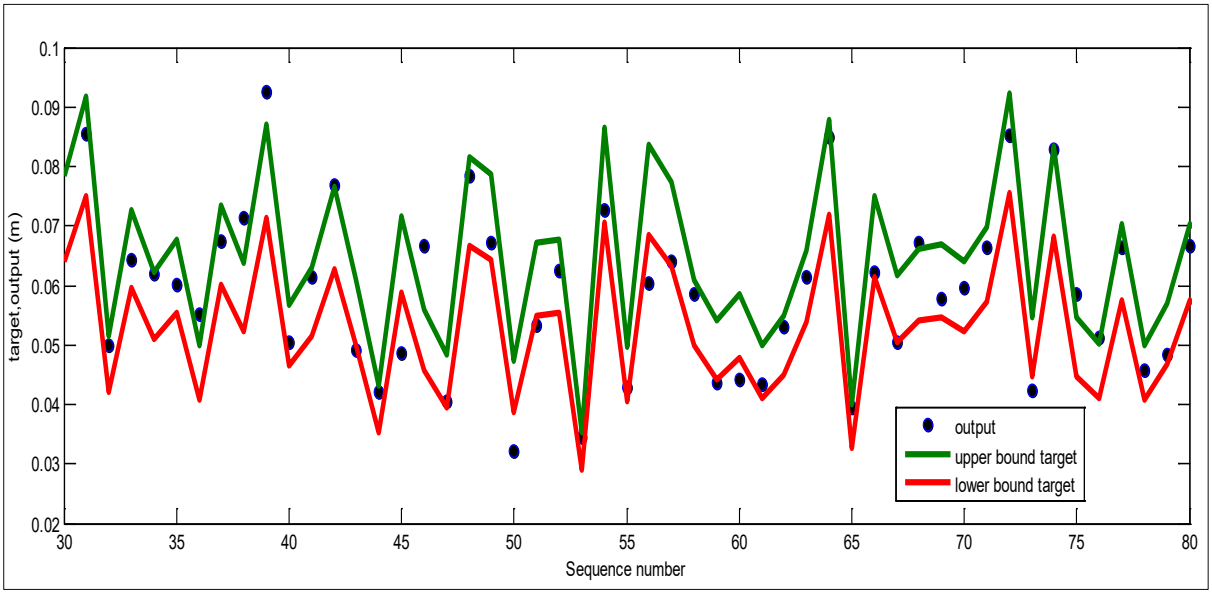

Figure 10: Comparing target and output from the surrogate model

This chapter develops the construction of neural network-based surrogate (data-driven) model to improve computational efficiency in fragility analysis of nonlinear frame structures under strong wind loads. Conventional simulations methods are computationally expensive and impractical for tasks requiring thousands of simulations, such as reliability analysis and optimization. The constructed surrogate model mimics the behaviour of the original simulation using a black-box (behavioural) modelling approach, focusing on input–output relationships rather than underlying physics. The process involves three key steps: selecting sample data, building, and optimizing the model, and validating its accuracy.

A pilot study is conducted using a two-storey nonlinear steel frame model implemented in MATLAB. The simulation generates wind-induced excitation forces and structural responses (displacement and velocity), highlighting the random nature of wind loads. Due to the high computational cost of repeated simulations, a trained neural network based surrogate mode is developed using key variables such as wind force and storey stiffness. The surrogate model significantly reduces computation time while

maintaining acceptable accuracy. Validation results ($R \approx 0.89$ and outputs mostly within 90–110% of targets) show good agreement with the original simulation.

Overall, the study demonstrates that surrogate modelling is an effective tool for efficient and reliable structural safety assessment under wind loading conditions. Similarly, model surrogation can be used in other areas of study, replicating the process carried out in Chapter 3. Applicability of the constructed surrogate model will be further discussed in Chapter 7.1. The following Chapter 4 will discuss the research work based on the numerical investigation of structures under seismic actions. Model surrogation was also applied for the analysis of the prototype replicating the true nature of the real-life silo structure in Chapter 5.

Chapter 4: Model surrogation for fragility analysis of nonlinear structures subjected to seismic actions

Earthquakes can create a massive challenge for humankind. It is necessary to build structures that can withstand the effects of seismic actions. Seismic actions are applied to the structure suddenly and can cause the structure to vibrate. Therefore, appropriate structural designs are required to be developed based on the seismic actions.

Traditional nonlinear dynamic analyses, although highly accurate, are computationally intensive and time-consuming, particularly when repeated analyses are required for probabilistic fragility assessments or optimisation studies. Recent advances in artificial intelligence have demonstrated that surrogate modelling techniques can significantly reduce computational effort while maintaining acceptable prediction accuracy.

This chapter extends the surrogate modelling methodology introduced in Chapter 3 by applying artificial neural networks to nonlinear seismic analysis. A neural network-based surrogate model is developed to reproduce the behaviour of a three-storey reinforced concrete building subjected to earthquake loading. Numerical data generated from ETABS through nonlinear time-history analysis are used to train and validate the surrogate models. The objective is to establish an efficient computational framework capable of accurately predicting structural responses while substantially reducing simulation time.

Chapter 4.1: Performance of structures under seismic actions

The structural response of a typical civil structure against any loads is used in the design of the structural members of the structure. Structural performance can be determined by analysing various load effects like bending moment, stress, strain, displacement, etc, which can occur within the structures. Under seismic loading, these response parameters become highly dynamic because earthquake forces vary continuously with time, making seismic analysis considerably more complex than static loading analysis. Thus, extensive research has been undertaken to improve the

understanding of structural behaviour and to develop effective methods for enhancing seismic resilience.

Several recent studies have focused on improving the seismic performance of reinforced concrete (RC) structures through innovative structural systems and retrofitting techniques. Kim and Lee (2024) investigated the use of slit-brace retrofitting for reinforced concrete beam-column systems through cyclic lateral loading tests. Their results demonstrated that the proposed retrofit delayed the initiation of shear cracking, reduced concrete spalling, enhanced energy dissipation capacity, and significantly improved the overall seismic resilience of the structural system.

Foundation systems have also been shown to influence seismic response. Sabermahany and Attarnejad (2021) evaluated the behaviour of buildings supported by shallow doubly curved shell raft foundations using nonlinear time-history analysis under four earthquake ground motions. Their numerical investigation showed that shell foundations reduced maximum structural displacement and inter-storey drift compared with conventional pile-raft foundations, although larger storey shear forces were observed.

The contribution of structural components to earthquake resistance has also been widely investigated. El-Ghareeb et al. (2024) conducted a numerical study on multi-storey reinforced concrete frames with masonry infill walls and reported that infill walls substantially enhanced the seismic performance of the structures. Similarly, Wu et al. (2024) experimentally examined Steel Reinforced Concrete–Reinforced Concrete (SRC–RC) hybrid structures using low-cycle loading tests. Their investigation evaluated hysteretic behaviour, skeleton curves, bearing capacity, residual deformation, damage progression, and energy dissipation, providing valuable insight into the seismic behaviour of hybrid structural systems.

Experimental investigations have further improved the understanding of individual structural components under earthquake loading. Apostolopoulos et al. (2018) assessed the seismic response of reinforced concrete columns subjected to combined constant axial loading and progressively increasing cyclic lateral loads. The resulting hysteresis curves were analysed in terms of strength degradation, displacement

capacity, and energy dissipation. Likewise, Rashidiyan et al. (2023) examined the seismic behaviour of non-straight steel beams, addressing an important gap in the understanding of irregular steel structural members and providing useful guidance for practical structural design.

Beyond conventional structural systems, researchers have also investigated methods for improving structural performance through supplemental control devices. Barroso et al. (2002) evaluated several structural control strategies, including friction pendulum base isolation systems, linear viscous dampers, and active tendon brace systems, demonstrating their effectiveness in mitigating earthquake-induced structural responses. Erdil et al. (2022) further examined the combined influence of seismic loading and harsh climatic conditions on masonry buildings, highlighting the importance of considering multiple environmental hazards in structural assessment.

These studies provide an important theoretical basis for the earthquake load-induced performance of the structures. Studies have been traditionally conducted on the beam and column of the structures in relation to earthquake loads. Since there has been increasing development of high-rise buildings around the globe, it is necessary to determine the earthquake load effects on walls and other exposed structural members. Though there have been studies conducted on the methods to estimate the seismic effect, most of the traditional methods are time-consuming and not feasible. To address these limitations, surrogate modelling techniques have emerged as an efficient alternative for approximating complex structural responses while significantly reducing computational effort. The following subchapter presents the development of a neural network-based surrogate model for the fragility analysis of nonlinear structures subjected to seismic actions.

Chapter 4.2: Model setup for Nonlinear hysteretic three-storey buildings subjected to seismic load.

The following sub-chapter discusses the numerical investigation for the safety assessment of a simple three-storey building under seismic actions. The primary objective of the numerical analysis is to generate a comprehensive dataset for the

development of a neural network-based surrogate model capable of efficiently predicting structural responses under seismic loading.

The data required to develop the surrogate model was generated using the ETABS software. ETABS software was used to develop a simple 3-storey building model. ETABS was used for this part of the research, i.e., seismic analysis, while it was not used in Chapter 3 for wind analysis. It is specifically optimized for designing building structures to understand its performance against earthquake action loads with use of international building codes. Time-history analysis was required to investigate the structure under seismic conditions.

A simple 3-storey building with the storey height of 3 m is designed in ETABS software. The plan configuration of the building is illustrated in Figure 11, while the three-dimensional numerical model is shown in Figure 12. The structural members were designed using reinforced concrete. Beams were modelled with cross-sectional dimensions of 230 mm × 350 mm, while columns were assigned dimensions of 350 mm × 350 mm. Both beams and columns were assumed to be constructed using M30 reinforced concrete. Reinforced concrete slabs with a thickness of 150 mm were used for both the intermediate floors and roof slab.

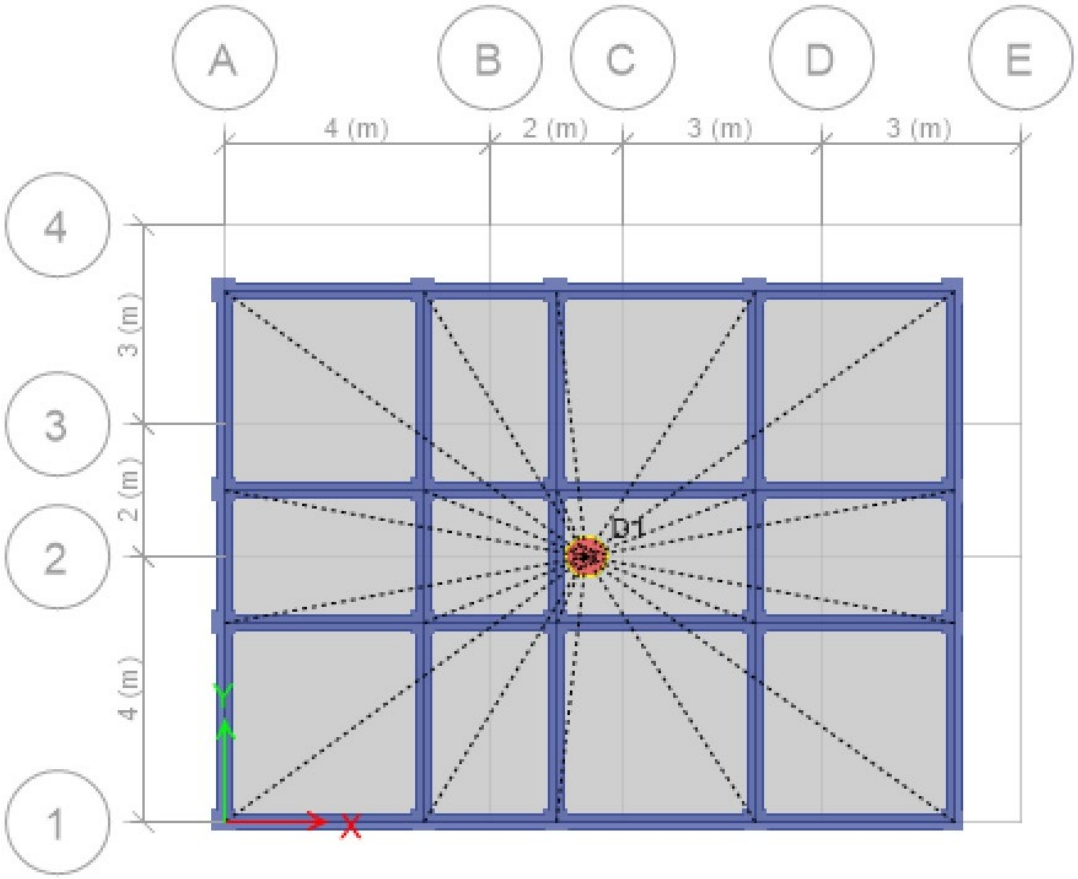

Figure 11: Plan view of the structure in ETABS model

Figure 11 displays the plan layout of the structure designed in ETABS software. It details the size of the room by laying out the distance between the columns. In horizontal direction, the distance between the consecutive columns are 4 m, 2 m, 3 m, and 3 m respectively, whereas in vertical direction, the distance between the consecutive columns are 4 m, 2 m, and 3 m, respectively. The resulting three-dimensional structural configuration is presented in Figure 12. It shows the number of stories in the building.

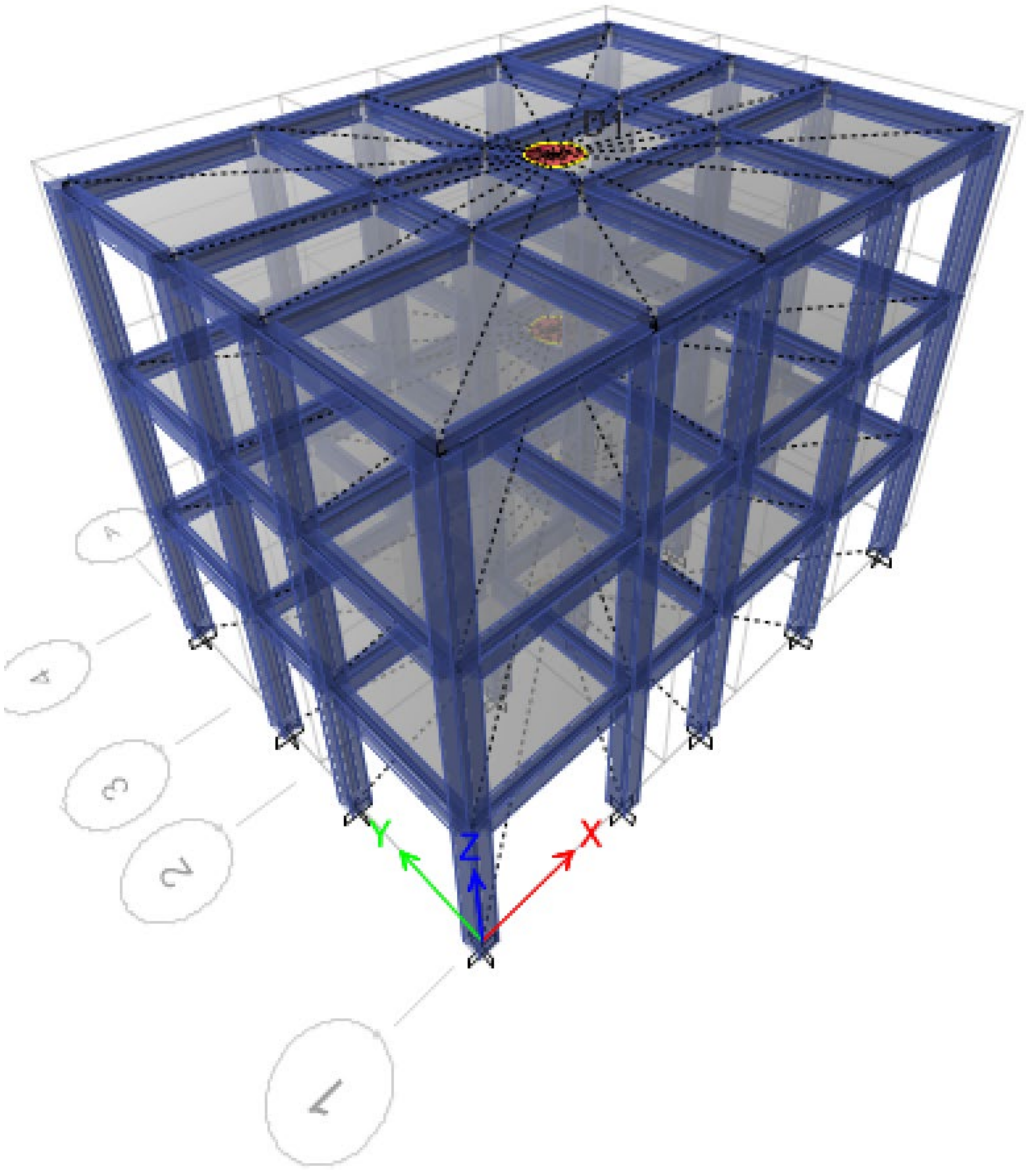

Figure 12: Three-dimensional view of the structure in ETABS model

The seismic performance of the building was evaluated using nonlinear time-history analysis. Effects of earthquake load on the structure, including joint displacements, velocities, and accelerations, can be changed according to the type of structure used for building it. It is understood that changing the Young's modulus of the concrete used in the structure can change the effects of the seismic actions. Initially, the young modulus of the concrete for designing the building is 30 GPa. However, to generate

the required output data, the young modulus of the concrete is changed consecutively to 40 GPa, and 50 GPa. Young modulus of the concrete was changed to derive the maximum storey displacement for the 3rd and 2nd stories of the building under the effect of seismic actions.

The maximum displacement in the 3rd storey of the building is assumed as the milestone to predict the fragility analysis of the building. It is known that seismic load is a dynamic load, where the force applied due to seismic load changes with time at each point of the building. Therefore, the El Centro time-history function embedded within ETABS was used to create the seismic load conditions. The most commonly used ground motion record (especially in the early day) for seismic analysis is the 1940 'El Centro' record. However, this has been renamed as the 1940 Imperial Valley earthquake based on the naming convention adopted in recent decades. Owing to its historical significance and extensive use in earthquake engineering research, this ground motion record provides a well-established benchmark for evaluating structural seismic performance. Time-history analysis was used to investigate maximum horizontal and vertical displacements in each storey of the building.

The numerical simulations were performed to determine the maximum horizontal and vertical displacements of each storey throughout the duration of the earthquake excitation. Although ETABS can also provide structural responses such as accelerations, velocities, internal forces, and member stresses, the present study focuses primarily on displacement responses because they directly relate to structural fragility assessment.

MATLAB was used to generate the 30 sets of random data around 3 different mean Young's Modulus or Modulus of Elasticity values. A normal distribution is used to generate these random data. The three different Young's Modulus are 30 GPa, 40 GPa, and 50 GPa. 30 sets of data were generated around each of these values using MATLAB with a coefficient of variation of 10 percent. These data were imported into MATLAB for creating a neural network-based surrogate model. Tables 2, 3, and 4 show the data collected from ETABS using the random numbers generated from MATLAB for different Young's Modulus.

From these data sets, a surrogate model was developed to replicate the behaviour of the simulation model as closely as possible. It was noticed during the simulation model that Young's Modulus is the only changing variable in the process. Therefore, the surrogate model needs to understand the behaviour pattern of the output based on this changing variable. Two MATLAB functions are required to complete the process of creating the surrogate model. Data were fetched and imported into MATLAB functions to train the function to understand the behaviour of the input-output pattern. It was developed into what is called a trained neural network surrogate model. The input was Young's Modulus, and the output were the 3rd storey maximum displacement in horizontal and vertical direction. It would be useful if the maximum displacement for all stories and inter-storey displacements were taken into consideration. However, to meet the objective of the research (i.e., to shorten the simulation time), the assumed milestone is only used in the upcoming subchapters.

Table 2: Data generated from ETABS when Young's Modulus is 30 GPa

Young's Modulus (MPa)	3rd storey max tha x (mm)	2nd storey max tha x (mm)	inter storey displacement x (mm)	3rd storey max tha y (mm)	2nd storey max tha y (mm)	inter-storey displacement y (mm)
31613.00	69.31	53.01	16.30	14.59	10.86	3.74
35501.66	64.43	49.30	15.13	12.81	9.53	3.28
23223.46	84.24	63.19	21.05	19.73	14.68	5.05
32586.52	68.00	52.08	15.91	14.07	10.47	3.60
30956.30	70.20	53.58	16.62	14.96	11.13	3.83
26076.94	77.31	57.93	19.38	17.87	13.29	4.57
28699.22	73.22	55.15	18.08	16.29	12.12	4.17
31027.87	70.10	53.52	16.58	14.92	11.10	3.82
40735.19	60.04	45.47	14.56	11.13	8.28	2.85
38308.31	61.82	46.96	14.86	11.80	8.78	3.02
25950.34	77.89	58.37	19.52	18.07	13.44	4.63
39104.77	61.19	46.41	14.78	11.56	8.60	2.96
32176.21	68.55	52.48	16.07	14.28	10.63	3.66

29810.84	71.71	54.40	17.31	15.63	11.63	4.00
32144.23	68.59	52.51	16.08	14.30	10.64	3.66
29385.10	72.27	54.67	17.61	15.88	11.82	4.07
29627.57	71.95	54.51	17.44	15.74	11.71	4.03
34469.09	65.59	50.24	15.35	13.22	9.83	3.39
34227.10	65.88	50.47	15.41	13.31	9.91	3.41
34251.58	65.85	50.45	15.40	13.30	9.90	3.41
32014.49	68.76	52.64	16.13	14.37	10.69	3.68
26377.54	76.81	57.55	19.26	17.68	13.16	4.53
32151.72	68.58	52.50	16.08	14.30	10.64	3.66
34890.71	65.10	49.85	15.25	13.05	9.71	3.34
31466.68	69.51	53.14	16.36	14.67	10.92	3.76
33104.08	67.31	51.57	15.74	13.80	10.27	3.53
32180.66	68.54	52.48	16.06	14.28	10.63	3.66
29089.68	72.68	54.86	17.81	16.06	11.95	4.11
30881.61	70.30	53.64	16.66	15.00	11.16	3.84
27638.15	74.81	56.11	18.70	16.93	12.60	4.33

Table 3: Data derived from ETABS when Young's Modulus is 40 GPa

Young's Modulus (MPa)	3rd storey max tha x (mm)	2nd storey max tha x (mm)	inter storey displacement x (mm)	3rd storey max tha y (mm)	2nd storey max tha y (mm)	inter-storey displacement y (mm)
43553.58	58.56	44.41	14.15	10.46	7.78	2.68
35411.72	64.52	49.38	15.15	12.85	9.56	3.29
35724.52	64.19	49.10	15.10	12.72	9.47	3.26
36762.01	63.17	48.20	14.97	12.34	9.18	3.16
28222.86	73.92	55.55	18.37	16.58	12.34	4.24
45753.52	57.80	43.91	13.90	9.99	7.43	2.56
41300.76	59.69	45.22	14.48	10.99	8.17	2.81
36980.29	62.97	48.01	14.96	12.26	9.12	3.14
45481.19	57.88	43.96	13.92	10.05	7.47	2.57

33153.93	67.25	51.52	15.72	13.78	10.25	3.53
39591.03	60.82	46.10	14.72	11.42	8.49	2.92
39034.21	61.24	46.45	14.79	11.58	8.61	2.97
41276.83	59.71	45.23	14.48	10.99	8.18	2.82
41251.43	59.72	45.24	14.49	11.00	8.18	2.82
36540.48	63.38	48.39	14.99	12.42	9.24	3.18
39879.79	60.61	45.92	14.69	11.34	8.44	2.90
39340.48	61.01	46.25	14.76	11.49	8.55	2.94
42510.83	59.05	44.75	14.30	10.70	7.96	2.74
44373.06	58.23	44.19	14.04	10.28	7.65	2.63
44437.09	58.21	44.17	14.03	10.26	7.64	2.63
36545.39	63.37	48.38	14.99	12.42	9.24	3.18
40309.44	60.31	45.69	14.63	11.23	8.36	2.88
35143.53	64.82	49.62	15.20	12.95	9.63	3.32
35546.00	64.38	49.26	15.12	12.79	9.52	3.28
39972.60	60.55	45.87	14.67	11.32	8.42	2.90
46130.52	57.71	43.85	13.86	9.91	7.37	2.54
36921.34	63.02	48.06	14.96	12.28	9.13	3.14
41485.52	59.59	45.14	14.45	10.94	8.14	2.80
39097.66	61.19	46.41	14.78	11.56	8.60	2.96
44469.42	58.19	44.16	14.03	10.26	7.63	2.63

Table 4: Data derived from ETABS when Young's Modulus is 50 GPa

Young's Modulus (MPa)	3rd storey max tha x (mm)	2nd storey max tha x (mm)	inter storey displacement x (mm)	3rd storey max tha y (mm)	2nd storey max tha y (mm)	inter-storey displacement y (mm)
52688.34	57.24	42.88	14.36	8.58	6.38	2.20
59169.43	59.03	43.70	15.33	7.53	5.60	1.93
38705.77	61.50	46.68	14.83	11.68	8.69	2.99
54310.87	57.57	42.82	14.75	8.29	6.17	2.12
51593.83	57.12	43.02	14.10	8.78	6.54	2.25

43461.56	58.60	44.44	14.16	10.48	7.80	2.68
47832.04	57.38	43.61	13.77	9.56	7.11	2.45
51713.12	57.13	43.01	14.13	8.76	6.52	2.24
67891.98	63.74	47.40	16.33	6.60	4.91	1.69
63847.19	61.09	45.35	15.74	6.99	5.20	1.79
43250.57	58.69	44.50	14.19	10.53	7.83	2.70
65174.62	61.85	45.94	15.91	6.85	5.10	1.75
53627.02	57.41	42.82	14.60	8.41	6.26	2.15
49684.73	57.15	43.34	13.81	9.17	6.82	2.35
53573.71	57.40	42.82	14.59	8.42	6.26	2.16
48975.17	57.22	43.45	13.77	9.32	6.93	2.39
49379.28	57.17	43.39	13.79	9.23	6.87	2.36
57448.49	58.46	43.27	15.20	7.78	5.79	1.99
57045.17	58.34	43.18	15.16	7.84	5.83	2.01
57085.96	58.35	43.19	15.16	7.83	5.83	2.01
53357.49	57.36	42.83	14.53	8.46	6.29	2.17
43962.57	58.39	44.29	14.09	10.37	7.71	2.65
53586.19	57.41	42.82	14.59	8.42	6.26	2.16
58151.18	58.69	43.43	15.26	7.68	5.71	1.97
52444.47	57.21	42.91	14.30	8.63	6.42	2.21
55173.47	57.79	42.88	14.92	8.14	6.05	2.08
53634.43	57.42	42.82	14.60	8.41	6.26	2.15
48482.80	57.28	43.52	13.76	9.42	7.01	2.41
51469.36	57.12	43.04	14.07	8.81	6.55	2.26
46063.59	57.73	43.86	13.87	9.92	7.38	2.54

Tables 2, 3, and 4 present the complete datasets generated for mean Young's Modulus values of 30 GPa, 40 GPa, and 50 GPa, respectively. These datasets constitute the training and validation database used throughout the subsequent surrogate modelling process.

Chapter 4.3: Model Implementation

This subchapter focuses on the creation and implementation of the neural network-based surrogate model. The proposed modelling approach follows the general workflow established in Figure 1 of Chapter 3 and is extended herein to depict the relationship between material properties and seismic response parameters under earthquake excitation. In this study, separate surrogate models are developed for different structural response outputs, each trained using datasets corresponding to three discrete levels of Young's Modulus of Elasticity. The predictive performance of the models is assessed using the mean squared error (MSE) and the coefficient of determination (R), which are commonly adopted measures for evaluating regression accuracy.

Initially, the surrogate model is created using data generated around a mean Young's Modulus of 30 GPa, with the target response defined as the 3rd storey maximum horizontal displacement. The training performance, illustrated in Figure 13, yields an MSE value of 0.065442, indicating satisfactory convergence of the neural network and an acceptable level of prediction error relative to the target response.

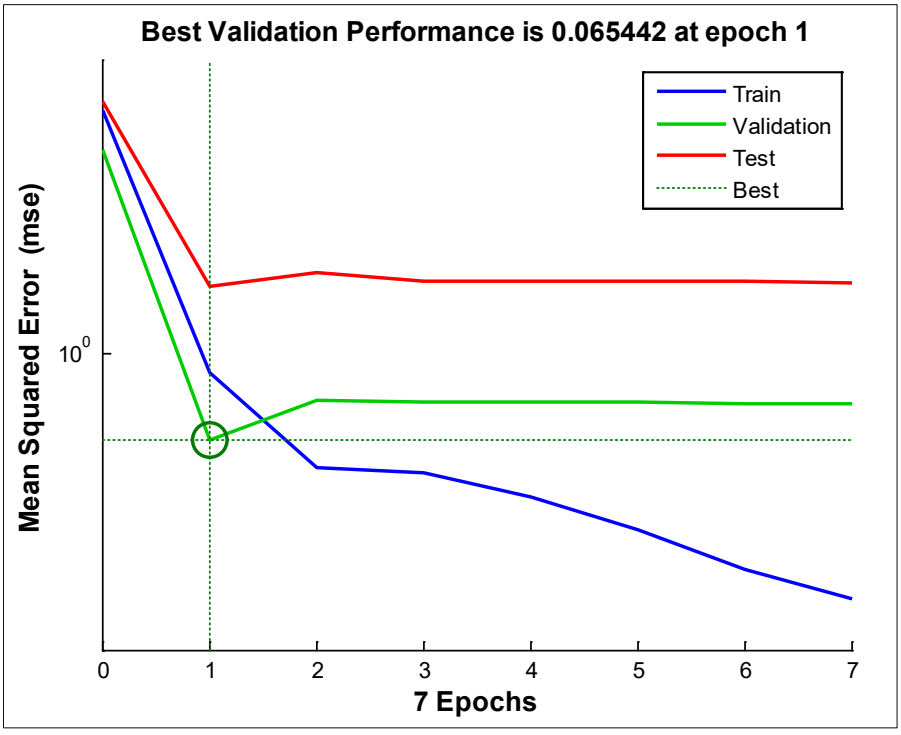

Figure 13: Neural network performance of the surrogate model for horizontal displacement when 30 GPa

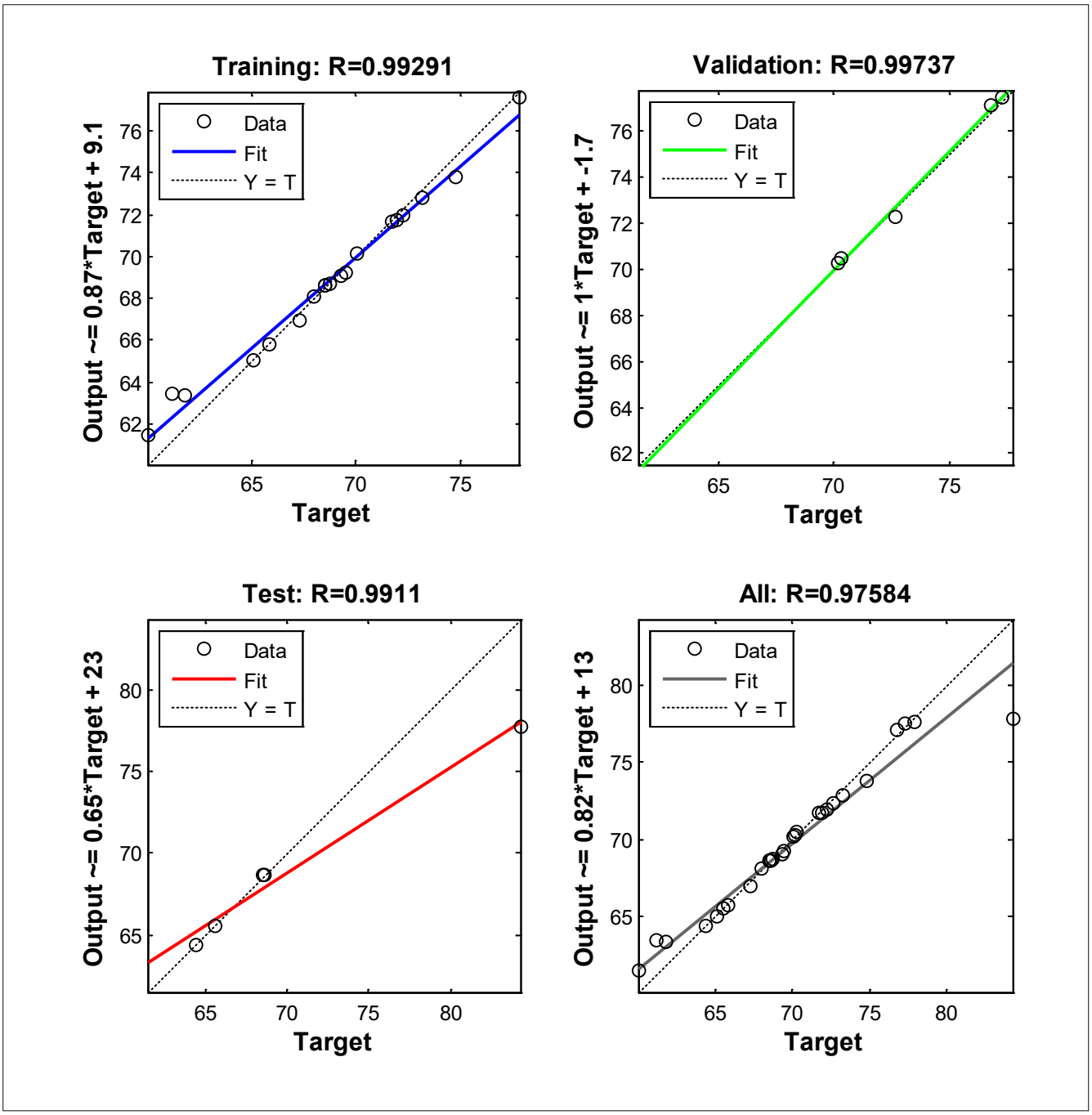

Figure 14: Regression values for the trained surrogate model

The corresponding regression analysis is presented in Figure 14, where a coefficient of determination of R = 0.97784 is obtained. This high value demonstrates a strong agreement between the predicted and target responses, confirming that the neural network has effectively captured the underlying functional relationship between input stiffness and structural response.

A second surrogate model is developed using the same input dataset (mean Young's Modulus of 30 GPa), with the output defined as the third-storey maximum vertical displacement. As shown in Figure 15, the model achieves an MSE value of 0.027855, which is lower than that of the horizontal displacement model, indicating improved predictive accuracy for this response component.

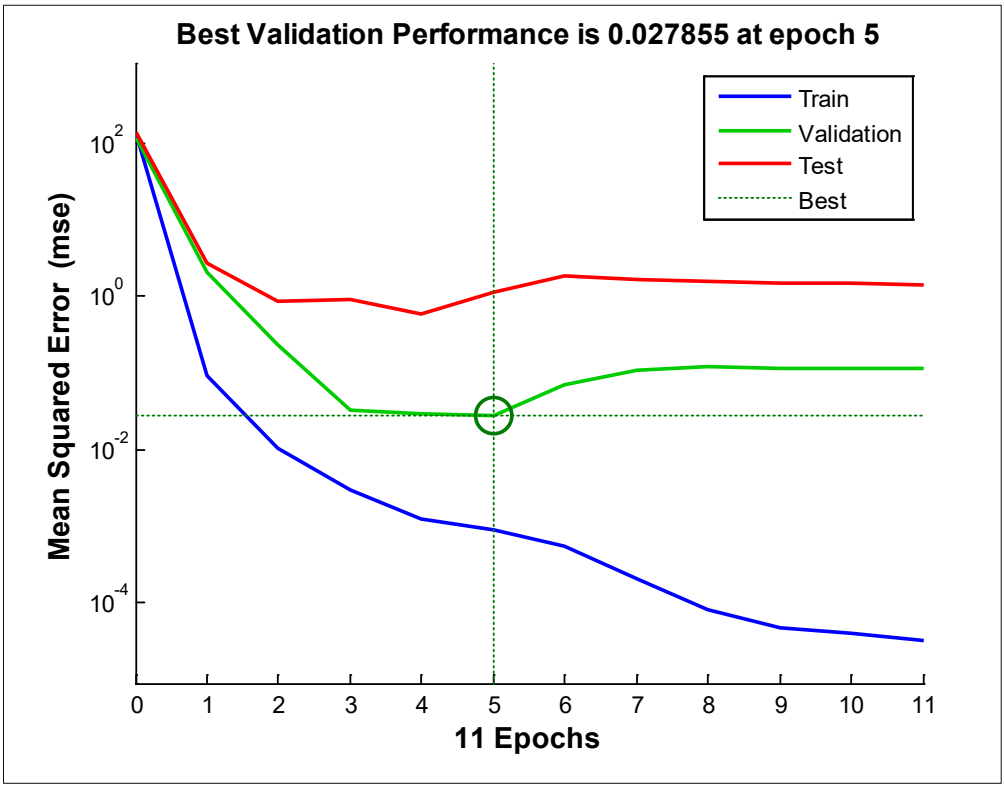

Figure 15: Neural network performance for vertical displacement in the 3rd storey when 30 GPa

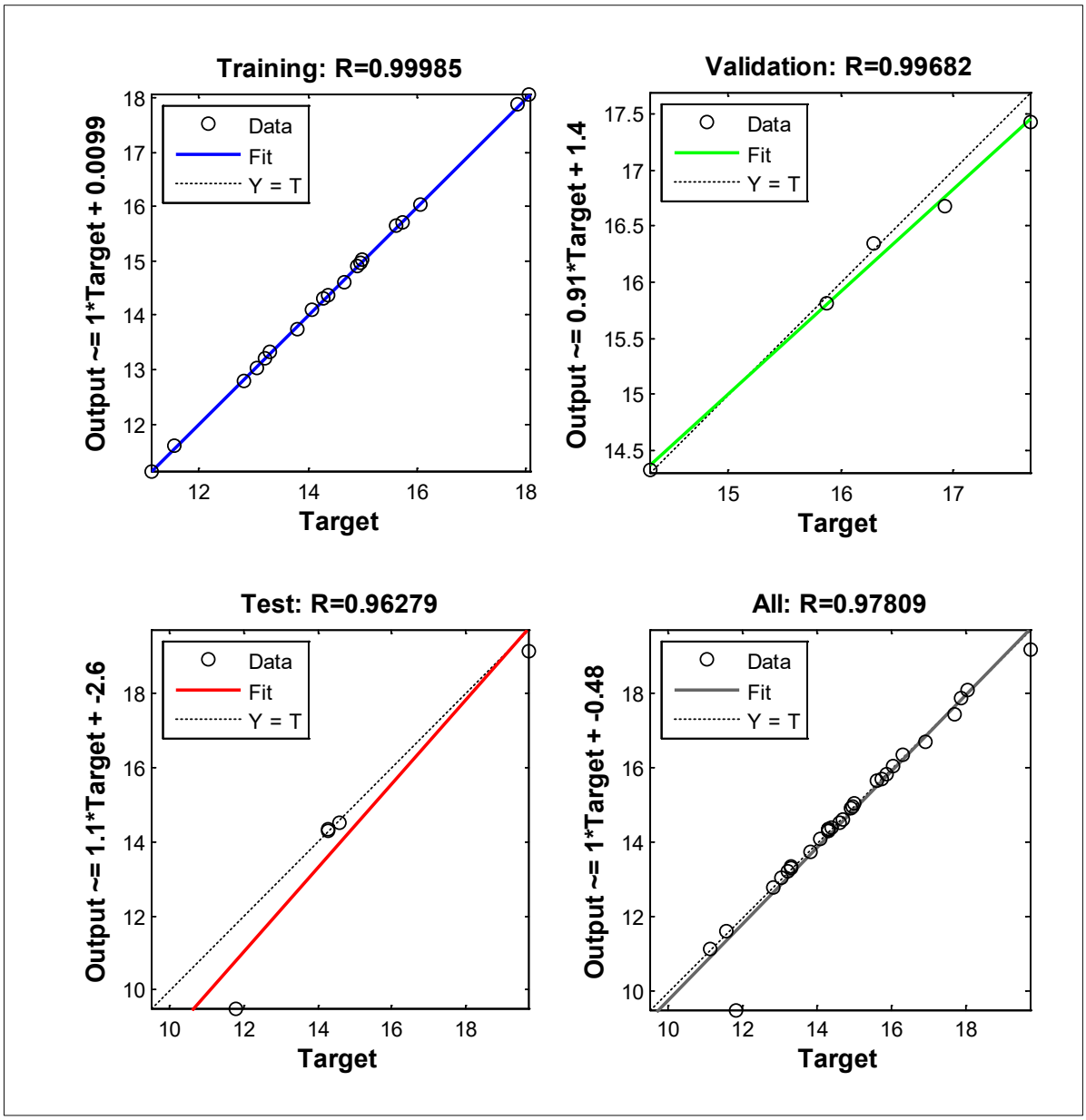

Figure 16: Regression values of the trained surrogate model

The corresponding regression performance, shown in Figure 16, yields an R value of 0.97809, further confirming a strong correlation between predicted and simulated responses and demonstrating the robustness of the trained network.

Subsequently, additional surrogate models are developed using datasets corresponding to a mean Young's Modulus of 40 GPa. For the model predicting third-storey maximum horizontal displacement, the training performance presented in Figure 17 indicates an MSE value of 0.012018, reflecting a high level of predictive accuracy and stable network convergence.

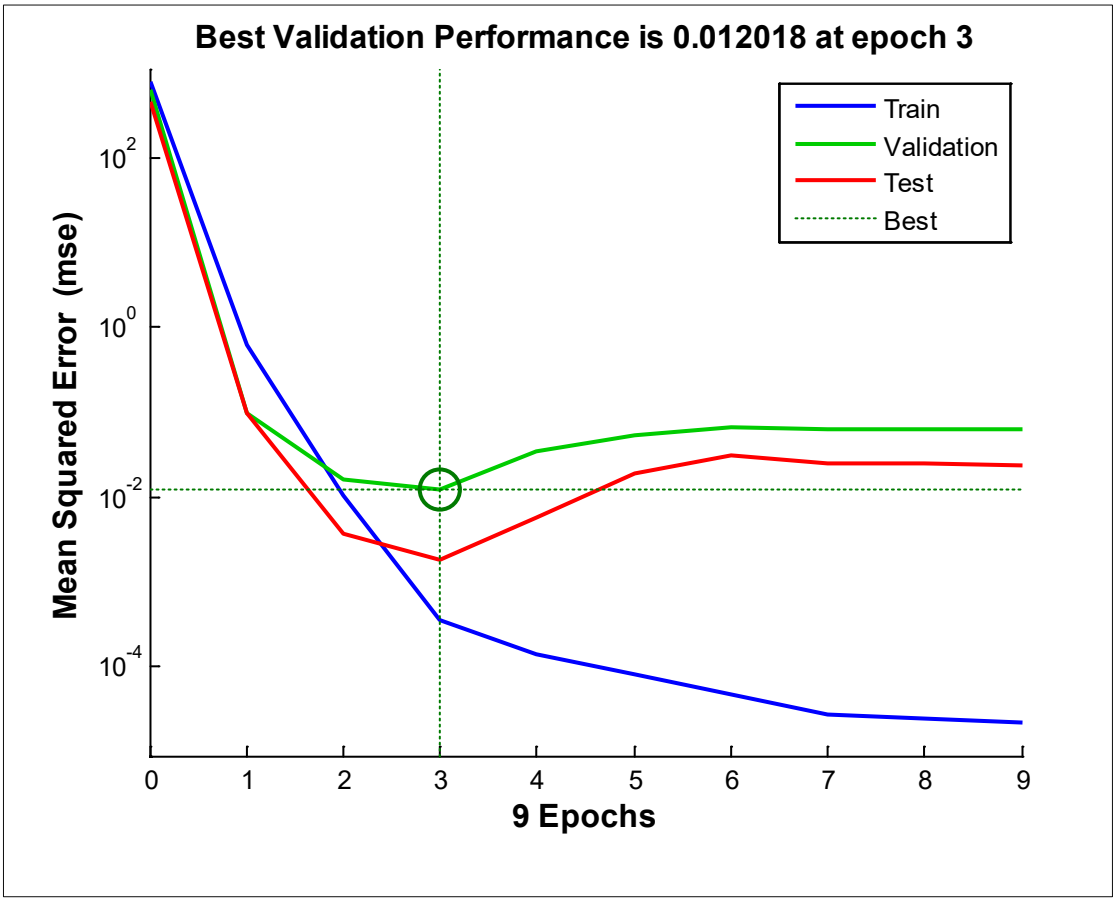

Figure 17: Neural network performance for horizontal displacement when 40 GPa

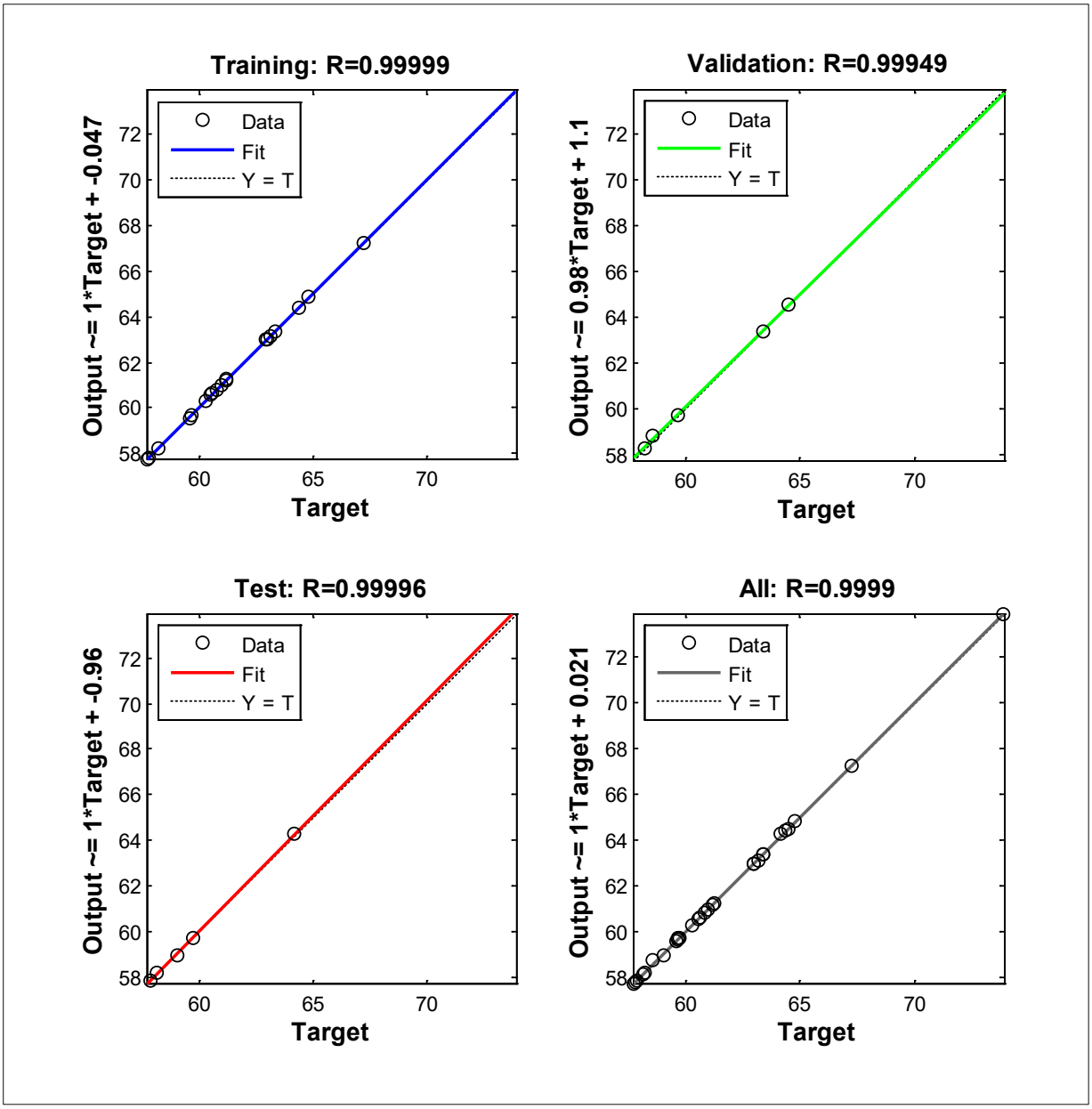

Figure 18: Regression values of the trained surrogate model

The regression results in Figure 18 show an R value of 0.9999, indicating an almost perfect linear relationship between predicted and target outputs and demonstrating excellent generalisation capability for this dataset.

For the corresponding vertical displacement model at 40 GPa, the training performance in Figure 19 yields an MSE value of 0.024209, confirming consistent predictive accuracy across response components.

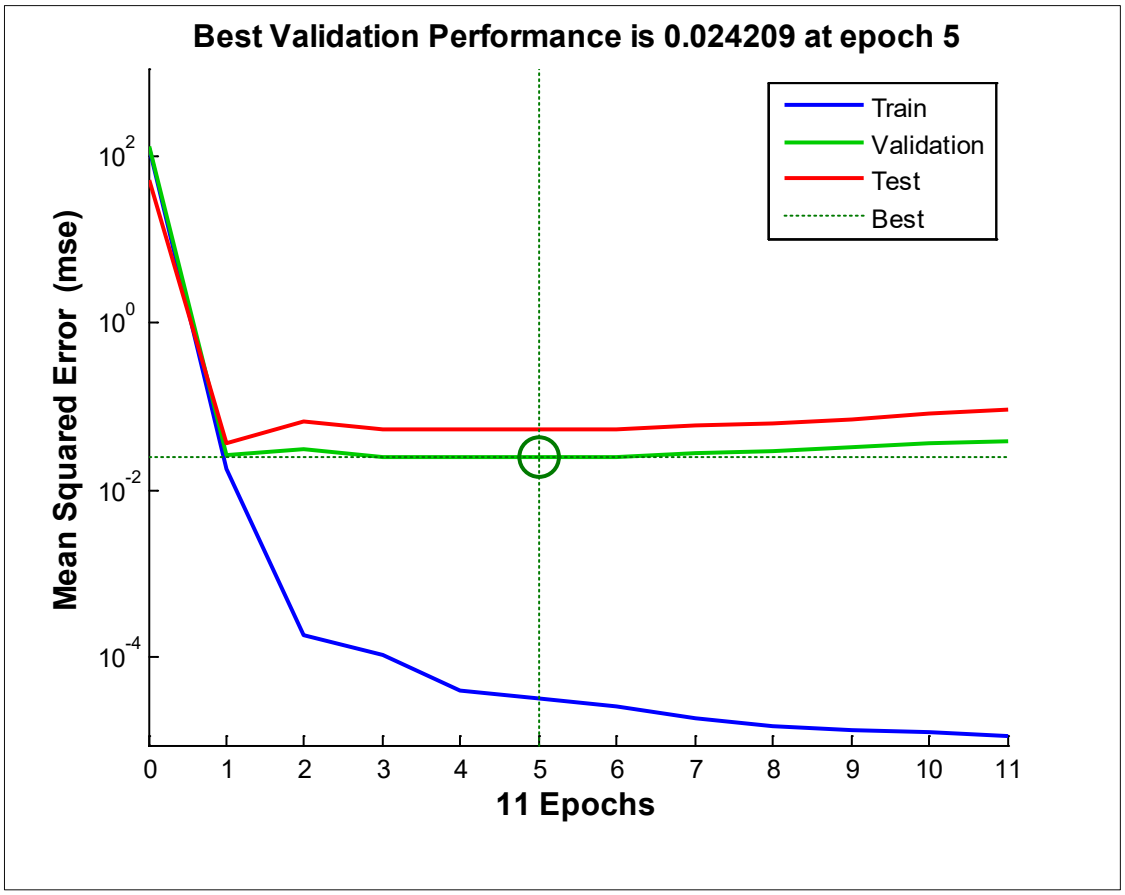

Figure 19: Neural network performance for vertical displacement when 40 GPa

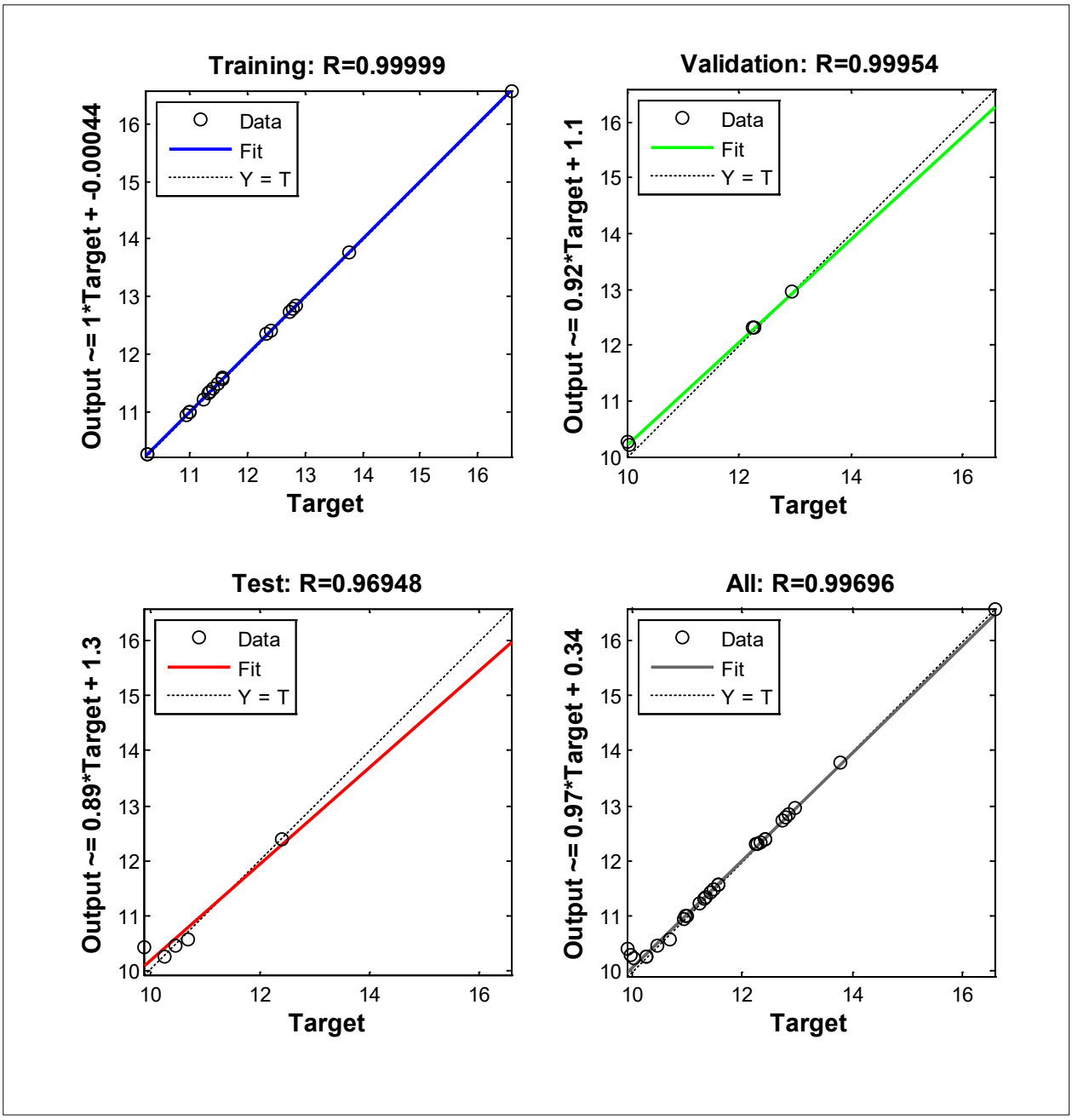

Figure 20: Regression values for the trained surrogate model

The regression analysis in Figure 20 produces an R value of 0.99696, which again suggests a very strong agreement between predicted and actual responses, further validating the reliability of the trained surrogate model.

Further surrogate models are developed for the 50 GPa datasets. For the horizontal displacement prediction model, Figure 21 reports an MSE value of 0.014288, indicating good predictive performance; however, the regression performance in Figure 22 yields an R value of 0.90904. This comparatively lower correlation suggests increased modelling difficulty in depicting the response behaviour at higher stiffness levels, potentially due to reduced variability or nonlinear sensitivity in the dataset.

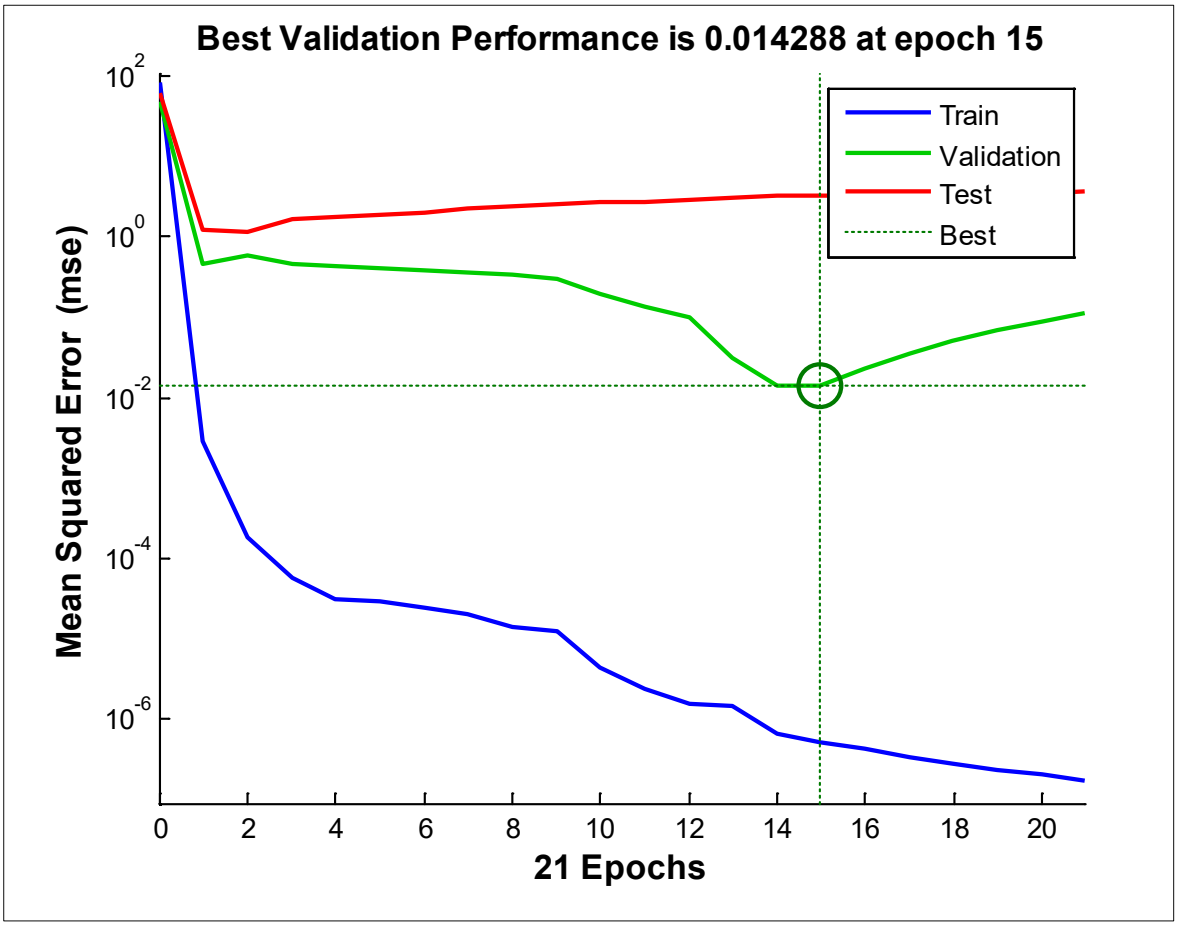

Figure 21: Neural network performance of the surrogate model for horizontal displacement for 50 GPa

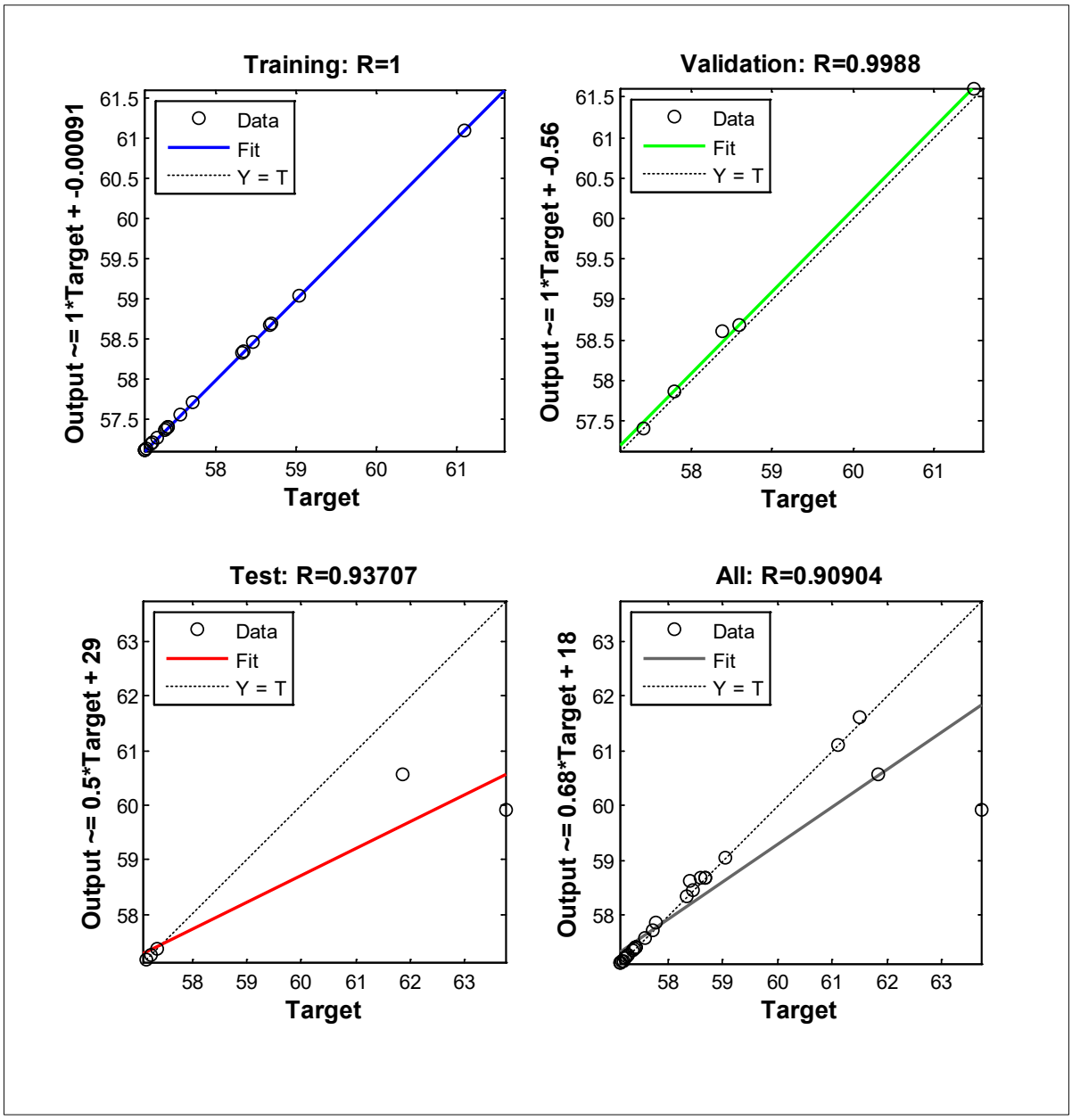

Figure 22: Regression values for the trained surrogate model

.

Finally, the surrogate model developed for the vertical displacement response at 50 GPa demonstrates superior performance. As shown in Figure 23, the model achieves an MSE value of 0.0013231, representing the lowest error among all developed models. The corresponding regression result in Figure 24 yields an R value of 0.9994, confirming an excellent agreement between predicted and target responses.

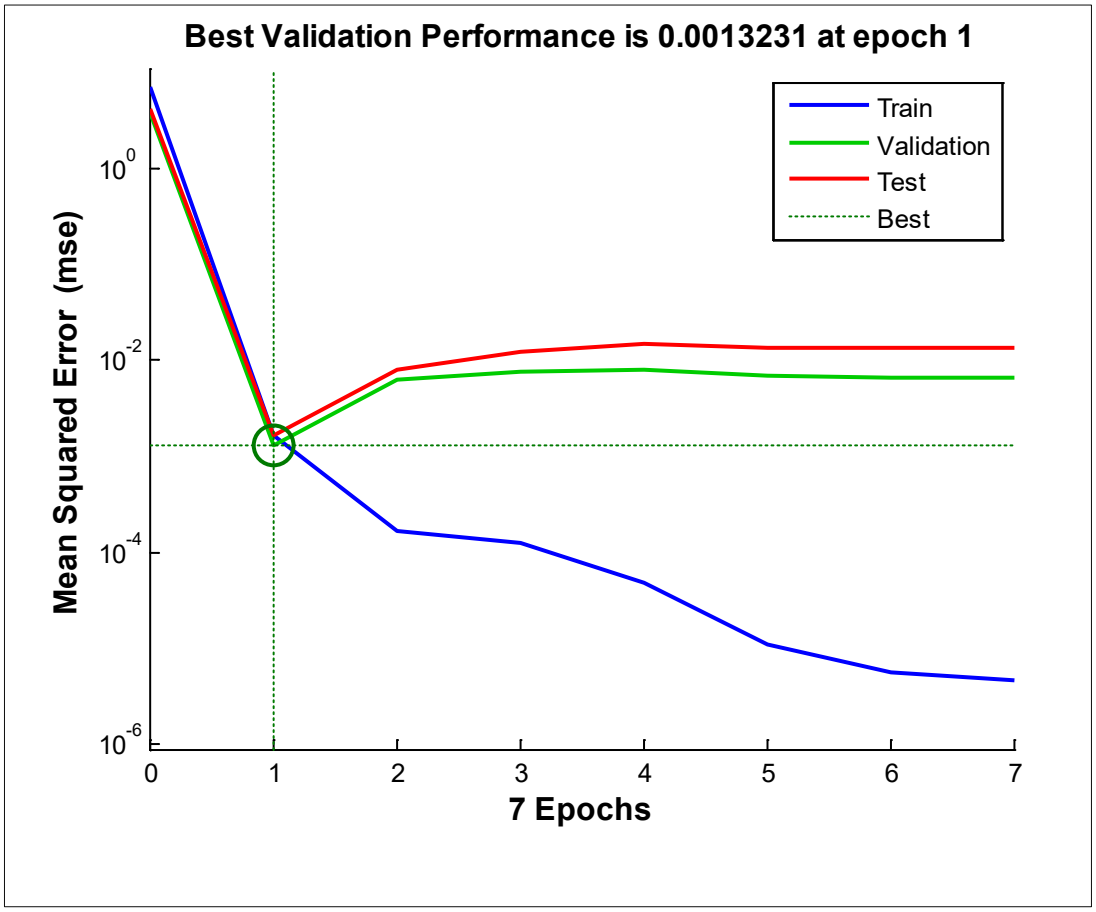

Figure 23: Neural network performance of the surrogate model for vertical displacement of 50 GPa

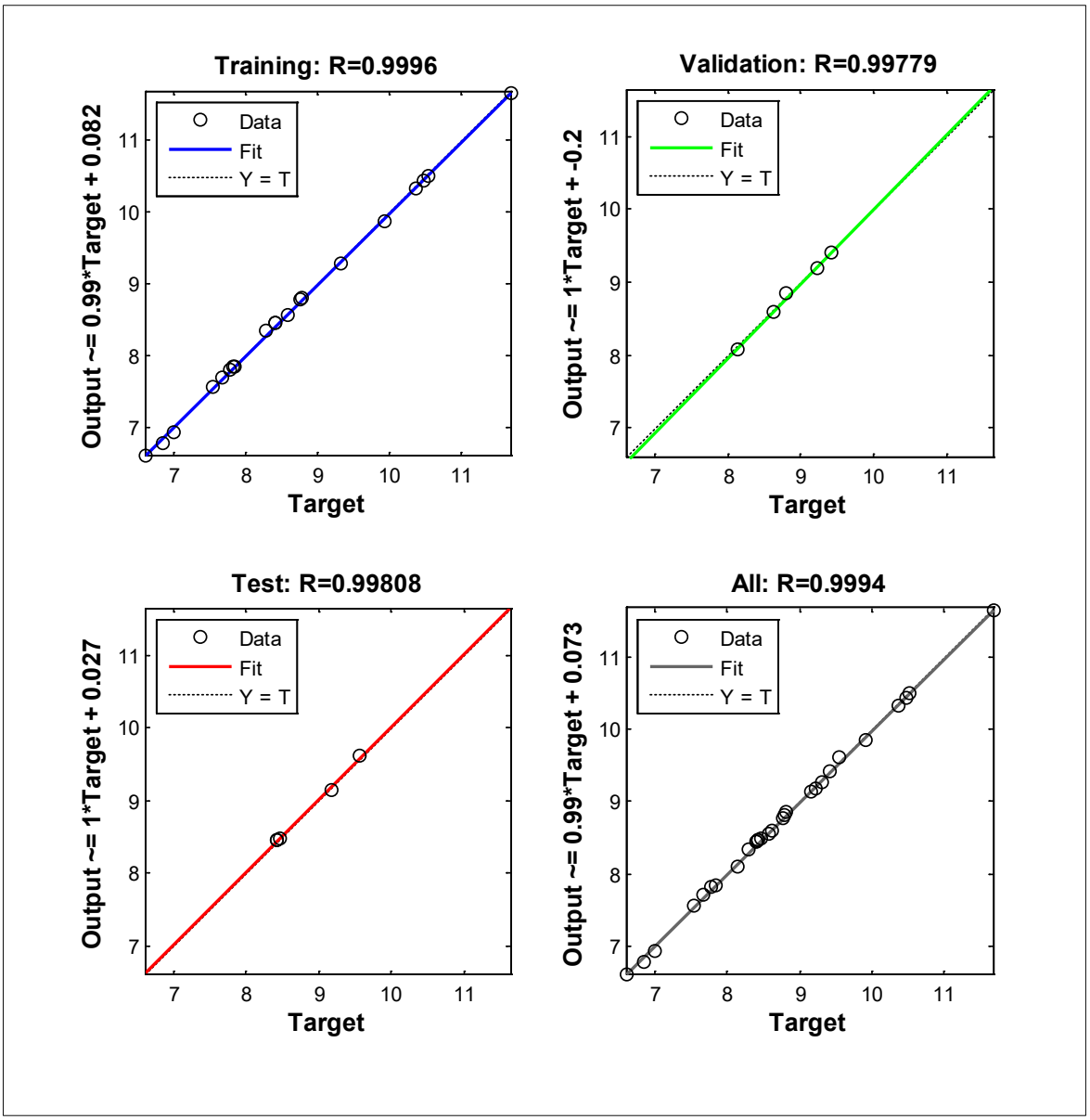

Figure 24: Regression values for the trained neural network

Overall, the results demonstrate that the proposed neural network–based surrogate modelling approach is capable of accurately approximating the seismic response of the nonlinear three-storey structure. Although minor variations in predictive accuracy are observed across different stiffness levels and response types, the models consistently demonstrate low error magnitudes and high regression values. This confirms the suitability of the proposed approach as an efficient alternative to computationally expensive nonlinear time-history analysis for seismic response prediction.

Chapter 4.4: Results and analysis

Following the development of the trained surrogate models, the effectiveness of each surrogate model was discussed in this sub-chapter. This sub-chapter provides insight into the further verification of the surrogate model.

Table 5: MSE values of each surrogate model

Strength of the concrete (GPa)	MSE values in horizontal displacement	MSE values in vertical displacement
30	0.0654	0.0279
40	0.0120	0.0242
50	0.0143	0.0013

Table 5 summarises the MSE values obtained for each surrogate model across horizontal and vertical displacement predictions. All models demonstrate low error magnitudes, with MSE values consistently below 0.1, indicating strong convergence and satisfactory predictive accuracy. The lowest error is observed for the 50 GPa vertical displacement model (0.0013), while the highest error corresponds to the 30 GPa horizontal displacement model (0.0654). Overall, the magnitude of these errors confirms that the neural network models have been effectively trained and can capture the nonlinear mapping between material stiffness and seismic response.

Table 6: Regression values of each surrogate model

Strength of the concrete (GPa)	Regression values in horizontal displacement	Regression values in vertical displacement
30	0.9758	0.9781
40	0.9999	0.9970
50	0.9090	0.9994

Similarly, Table 6 presents the corresponding regression coefficients for all surrogate models. Most R values exceed 0.97, demonstrating a strong correlation between predicted and target responses. The only comparatively lower value (R = 0.9090 for the 50 GPa horizontal displacement model) still indicates an acceptable level of

predictive agreement, although it suggests a reduction in model accuracy under higher stiffness conditions. Nevertheless, the overall regression performance confirms that the developed surrogate models exhibit effective predictive capability.

To further verify the developed surrogate models, the relationship between the target boundaries against the output from the surrogate model was demonstrated. It is assumed that the surrogate model is valid and acceptable if the output data falls between the limits of 110% and 90% of the target. Therefore, the first and second developed surrogate models were tested.

For this purpose, 6 random numbers around Young's Modulus 30 GPa using a standard deviation of 10 percent were generated on MATLAB. Horizontal and vertical displacements of the 3rd storey were generated manually again on ETABS according to the random numbers, respectively. This was the target data. A surrogate model was used to generate the horizontal and vertical displacements, respectively, on MATLAB. Data generated on MATLAB was output data.

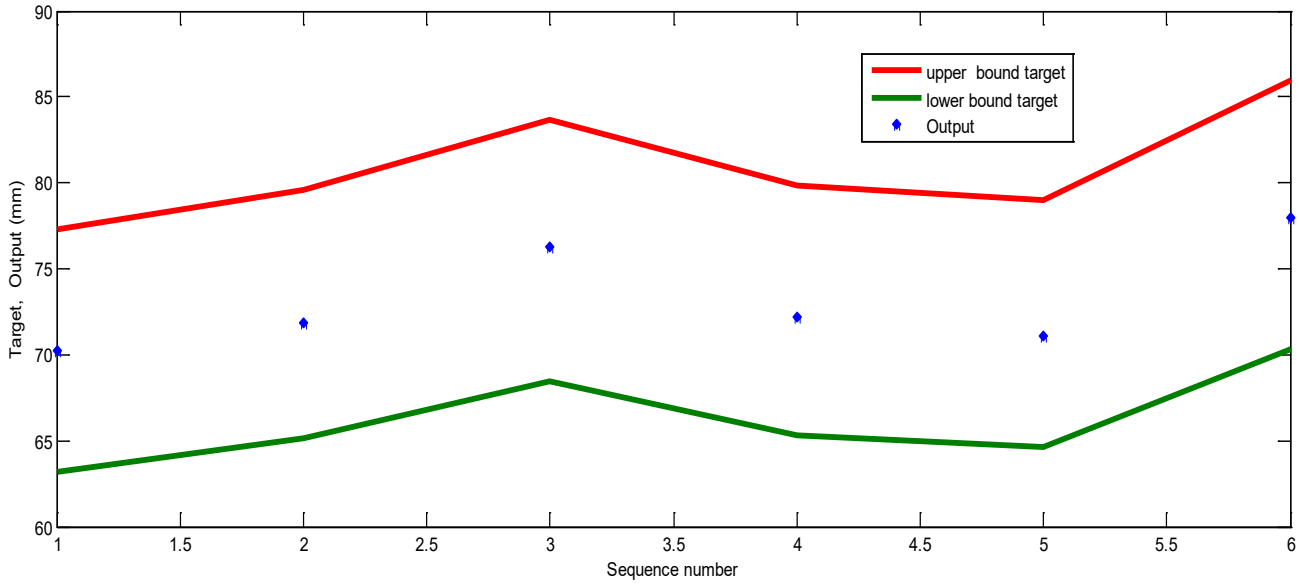

Figure 25: Comparing target and output for horizontal displacement

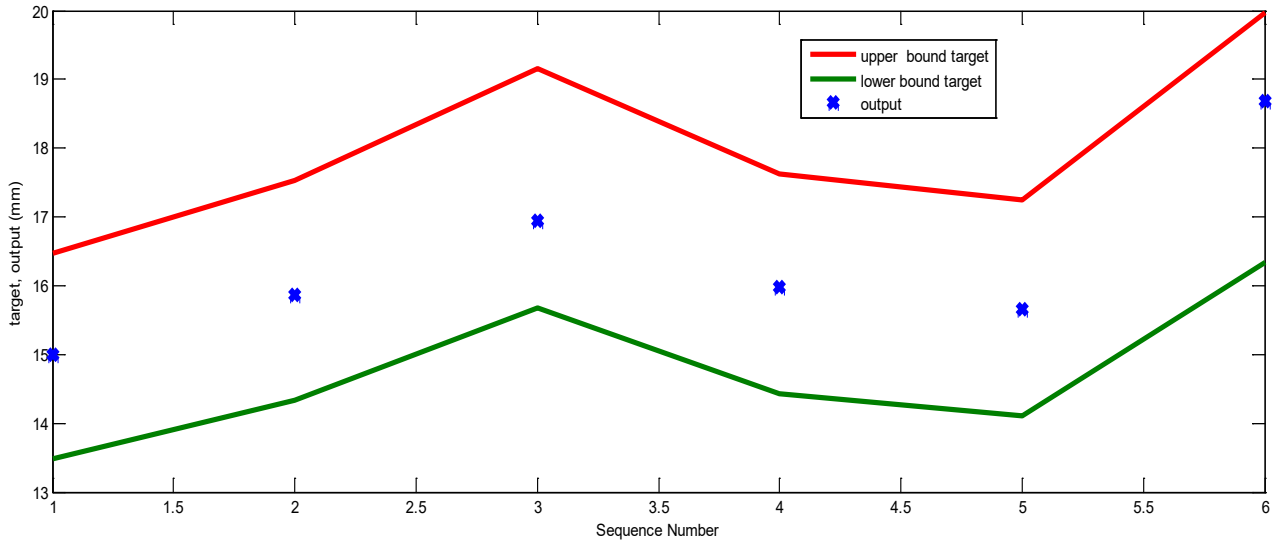

Figure 26: Comparing target and output for vertical displacement

Figures 25 and 26 present the comparison between target and predicted outputs for horizontal and vertical displacements, respectively. The results indicate that, in most cases, the surrogate model predictions lie within the predefined ±10% acceptance bounds, confirming satisfactory agreement with the ETABS-generated responses. This demonstrates that the proposed surrogate modelling approach is capable of reliably approximating nonlinear seismic responses within acceptable engineering tolerance limits.

In addition to the primary response variables considered in this study, it is noted that surrogate modelling can also be extended to other structural response parameters, such as inter-storey drift and acceleration. This would have made the results more applicable and suitable in terms of real-life situations. However, keeping in mind the objective of the research, which is to shorten the simulation process, the surrogate model can be effective, and it can help to shorten the analysis process by simulating the real-life behaviours as accurately as possible.

This subchapter has focused on the model surrogation based on the changing structural properties of the members of the structure. However, to make the model surrogation more effective, a parametric study can also be conducted. It includes changing the number of neurons during the training of the neural network in MATLAB simulation. This process is further described in the upcoming Chapter 5.

This chapter presents a neural network–based surrogate modelling approach for the fragility analysis of a nonlinear three-storey building under seismic actions. It begins by reviewing how structures respond to earthquake loading, highlighting previous research on seismic performance and structural retrofitting, and noting that conventional traditional analysis methods are often time-consuming.

A numerical model of a three-storey reinforced concrete building is created in ETABS and analysed using nonlinear time-history analysis with the El Centro earthquake (1940 Imperial Valley earthquake) record. To generate training data for the surrogate model, the Young's Modulus of concrete is varied (30, 40, and 50 GPa), and 30 random samples around each value are produced in MATLAB. The corresponding structural responses (third-storey horizontal and vertical displacements) are extracted.

These datasets are used to train multiple neural network surrogate models that map Young's Modulus to structural displacement responses. Model performance is evaluated using mean squared error (MSE) and regression (R) values, showing generally high accuracy and strong correlation between predicted and simulated results.

Finally, validation confirms that the surrogate models reliably approximate ETABS results within acceptable error bounds (90–110% of target values), demonstrating that neural networks can effectively reduce computational effort in seismic fragility analysis while maintaining accuracy.

Hence, developed trained surrogate models developed in Chapter 4 are effective and efficient. Model surrogation can be used in other areas of study, replicating the process carried out in Chapters 3 and 4. Applicability of the constructed surrogate model is further discussed in Chapter 7.1. The following Chapter 5 discusses about the research work based on the silo structures. Model surrogation is also applied for the analysis of the prototype replicating the true nature of the real-life silo structure in Chapter 5.

Chapter 5: Model surrogation for the safety assessment of silo structures.

In Australia, the design of reinforced concrete (RC) silos is governed by per AS 3774-1996 (Standards Australia 1996) which specifies design procedures and loading requirements for structures used to store bulk solids. Like international standards such as ACI 313-16 (American Concrete Institute 2016), the Australian standard adopts conservative design assumptions to ensure adequate structural safety under a wide range of loading conditions. Although such traditionalism provides a desirable level of safety, it may also result in overdesign, leading to unnecessary construction costs and inefficient use of materials. Improving the accuracy of structural safety assessment therefore has the potential to optimise silo design while maintaining the required reliability.

One of the main challenges in reliability-based design is the substantial computational effort required to perform repeated structural analysis, particularly in probabilistic methods such as Monte Carlo Simulation (MCS). Each simulation typically requires repeated evaluation of structural responses under varying input parameters, making conventional numerical approaches computationally expensive. To address this limitation, this research proposes the development of surrogate models capable of accurately approximating the structural response while significantly reducing computational cost.

To achieve this, it is proposed in this research to construct suitable surrogate models based on a limited amount of experimental and numerical simulation, replacing the otherwise indispensable, much larger amount of data. Specifically, the experimental simulation was developed from the prototype illustrated in Figure 27.

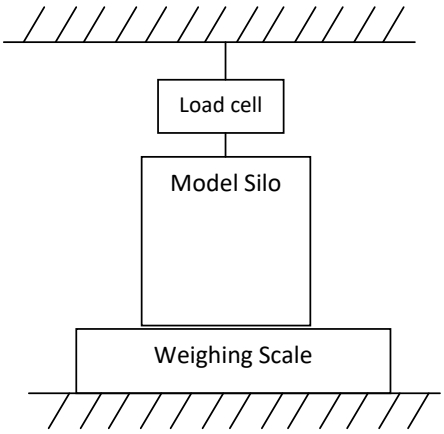

Figure 27: A prototype for the laboratory testing of the silo (Widisinghe et. al, 2014)

Figure 27 illustrates the prototype of the laboratory apparatus developed to simulate the behaviour of a silo during the filling process. The prototype consists of the following components: the load cell, the model silo, and the weighing scale. The load cell is basically the equipment to measure the load distributed along the wall of the model silo, and the weighing scale measures the load acting at the silo base. The model silo is made up of the transparent cylindrical tube with the sandpaper attached to its wall for providing the friction on the surface of the tube.

During the testing, the suspended model silo shown in the figure was filled with material particles while the weighing scale and the load cell registering the loads acting at the silo base and wall, respectively. The proposed testing parameters include moisture content, surface properties of the silo, type of filling materials, etc. During the testing, different sets of data were acquired according to changes in parameters. For example, the study conducted how the prototype of silo behaves if the type of filling materials is changed. Some experiments were conducted on food grains of various sizes, whereas other experiments were conducted on sand particles. Similarly, other parameters were changed accordingly to derive more versatile and sufficiently large datasets required for the analysis purpose.

Following collection of data from laboratory experiments, the experimental datasets were imported into the MATLAB software, where neural networks were trained to establish the nonlinear relationships between the governing input parameters and the

resulting structural responses. The trained surrogate models developed in this chapter provide a computationally efficient substitute to repeated experimental testing or numerical simulations and form the basis for the reliability analysis presented in the subsequent chapters.

Chapter 5.1: Performance of silo structures

The structural performance of silos has been the subject of extensive research due to their widespread application in agricultural, industrial, mining, and bulk material handling industries. The safe design of silo structures depends largely on accurately predicting the complex interaction between stored granular materials and the surrounding structural components. Unlike conventional liquid storage structures, silos are subjected to highly nonlinear loading conditions arising from particle interaction, wall friction, arching, segregation, flow patterns, and material properties. Accordingly, numerous analytical, experimental, and numerical studies have been undertaken to better understand these mechanisms.

Early investigations primarily focused on determining the engineering properties of stored materials required for structural design. For example, Kibar et al. (2014) studied selected engineering properties (physical and mechanical) of dry bean under non-irrigation and drip-irrigation conditions necessary in the design of handling equipment and storage facilities for dry bean. Their study examined parameters including average length, width, thickness, the geometric mean diameter, sphericity, surface area, volume, thousand grain mass (M1000), bulk and true densities, porosity, angle of internal friction, static coefficient of friction, Poisson ratio, and pressure ratio. These properties provide essential input parameters for predicting the behaviour of bulk materials during storage and discharge.

With improvements in computational methods, finite element modelling has become an important tool for analysing silo behaviour. Yu et al. (2017) developed and validated a complex finite element model to understand the structural behaviour of silos when filled with bulk corn by calculating the stresses and displacements occurred. Their work demonstrated the capability of numerical methods to capture complex structural

responses while highlighting the computational demands associated with detailed finite element analyses.

Similarly, Fang et al. (2022) combined laboratory experiments with Discrete Element Method (DEM) simulations to investigate the distribution of static stresses within granular silos. Their study examined the influence of construction history, internal friction angle, and wall-particle friction coefficient on stress distribution, with particular attention given to the stress dip phenomenon and the load-bearing characteristics of silo walls. The results confirmed that loading history and particle interaction significantly influence stress development within bulk storage systems.

Several researchers have investigated the influence of structural characteristics on silo performance. Pantaleev et al. (2018) examined the effect of wall flexibility on bulk stress distribution and wall pressures using finite element analysis, while Makhinko (2018) analysed the structural response of steel grain silos with varying shell thicknesses and stiffener arrangements subjected to asymmetric wind loading. Likewise, Gökalp (2010) used finite element analysis to investigate displacement and bending stresses in folded steel plate silos storing shelled corn.

Other studies have focused on improving analytical approaches for silo design. Kumar et al. (2023) designed reinforced concrete silos for cement clinker storage using Janssen's theory, considering pressures generated during both filling and discharge operations together with hoop stresses, temperature effects, and hoop tension. In addition, Fank et al. (2018) experimentally investigated the variation of vertical pressures at the silo base during loading, storage and unloading phases, providing valuable insights into the evolution of stress distributions throughout the storage cycle.

Dynamic loading has also attracted considerable research interest. Butenweg et al. (2017) compared two analytical approaches for evaluating silo behaviour under seismic excitation. Their study assessed both equivalent static loading procedures and nonlinear time-history analyses, demonstrating that dynamic effects may significantly influence shell buckling and overall structural stability.

The existing literature clearly demonstrates that the behaviour of silo structures is governed by a complex interaction between material properties, wall friction, structural geometry and loading history. Experimental investigations, analytical formulations, and advanced numerical methods have substantially improved the understanding of these mechanisms. Nevertheless, many of these approaches remain computationally demanding, particularly when repeated analyses are required for probabilistic structural reliability assessments such as Monte Carlo Simulation.

Furthermore, although sophisticated numerical methods such as finite element analysis and the discrete element method provide detailed predictions of stress distributions, their computational expense limits their practical application in large-scale reliability analyses involving thousands of simulations. This limitation provides a strong motivation for the development of surrogate modelling techniques capable of reproducing the behaviour of high-fidelity models while significantly reducing computational effort.

Accordingly, the methodology presented in this chapter investigates the development of artificial neural network-based surrogate models for predicting the stress behaviour of silo structures. The proposed approach utilises experimentally generated datasets to train computationally efficient models that can subsequently be integrated into Monte Carlo Simulation frameworks for rapid safety and reliability assessment. The following sections describe the experimental procedures, data acquisition procedures, surrogate model development, validation, and application to structural reliability analysis.

Chapter 5.2: Pilot study based on data in relevant literature review

This subchapter presents a pilot study developed using data reported in the literature, with reference to experimental investigations on silo and vertical containment systems. The study by Widisinghe (2014) is used as the primary basis for this preliminary analysis. In that work, a laboratory-scale experimental setup was employed to investigate the development of arching effects in vertically confined granular systems during progressive backfilling. The study provided measurements of both vertical and

shear stress evolution along the container walls and base, which are particularly relevant for the development of surrogate modelling frameworks.

The dataset extracted from Widisinghe (2014) is summarised in Table 7. It includes measurements obtained at successive filling steps, such as load cell readings, total system mass, and derived quantities including mass redistribution on the walls and base of the container. From these measurements, the corresponding vertical stress (σ) and shear stress (τ) were calculated.

Table 7: Experimental data adapted from Widisinghe (2014)

filling step i	load cell reading	mass on load cell (kg)	initial mass of setup (kg)	mass on walls mi (kg)	mass on base ni (kg)	σ (kPa)	τ (kPa)
0	-20.08	9.77	9.77	0	0	0.00	0.00
1	-19.26	10.33	9.77	0.56	2.11	0.92	0.12
2	-17.27	11.67	9.77	1.91	3.4	1.48	0.29
3	-14.65	13.45	9.77	3.68	4.26	1.86	0.39
4	-11.62	15.5	9.77	5.74	4.83	2.11	0.45
5	-8.37	17.71	9.77	7.94	5.23	2.28	0.48
6	-4.95	20.03	9.77	10.26	5.54	2.42	0.51
7	-1.4	22.43	9.77	12.66	5.825	2.54	0.52
8	2.15	24.84	9.77	15.07	6.075	2.65	0.53
9	5.59	27.17	9.77	17.4	6.31	2.75	0.51
10	9.28	29.67	9.77	19.9	6.475	2.82	0.55
11	12.56	31.9	9.77	22.13	6.775	2.95	0.49
12	16.13	34.32	9.77	24.55	6.94	3.03	0.53

Given that the main objective of this research is the development of surrogate models for stress prediction, the dataset was subsequently reduced to focus only on the most influential variables. In particular, the analysis identifies that the mass redistributed to the walls and the mass transferred to the base are the influential variables governing shear and vertical stress development, respectively. Other intermediate variables,

although useful for experimental interpretation, were not directly required for surrogate model construction.

This sub-chapter discusses the construction of a surrogate model to predict vertical stresses and shear stresses on the vertical containment caused by backfilling. A rectangular cross-sectional vertical container was selected as a specific civil structure for the purposes of the pilot study. The study comprises a simulation model and a developed surrogate model that mimics the true simulation model behaviour as closely as possible. The input variables are the load cell reading, the mass on the load cell (kg), the initial mass of the setup (kg), the mass on the walls mi (kg), and the mass on the base ni (kg). The output variables were calculated experimentally. The output variables are the vertical stress σ (kPa) and the shear stress τ (kPa).

Now, a surrogate model is developed to replicate the behaviour of experimental studies as closely as possible. It was noticed during the experimental studies that the mass on the walls and the mass on the base are the only changing variables in the process. Therefore, the surrogate model needs to understand the behaviour pattern of the output based on these two changing variables. Two separate surrogate models were made for two different outputs. The vertical stress is based on the mass on the base, whereas the shear stress is based on the mass on the walls. For each surrogate model, the sample data will be fetched and imported into MATLAB functions to train a neural network to understand the behaviour of the input-output pattern. It will develop into what is called a trained neural network surrogate model.

The performance of the surrogate model developed for vertical stress prediction is illustrated in Figure 28. The trained network achieved a mean squared error (MSE) of 0.0027192, indicating a low average deviation between predicted and observed values. The consistency between training, validation, and test datasets further indicates that the model displays stable generalisation performance across unseen data.

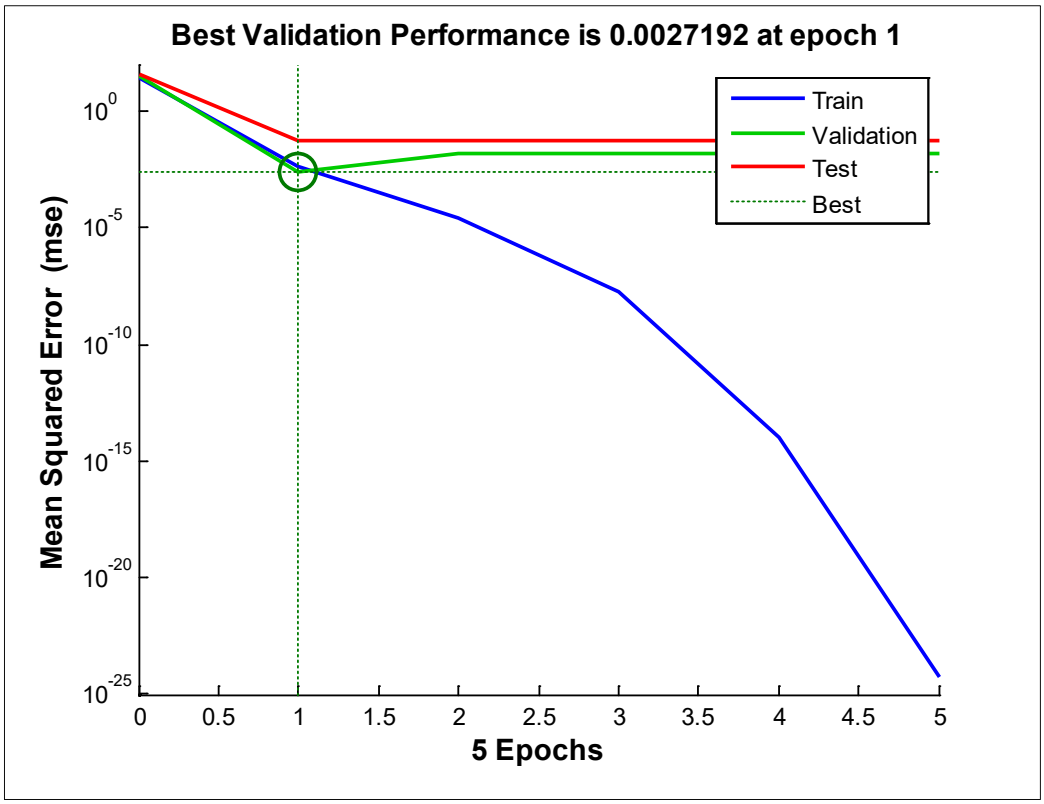

Figure 28: Performance of the trained surrogate model for vertical stress prediction

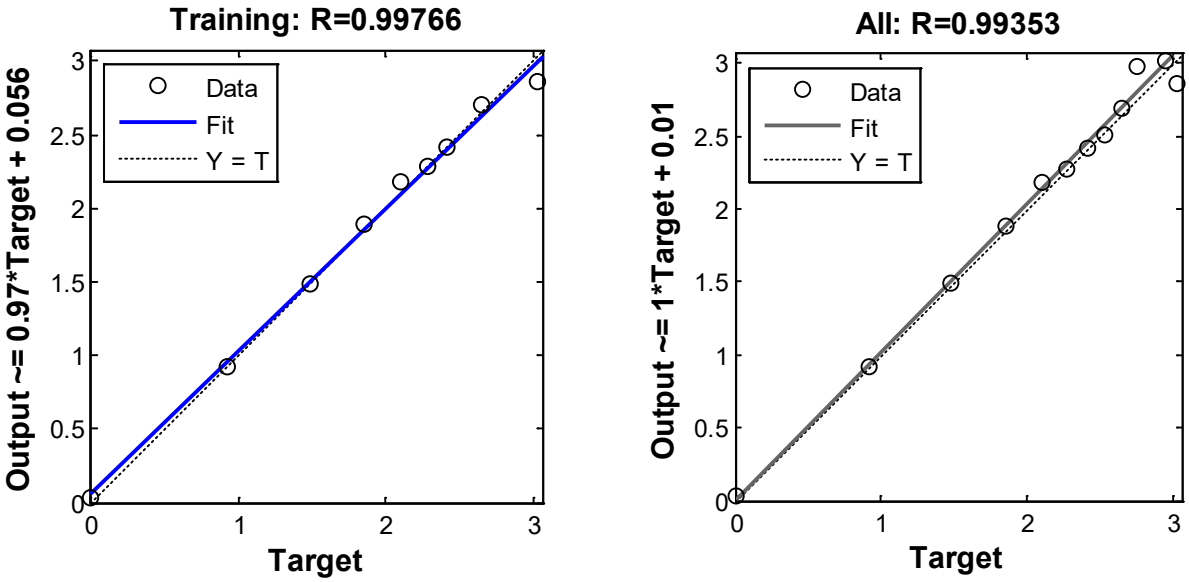

Figure 29: Regression analysis for vertical stress surrogate model

Due to availability of the limited size of the dataset, model evaluation was primarily based on regression analysis of training and overall fitted neural network. Figure 29

presents the regression relationship between predicted and target outputs, yielding a coefficient of determination (R) of 0.99766. This high correlation indicates strong agreement between the surrogate model predictions and experimental observations, suggesting that the model is capable of accurately capturing the underlying functional relationship. In chapter 5.2 and chapter 5.3, only regression analyses for training and overall fitted neural network are provided due to the availability of limited size of the dataset.

Further validation was conducted by comparing predicted outputs with experimentally derived target boundaries. Figure 30 shows the relationship between the target boundaries against the output from the surrogate model. It is assumed that the surrogate model is valid and acceptable if the output data falls between the limits. Figure 30 indicates that the developed surrogate model is valid and acceptable since, in most cases, the data falls between the limitations.

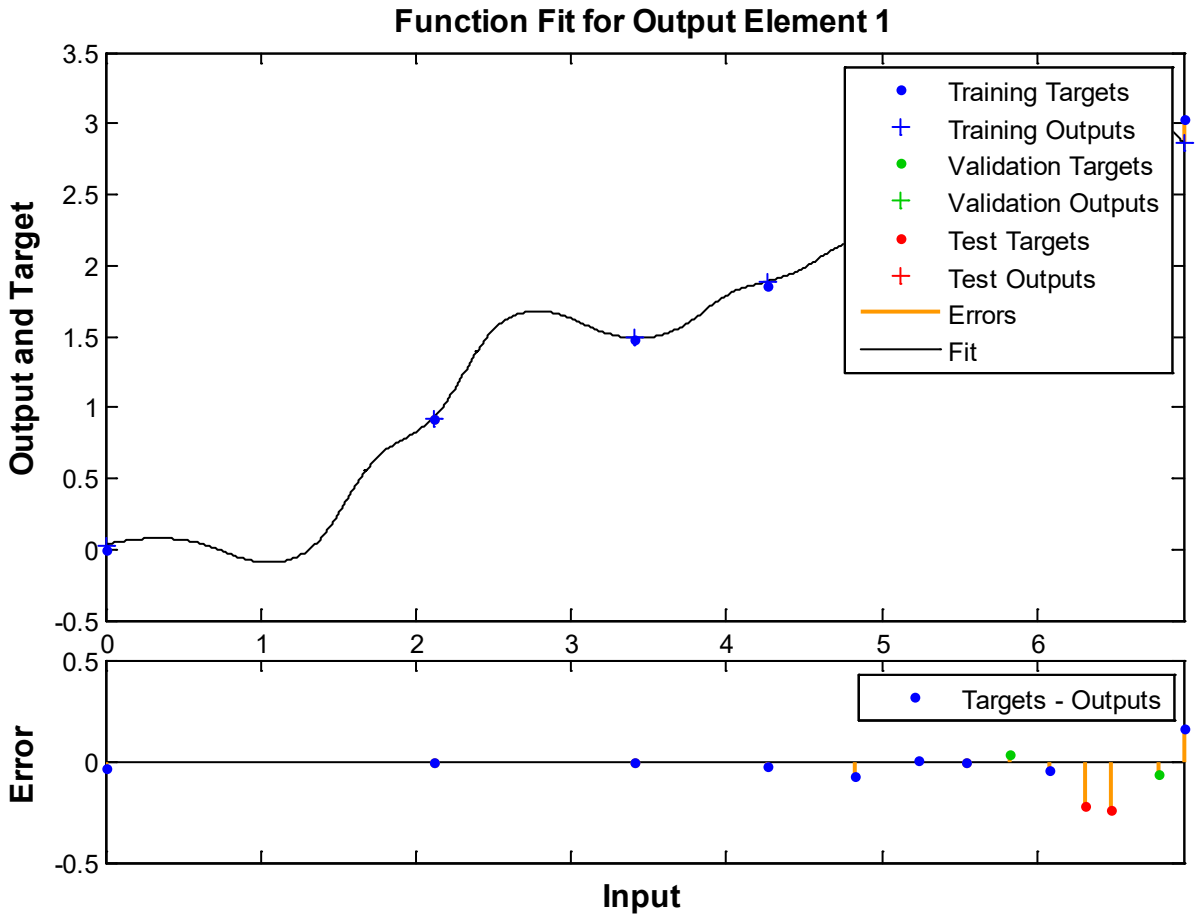

Figure 30: Comparison of target boundaries and surrogate model outputs (vertical stress)

A similar modelling procedure was applied to shear stress prediction. The corresponding neural network based surrogate model exhibited strong convergence behaviour during training, as illustrated in Figure 31. Figure 31 shows the neural network performance of the trained surrogate model. The test data and the validation data seem to be coherent with each other to show the acceptable validation performance.

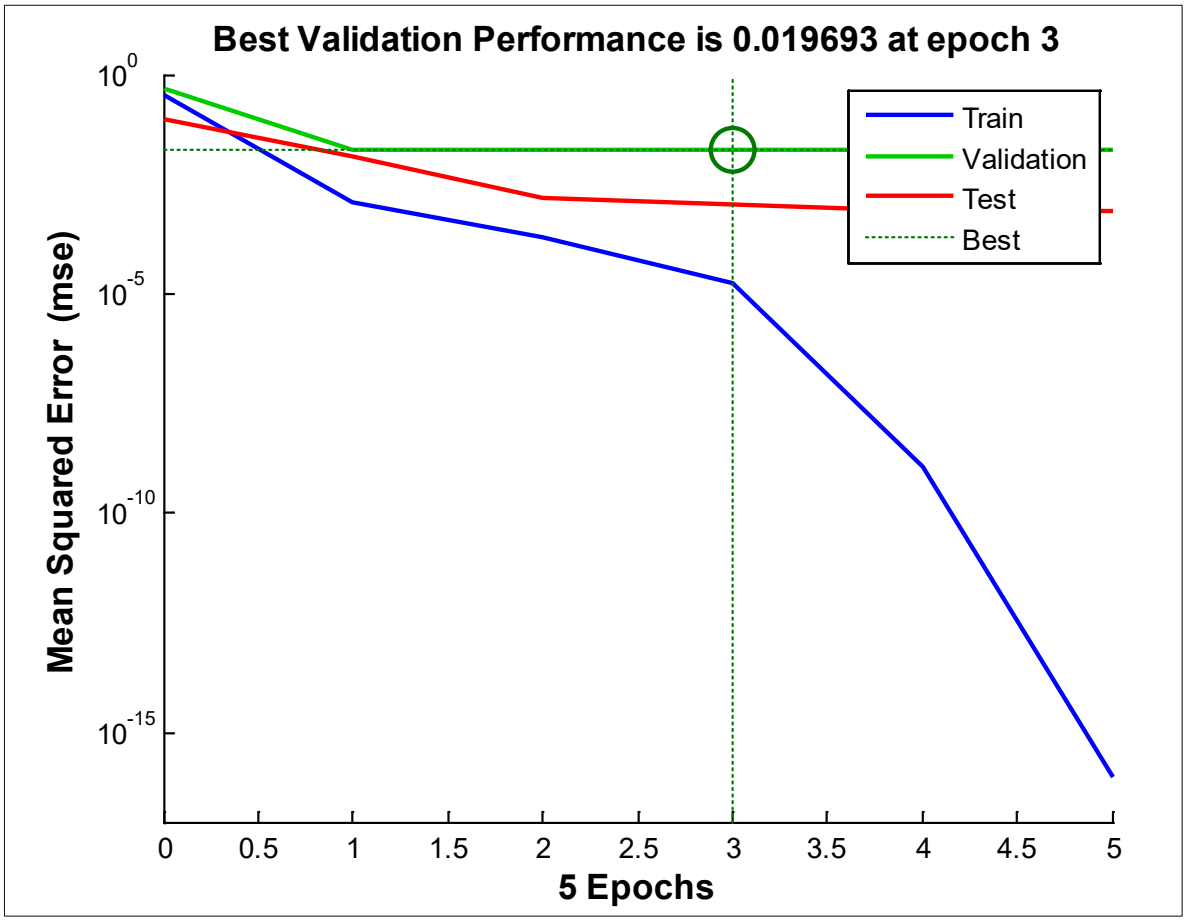

Figure 31: Performance of the trained surrogate model for shear stress prediction

The regression analysis for the shear stress model (Figure 32) indicates a very high level of agreement between predicted and target values, with an R-value approaching unity. This suggests that the surrogate model effectively captures the nonlinear relationship between wall-associated mass transfer and shear stress development.

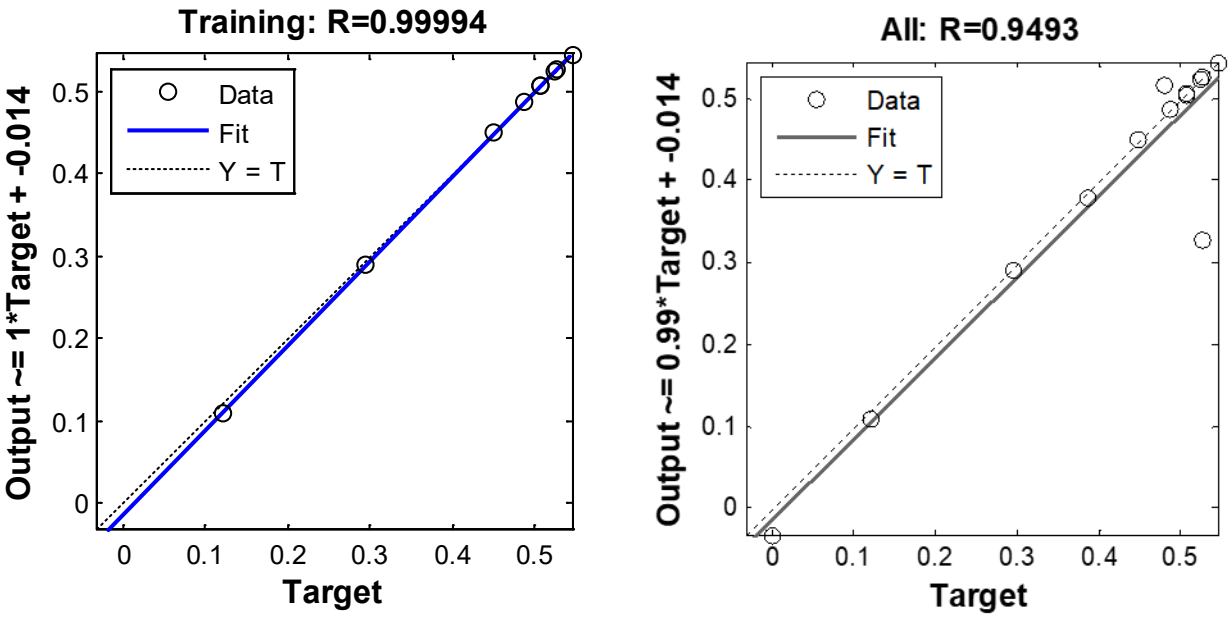

Figure 32: Regression analysis for shear stress surrogate model

Finally, figure 33 presents the relationship between the target boundaries against the output from the surrogate model. Since the output data falls between the limitations, the surrogate model is valid and acceptable.

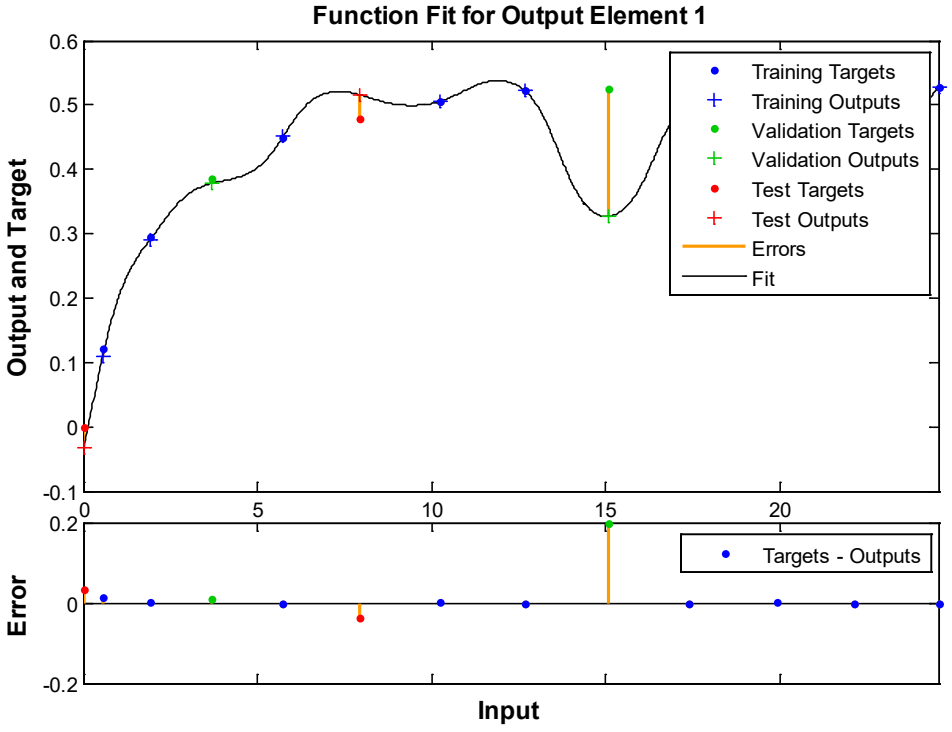

Figure 33: Comparison of target boundaries and surrogate model outputs (shear stress)

The results of this pilot study demonstrate that neural network-based surrogate models can effectively replicate experimentally derived stress responses in vertically confined granular systems. Despite the relatively small dataset, the models achieved high regression accuracy and acceptable prediction consistency within defined tolerance limits.

This pilot study therefore provides a foundational validation of the proposed surrogate modelling framework and establishes its suitability for extension to more complex geometries and experimental configurations, including the circular-base containment system considered in subsequent sections.

Chapter 5.3: Parametric study

The pilot study presented in Chapter 5.2 established the feasibility of developing neural network-based surrogate models for predicting vertical and shear stresses in silo structures. Building on this foundation, the present chapter conducts a parametric investigation to evaluate the sensitivity of surrogate model performance to variations in key neural network architecture parameters.

The neural network consists of an input layer, a hidden layer, and an output layer. The effectiveness of the trained neural network depends on these layers. These layers are interconnected by neurons. Therefore, a change in the number of neurons can effectively change the performance of the neural network-based surrogate model. Parameters, including the number of hidden layers and the number of neurons applied during the training phase of the surrogate model, can alter the performance of the neural network.

In this study, Feed-Forward Networks (FNN) is selected as the neural network structure for creating surrogate models with 1 hidden layer is selected for constructing neural network. Input and output variables were predetermined in each chapter. Same neural network structure has been used for all parts of the thesis that have adopted neural network algorithms.

Some of the scenarios that can be created by altering these parameters are:

1) The number of hidden layers can be changed
2) The number of neurons can be changed while keeping the same number of hidden layers
3) Equal or uneven distribution of neurons among the hidden layers

This chapter focuses on the second scenario. The performance of the trained surrogate model will be evaluated by changing the number of neurons. During the pilot study in chapter 5.2, the number of neurons applied during the training of the neural network is 10. The number of neurons will be changed to 5, 15, 20, and 25 to examine the effect of this parameter.

The performance of the neural network will be evaluated using the mean squared error (MSE) value and regression R value. The Mean Squared Error (MSE) is the average squared difference between the predicted outputs and target values. A lower MSE value implies better predictive accuracy, with a value of zero corresponding to a perfect prediction with no error. The regression coefficient R measures the strength of the linear correlation between the predicted outputs and target values. An R value of 1 means a strong linear relationship, while R value of 0 means a random relationship. These values will be tabulated to analyse the performance of the trained surrogate model.

Given that two surrogate models were previously developed—one for vertical stress and one for shear stress—the parametric analysis is conducted separately for each output variable to ensure consistent and comparable evaluation.

Vertical Stress Surrogate Model

Neural network with 5 neurons

The surrogate models based on the vertical stress were evaluated first, and secondly, the surrogate models based on the shear stress were evaluated. When the hidden layer consists of 5 neurons, the model exhibits strong predictive performance, with a very low MSE of 0.00015321. The corresponding regression analysis (Figure 35)

yields an R-value of 0.99996, indicating near-perfect correlation between predicted and target values. The output–target comparison (Figure 36) further confirms that predicted values lie within the defined acceptance limits, demonstrating high model accuracy.

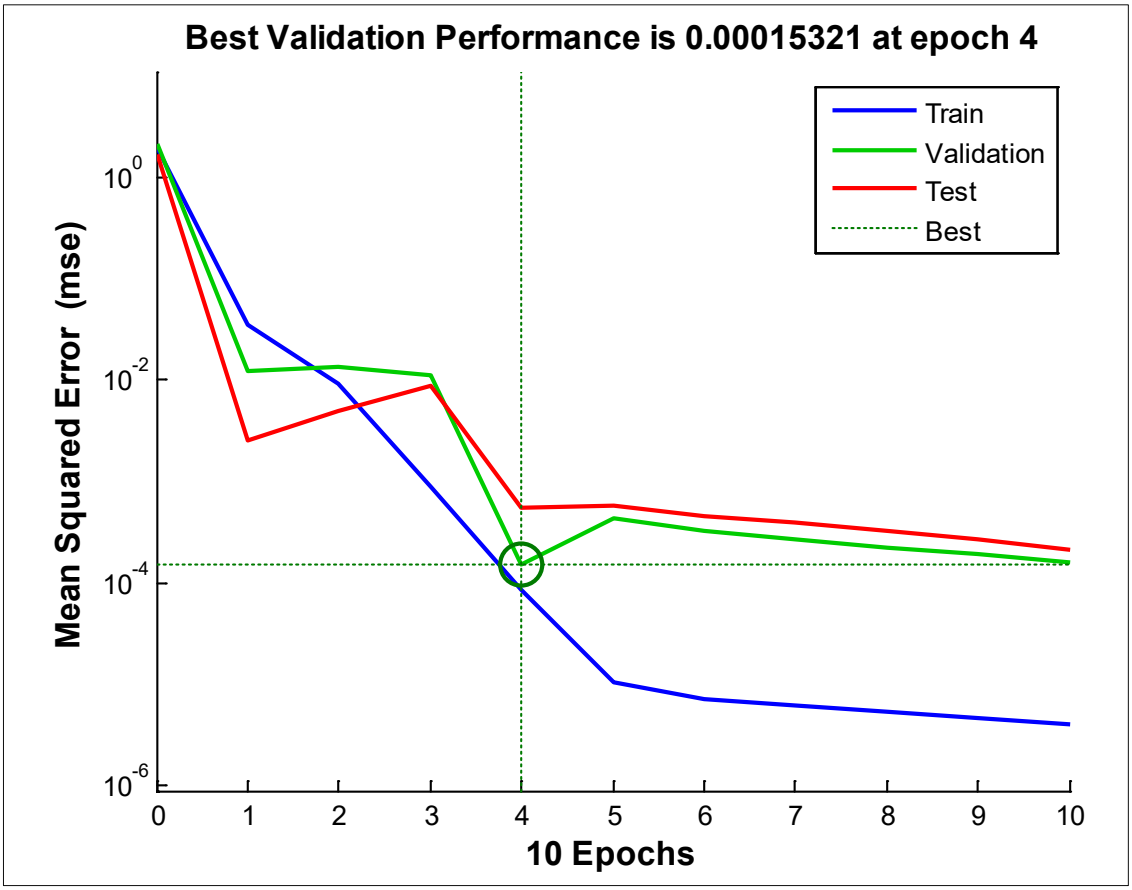

Figure 34: Performance of the trained surrogate model for vertical stress prediction with the number of neurons set to 5

Figure 34 displays the performance of the trained surrogate model, quantified in terms of Mean Squared Error (MSE).

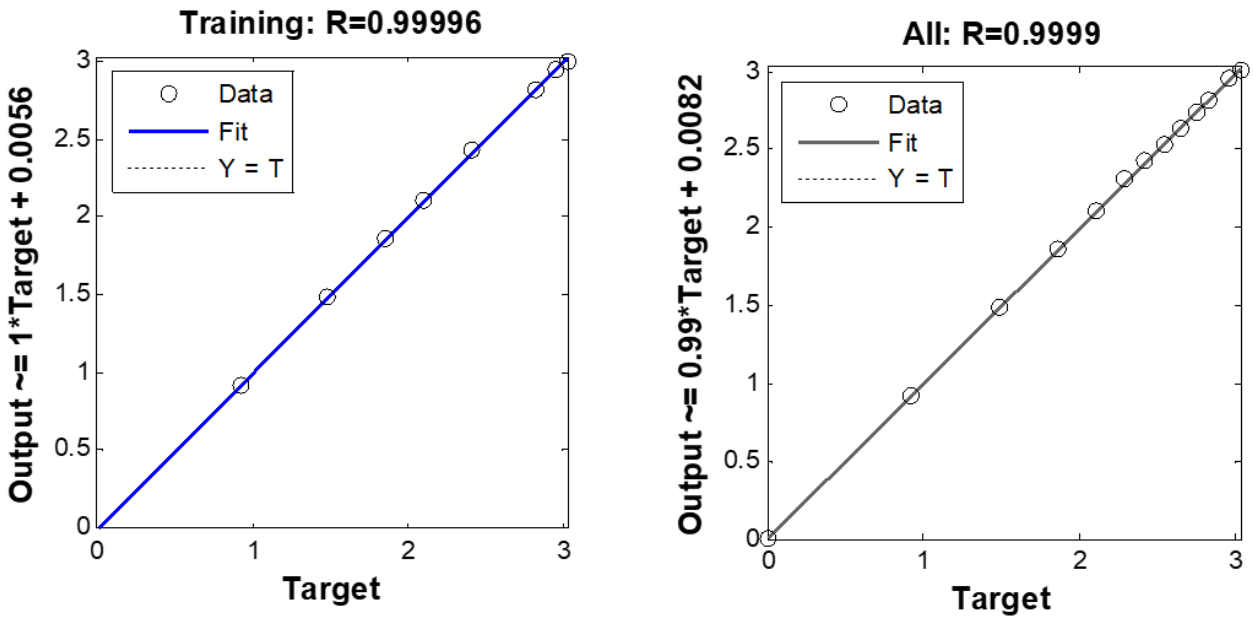

Figure 35: Regression analysis for vertical stress surrogate model with the number of neurons set to 5

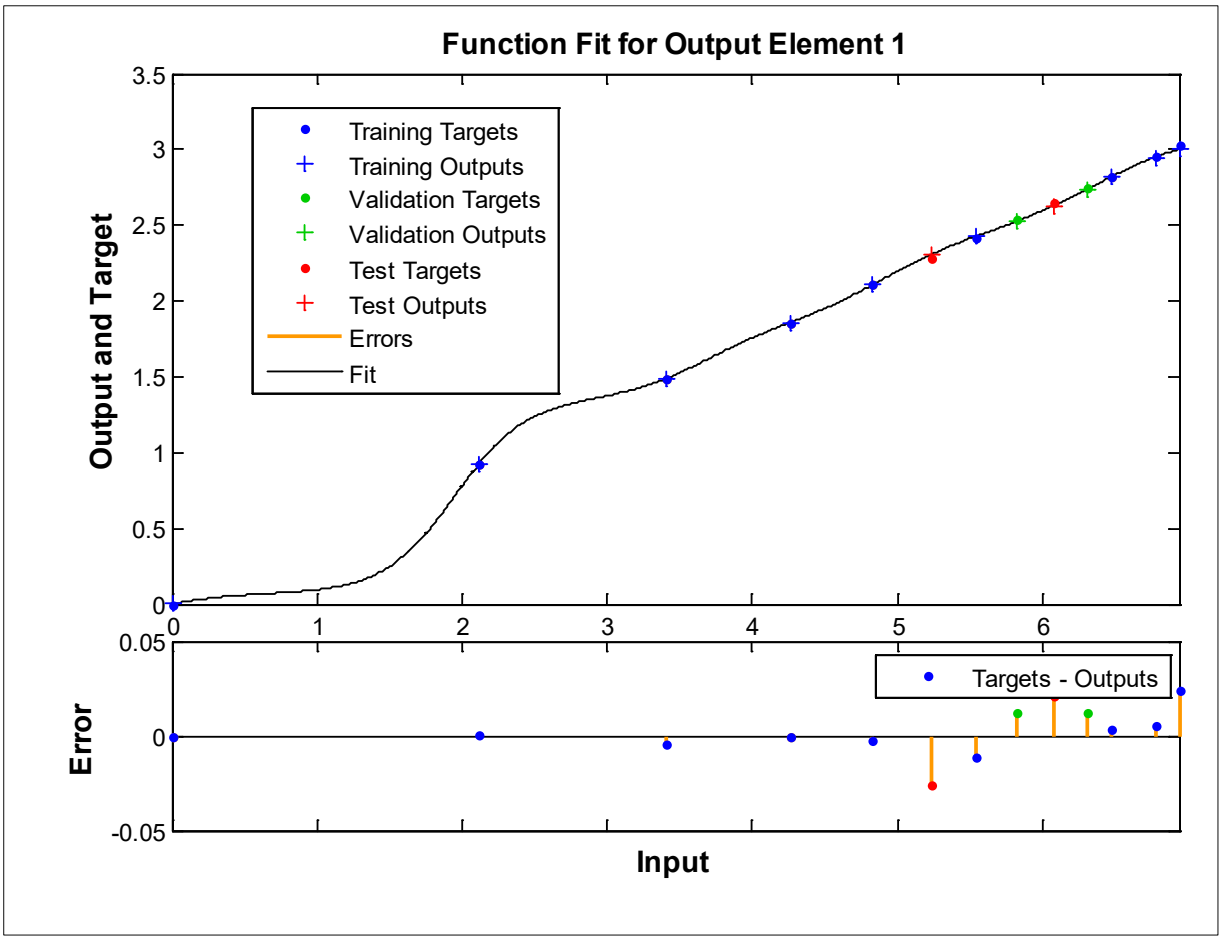

Figure 36: Comparison of target boundaries and surrogate model outputs (vertical stress)

Neural Network with 15 Neurons

Increasing the number of neurons to 15 results in a significant deterioration in performance as displayed in figure 37. The MSE increases substantially to 5.0396, indicating reduced predictive accuracy. Similarly, the regression coefficient decreases to 0.46347, reflecting weak correlation between predicted and observed values. This pattern can be observed in figure 38. The corresponding output–target distribution (Figure 39) shows increased scatter, suggesting unstable learning and poor generalisation.

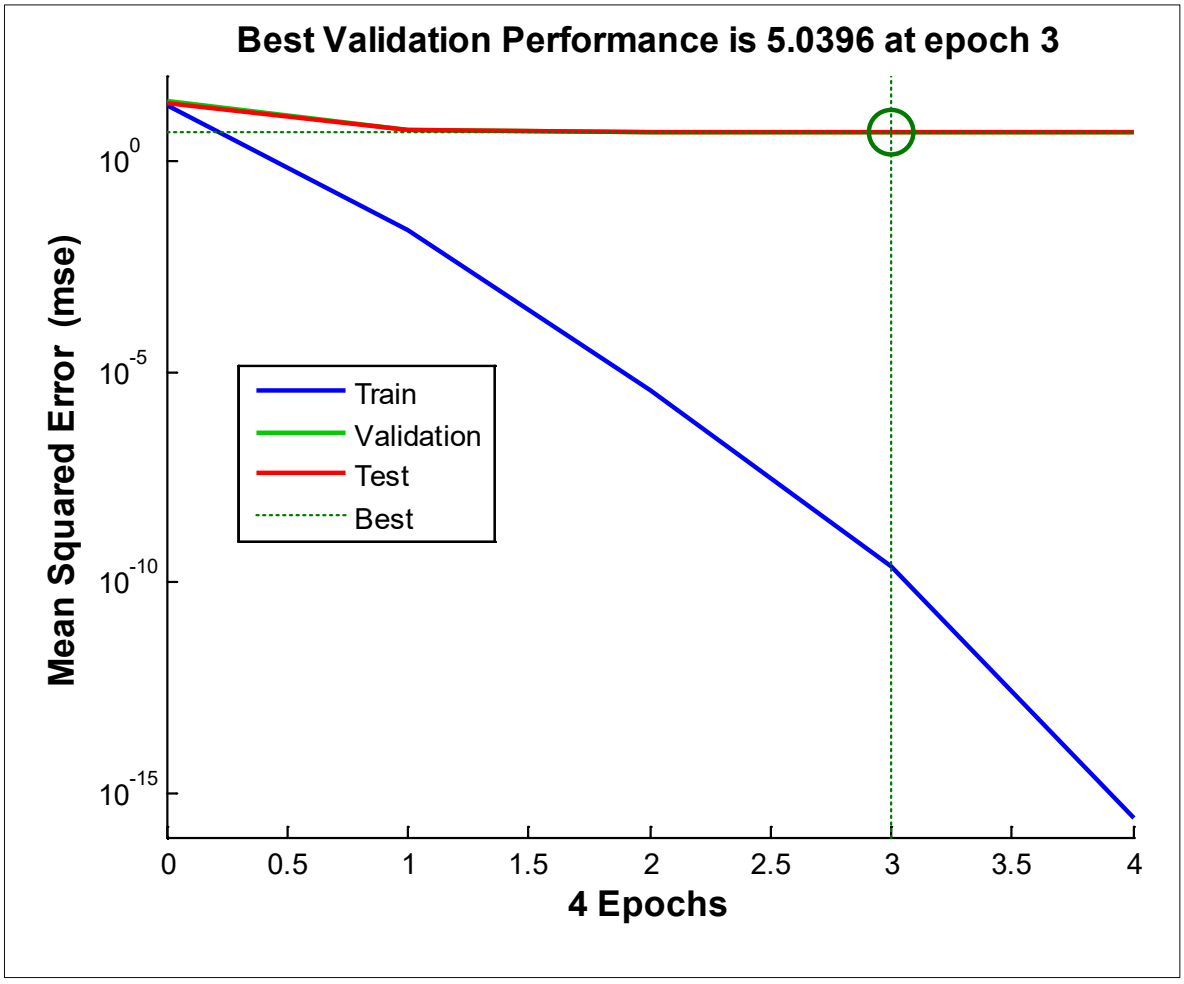

Figure 37: Performance of the trained surrogate model for vertical stress prediction with the number of neurons set to 15

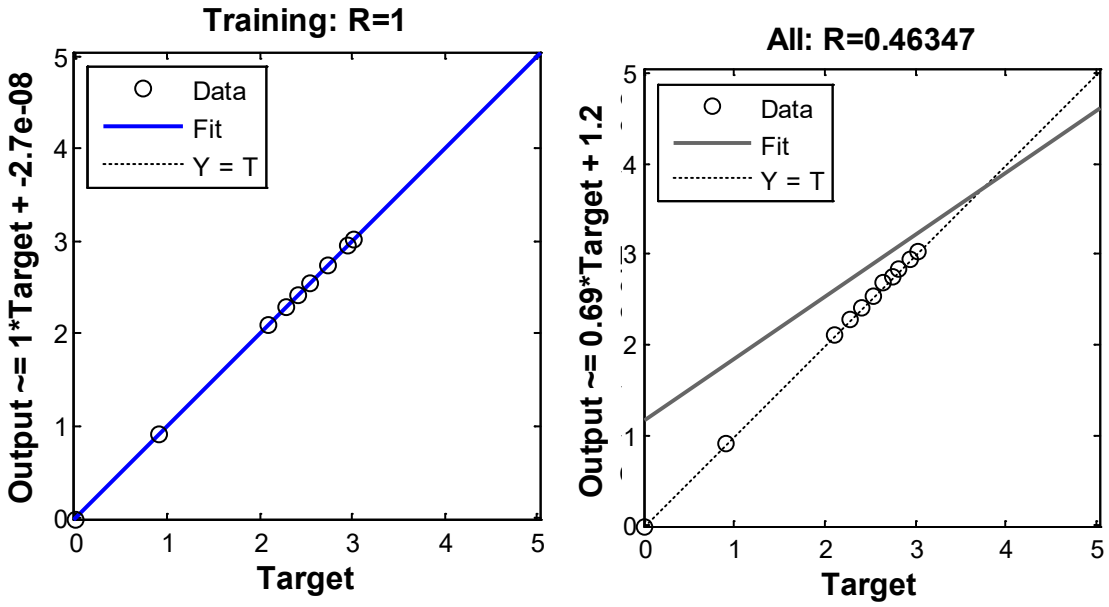

Figure 38: Regression analysis for vertical stress surrogate model with the number of neurons set to 15

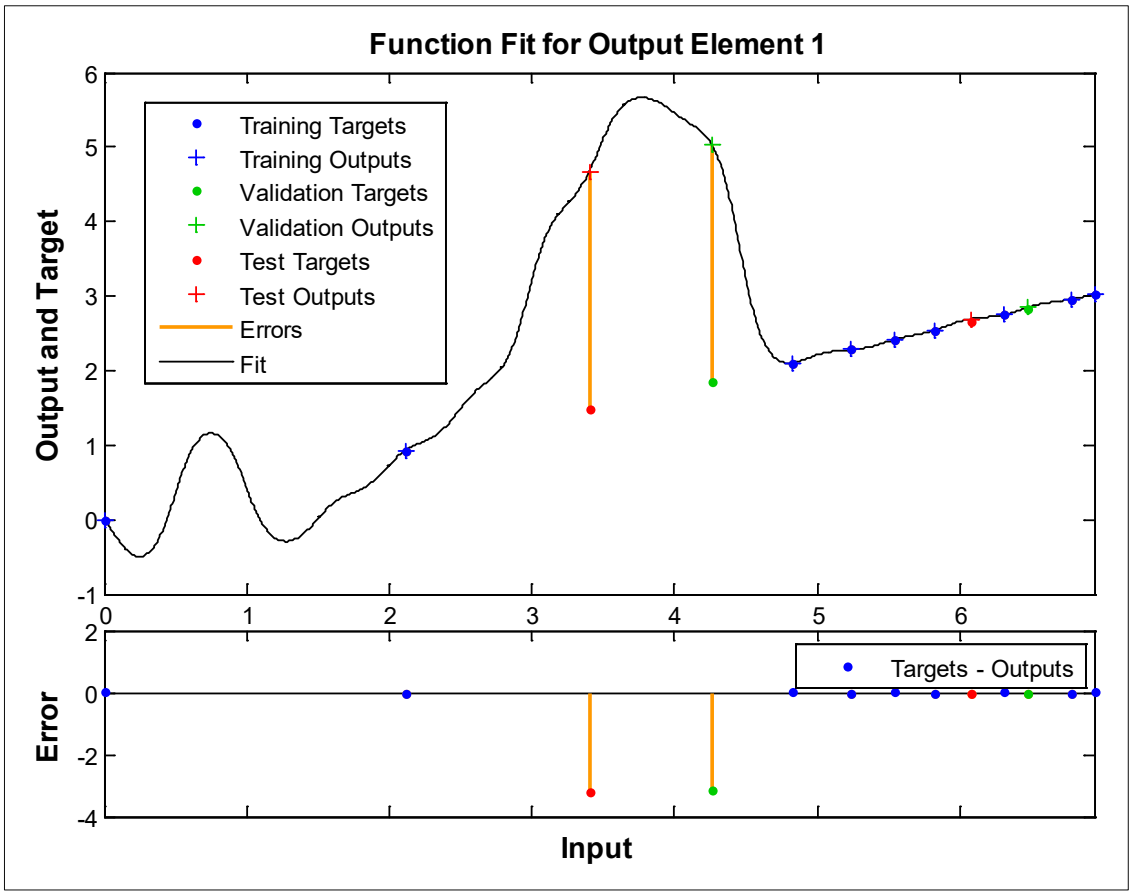

Figure 39: Comparison of target boundaries and surrogate model outputs (vertical stress)

Neural Network with 20 Neurons

For 20 neurons, the model shows partial recovery in performance, with an MSE of 1.8613 and a regression coefficient of 0.83085 via figures 40 and 41, respectively. Although improved compared to the 15-neuron configuration, the performance remains inferior to the lower neuron configurations, particularly 5 and 10 neurons. Output comparisons (Figure 42) indicate persistent deviations from target values.

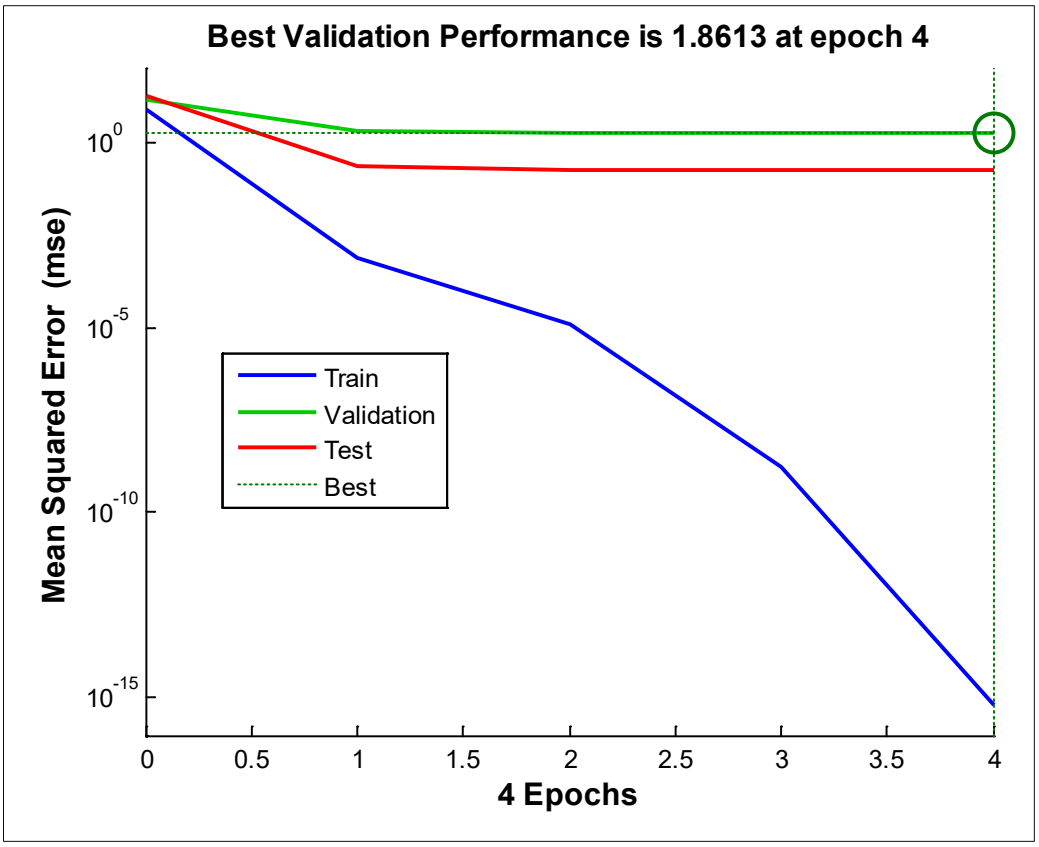

Figure 40: Performance of the trained surrogate model for vertical stress prediction with the number of neurons set to 20

Figure 41 shows the regression line with a value of 0.83085. It is still not effective compared to values of R when the number of neurons were 5 and 10.

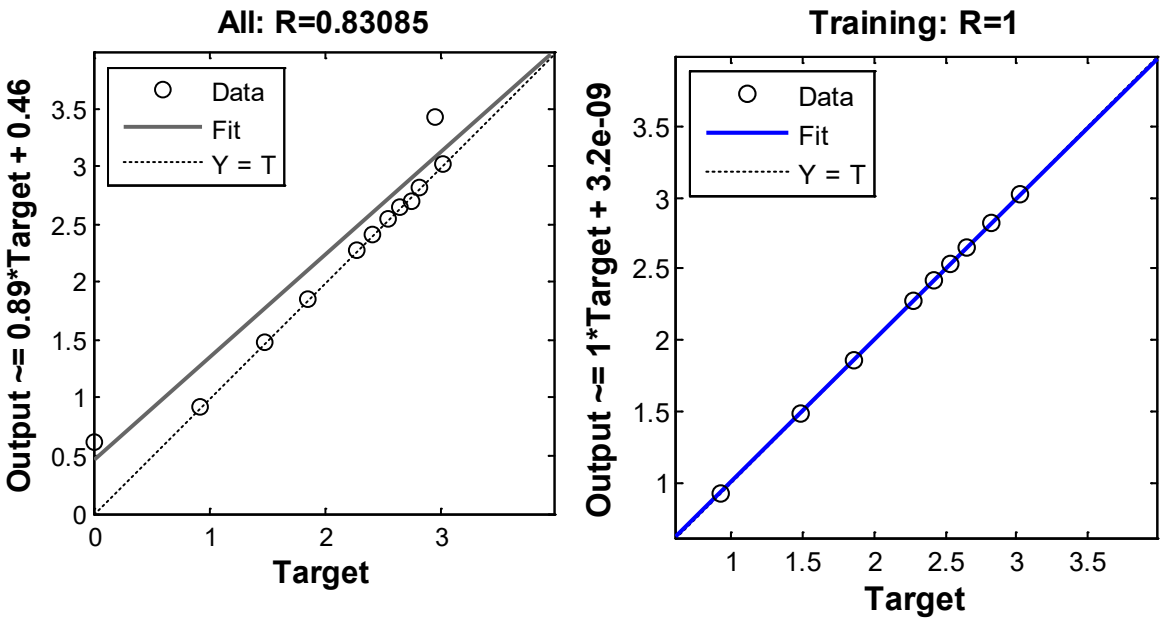

Figure 41: Regression analysis for vertical stress surrogate model with the number of neurons set to 20

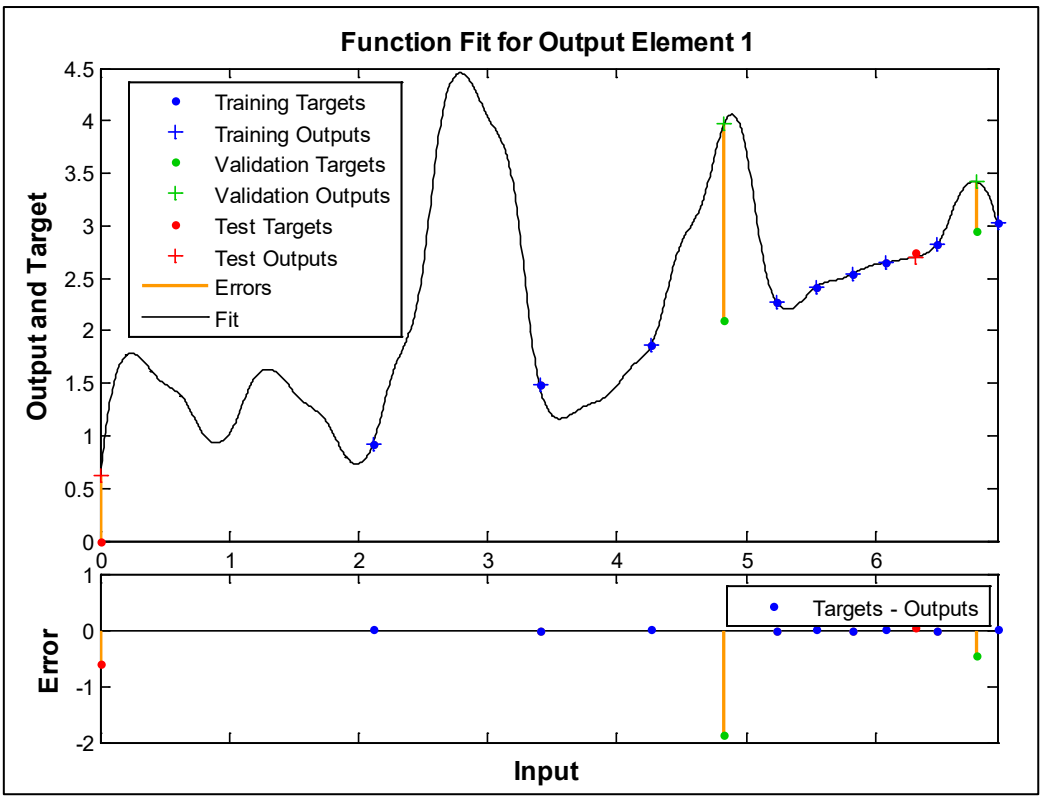

Figure 42: Comparison of target boundaries and surrogate model outputs (vertical stress)

Neural Network with 25 Neurons

When the number of neurons is increased to 25, model performance improves further, with an MSE of 0.32036 and an R-value of 0.96866. The results indicate that increasing model complexity beyond a certain threshold can partially restore learning capability. However, the performance still does not exceed that of the optimal low-neuron configuration.

The mean squared error is 0.32036 as can been seen in figure 43.

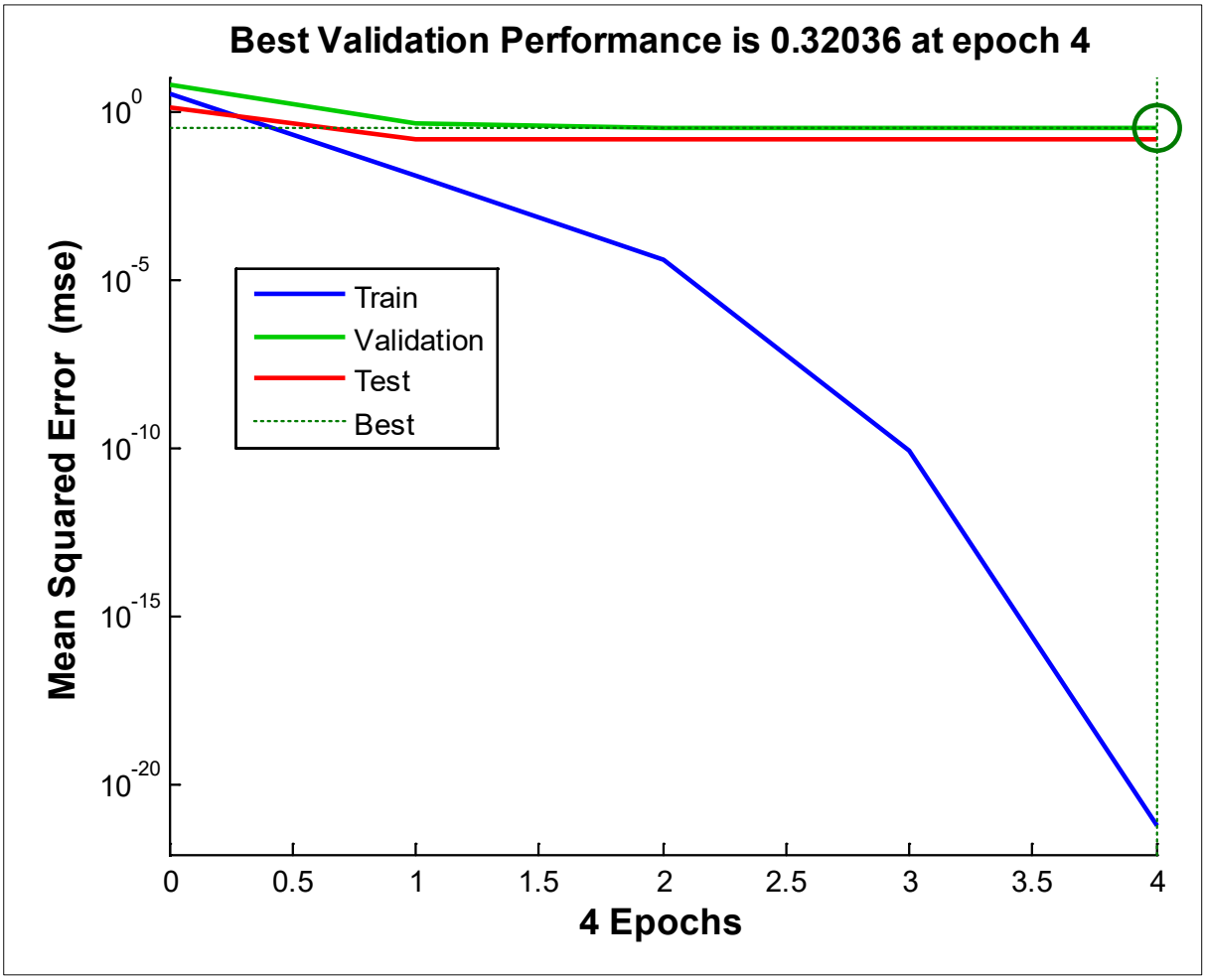

Figure 43: Performance of the trained surrogate model for vertical stress prediction with the number of neurons set to 25

Figure 44 shows the regression line with an improved value of 0.96866. Also, Figure 45 shows the relationship between target and output variables to show the improvement in the performance of the surrogate model.

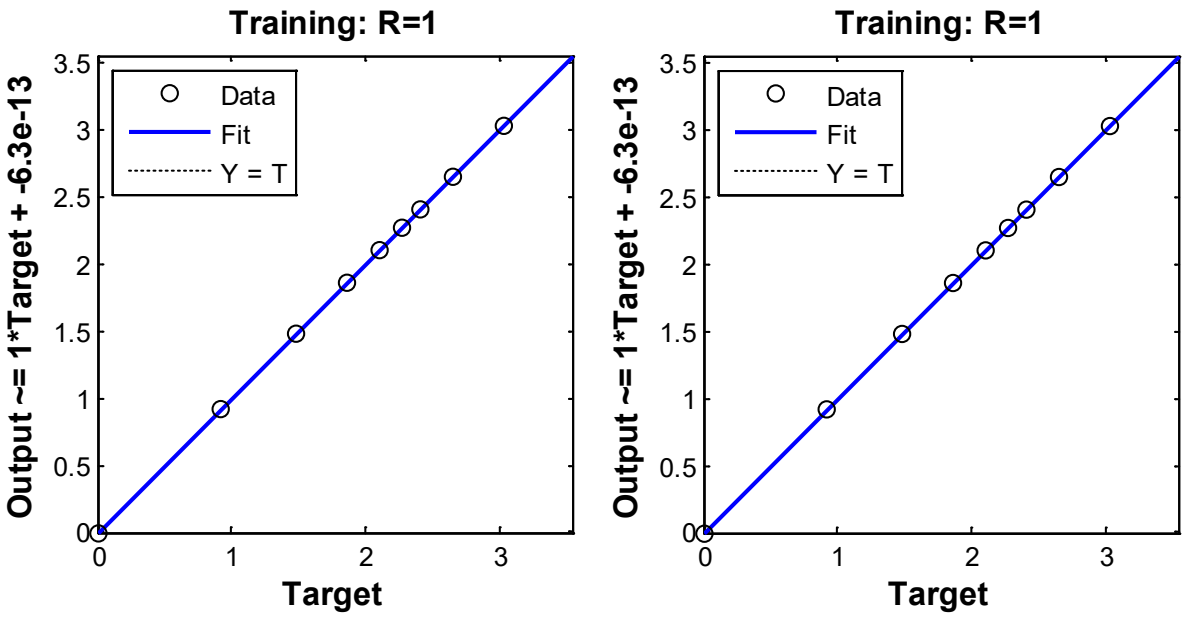

Figure 44: Regression analysis for vertical stress surrogate model with the number of neurons set to 25

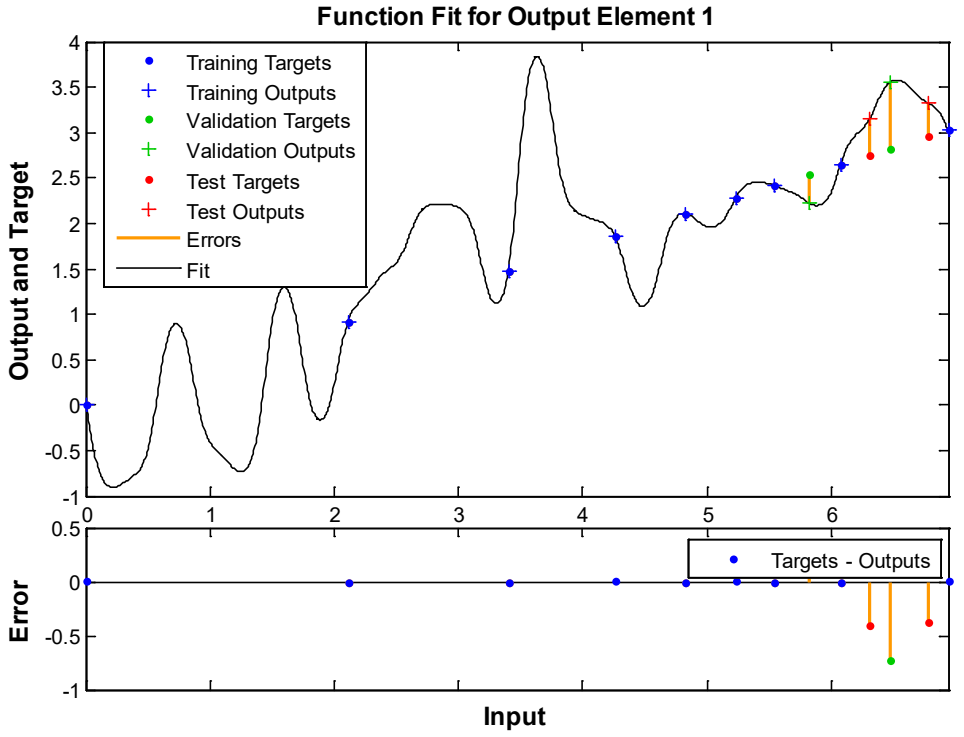

Figure 45: Comparison of target boundaries and surrogate model outputs (vertical stress)

The performance of the surrogate models developed by changing the number of neurons is tabulated below in table 8.

Table 8: Comparing the performance of the vertical stress surrogate models

Number of neurons	Mean squared error mse	Regression R
5	0.0002	1.0000
10	0.0027	0.9977
15	5.0396	0.4635
20	1.8613	0.8309
25	0.3204	0.9687

The comparative results are summarised in Table 8. The findings indicate that the best performance is achieved with a relatively small number of neurons (5–10), while intermediate configurations (particularly 15 neurons) result in substantial degradation in accuracy. This suggests that the dataset size may be insufficient to support more complex network structures, leading to unstable parameter estimation and reduced generalisation capability. There can be various reasons for this phenomenon. The neural network might get misled by an increasing number of neurons that connect the input and output. But when the neurons are again increased to 20, it shows that the performance of the surrogate model is improving. It can be due to the neural network, while training, which can effectively understand the input-output behaviour, reducing errors.

Shear Stress Surrogate Model

Similarly, a similar process was carried out for the development of the surrogate models to analyse the shear stress. At 5 neurons, the model demonstrates strong predictive performance, with an MSE of 0.0014843 and an R-value of 0.9917. The regression and output–target plots confirm a strong correlation and acceptable predictive accuracy. Figure 46 shows the validation performance of the surrogate model using a mean squared error value of 0.0014843.

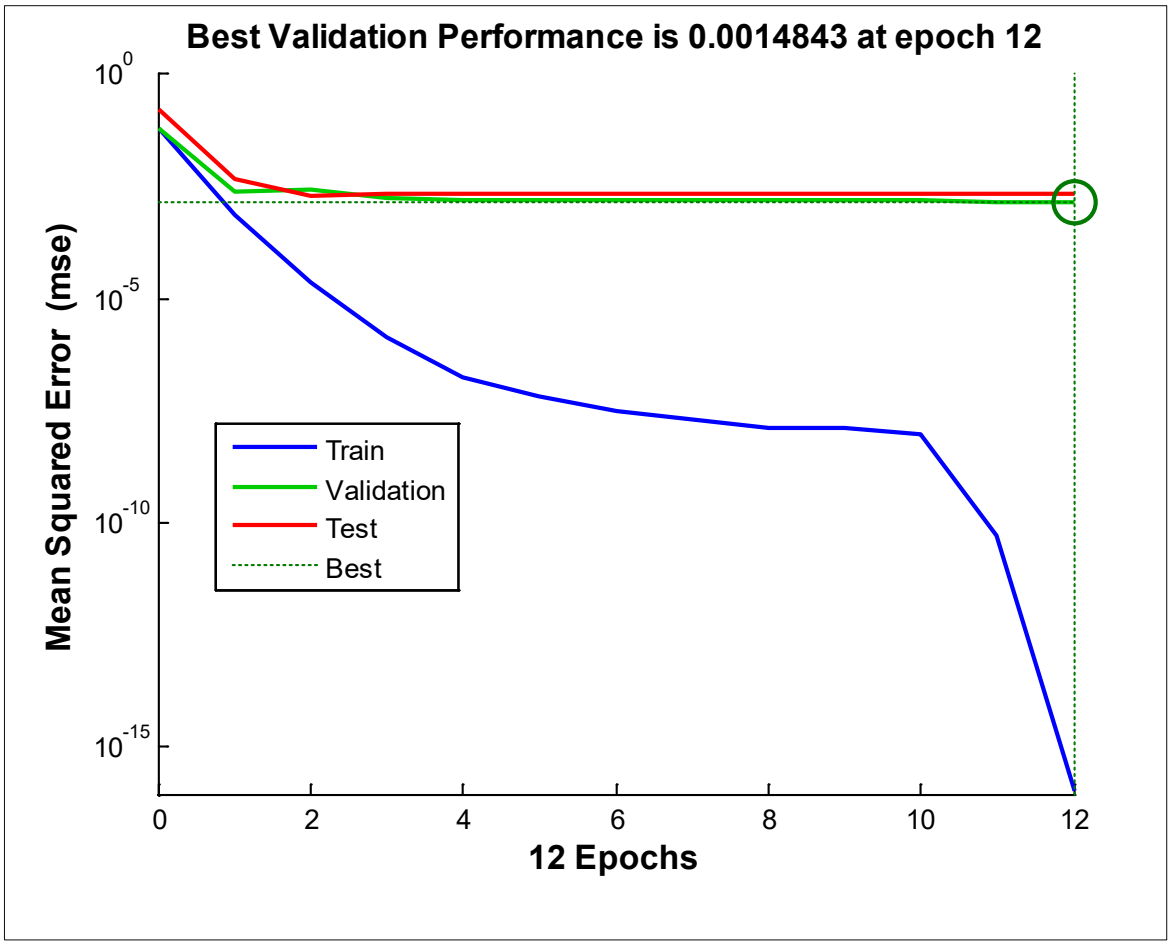

Figure 46: Performance of the trained surrogate model for shear stress prediction with the number of neurons set to 5

Figure 47 shows the regression line to validate the trained surrogate model. The value of R is 0.9917, which shows the surrogate model is effective. The 45-degree linear line also shows the consistency of output and target variables.

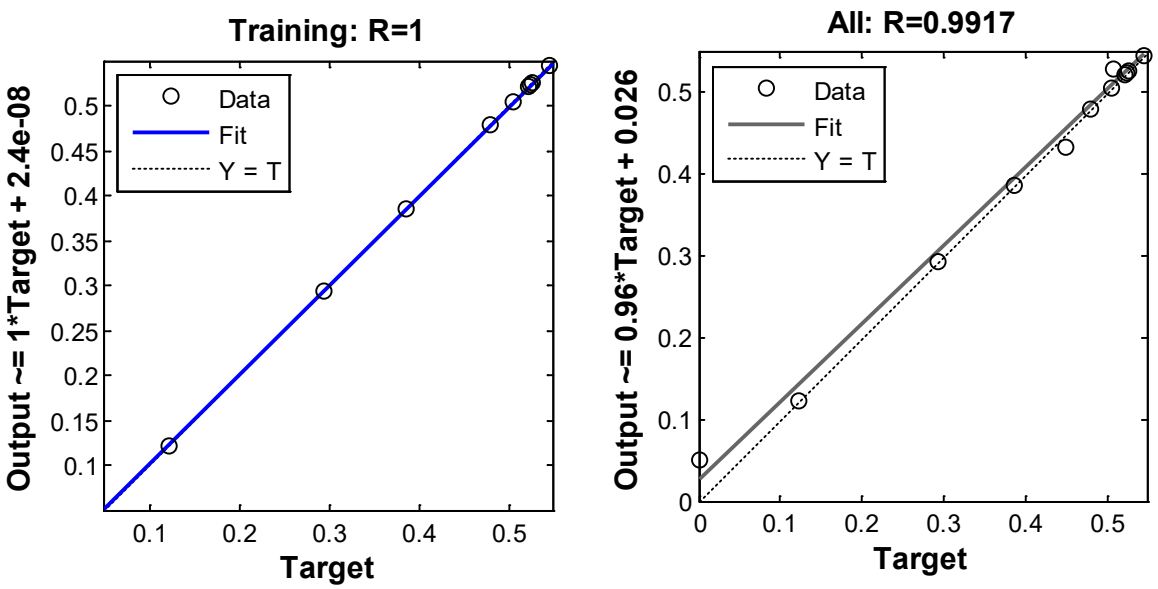

Figure 47: Regression analysis for shear stress surrogate model with the number of neurons set to 5

Figure 48 shows the relationship between the target and output. It can also be observed that the output is within the limits of the target.

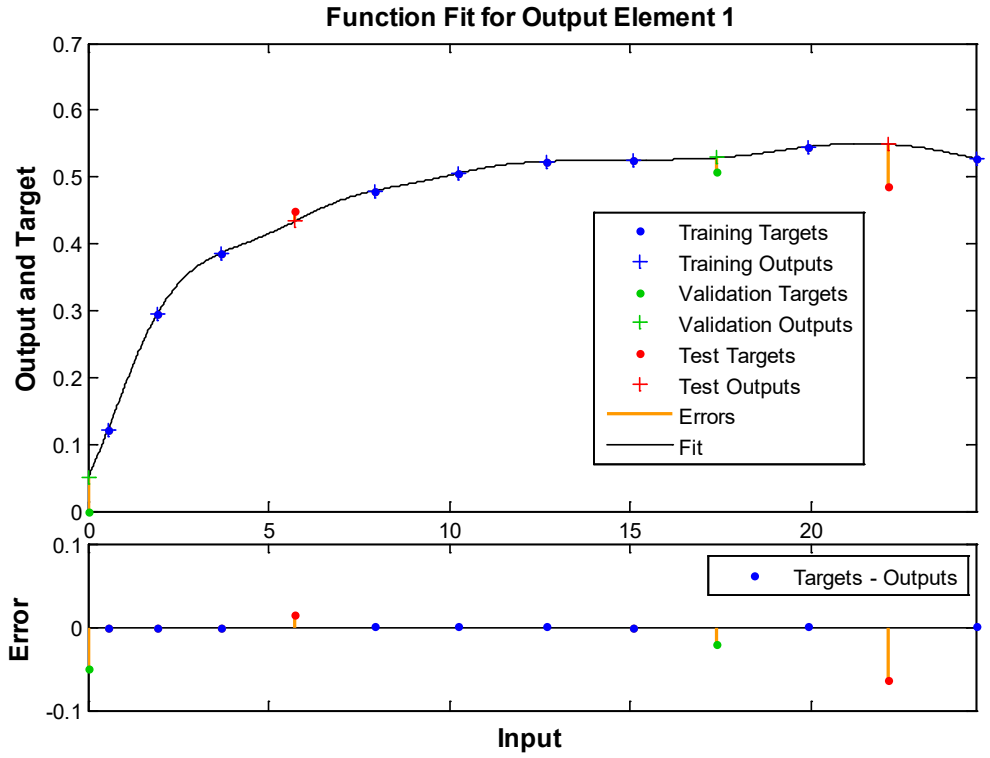

Figure 48: Comparison of target boundaries and surrogate model outputs (shear stress)

Neural Network with 15 Neurons

With 15 neurons, model performance declines significantly, with the MSE increasing to 0.030008 and the regression coefficient decreasing to 0.78931. The increased scatter in predicted values indicates reduced stability in learning the input–output relationship. The mean squared error is changed to 0.030008 as seen in figure 49. MSE value seems to be higher, so it can be assumed that the surrogate model might not be as effective compared to the previous surrogate models developed when the neurons were set to 5 and 10, respectively.

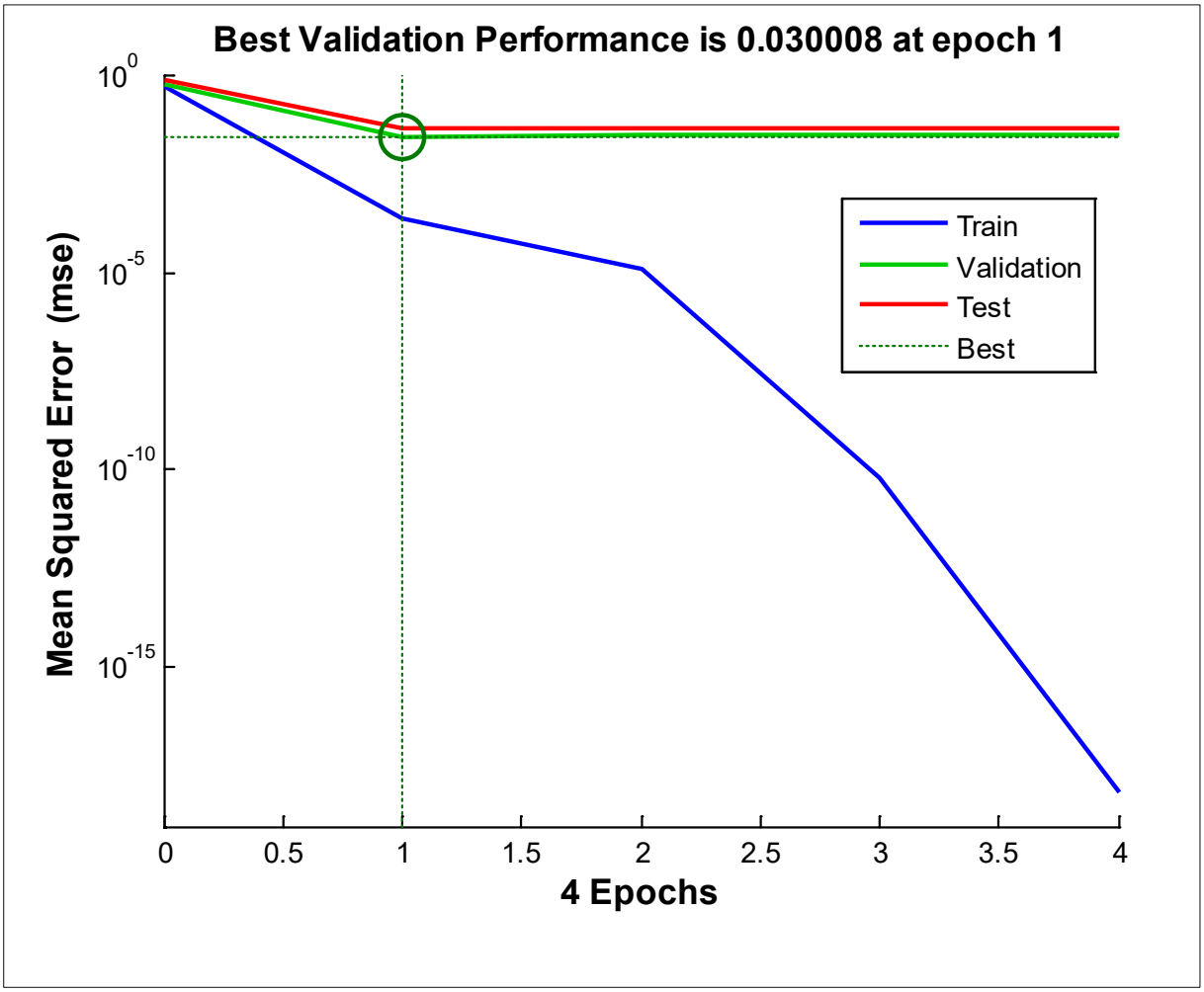

Figure 49: Performance of the trained surrogate model for shear stress prediction with the number of neurons set to 15

The regression line with the value of R 0.78931 also proves the fact that the surrogate model might not be as effective as stated in figure 50. The linear curve is also not at 45 degrees.

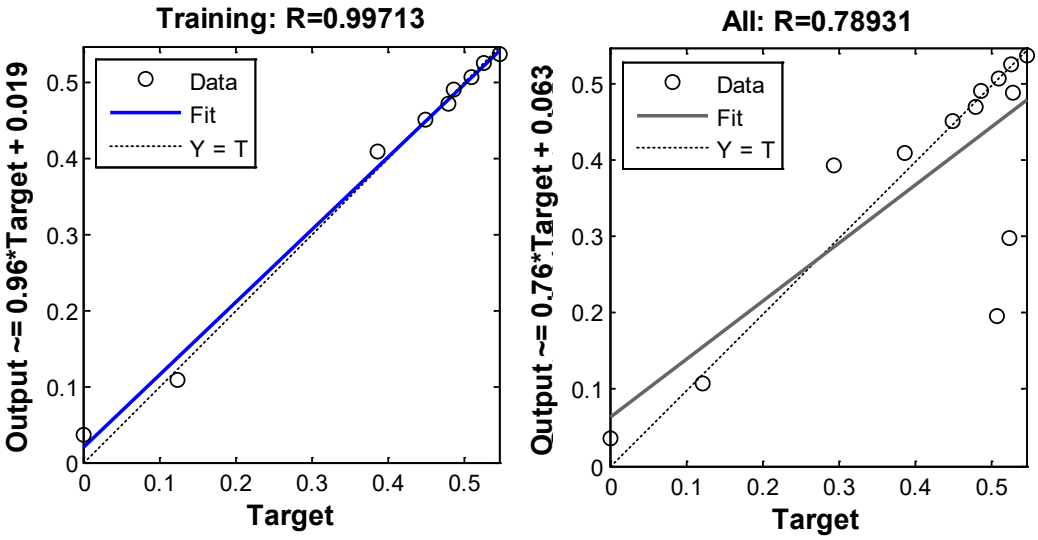

Figure 50: Regression analysis for shear stress surrogate model with the number of neurons set to 15

To further prove the claim, Figure 51 will show the relationship between output and target. Furthermore, the sparsely distributed output and target variables support the claim.

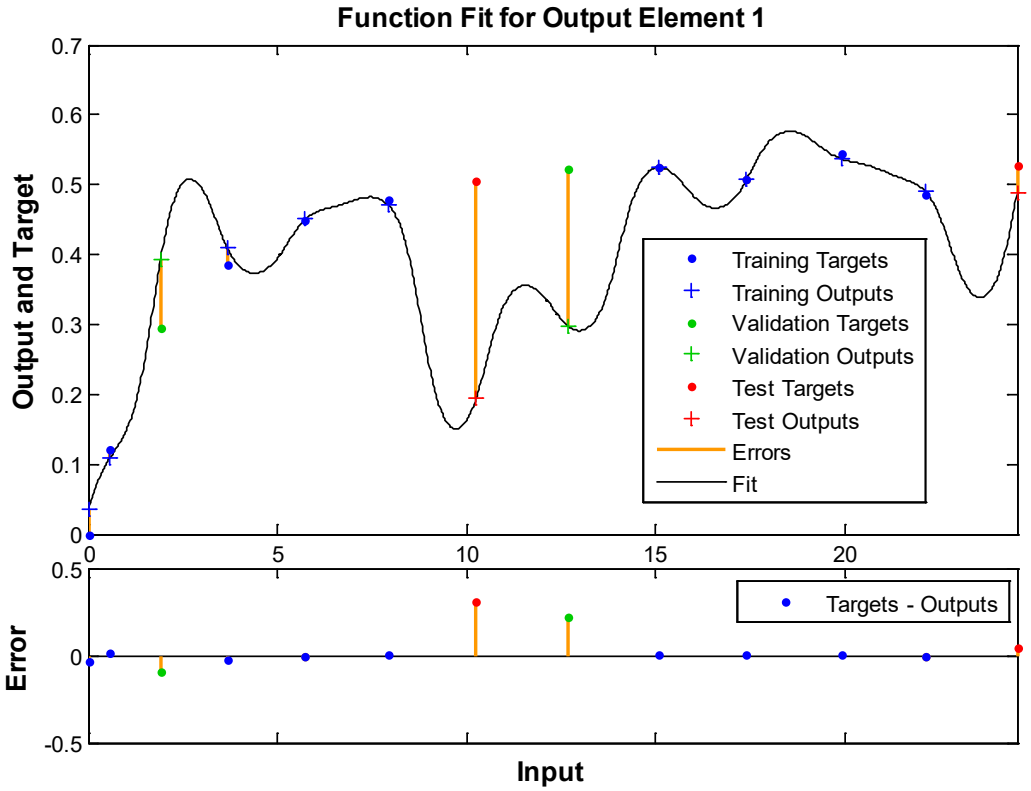

Figure 51: Comparison of target boundaries and surrogate model outputs (shear stress)

Neural Network with 20 Neurons

At 20 neurons, the model exhibits further degradation, with an MSE of 0.090377 and an R-value of 0.81974. The output–target comparison (Figure 54) shows noticeable deviation from the ideal prediction band. Figure 52 shows the effectiveness of the surrogate model by providing MSE value.

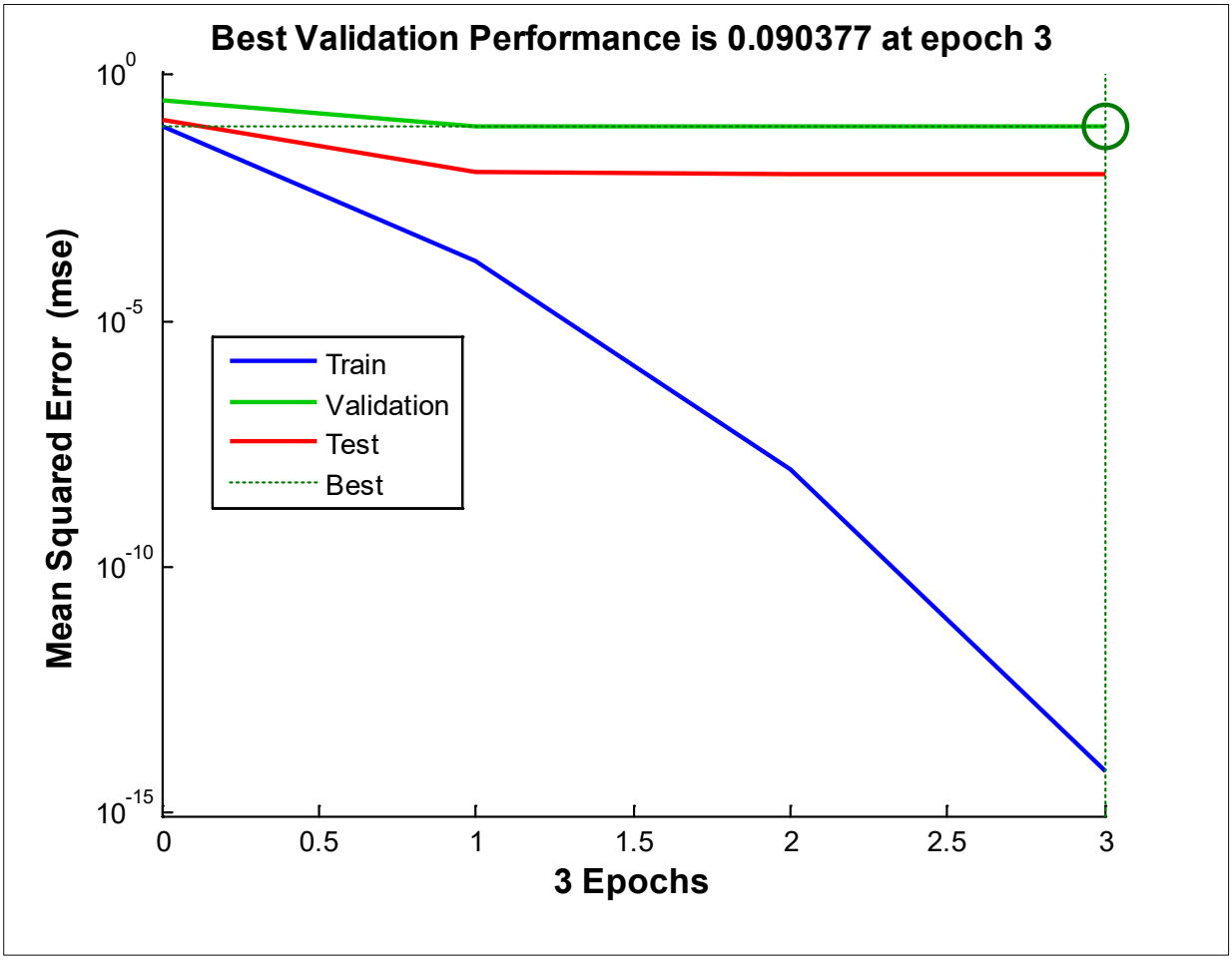

Figure 52: Performance of the trained surrogate model for shear stress prediction with the number of neurons set to 20

Figure 53 shows the regression line with a value of 0.81974. It is still not effective compared to values of R when the number of neurons were 5 and 10.

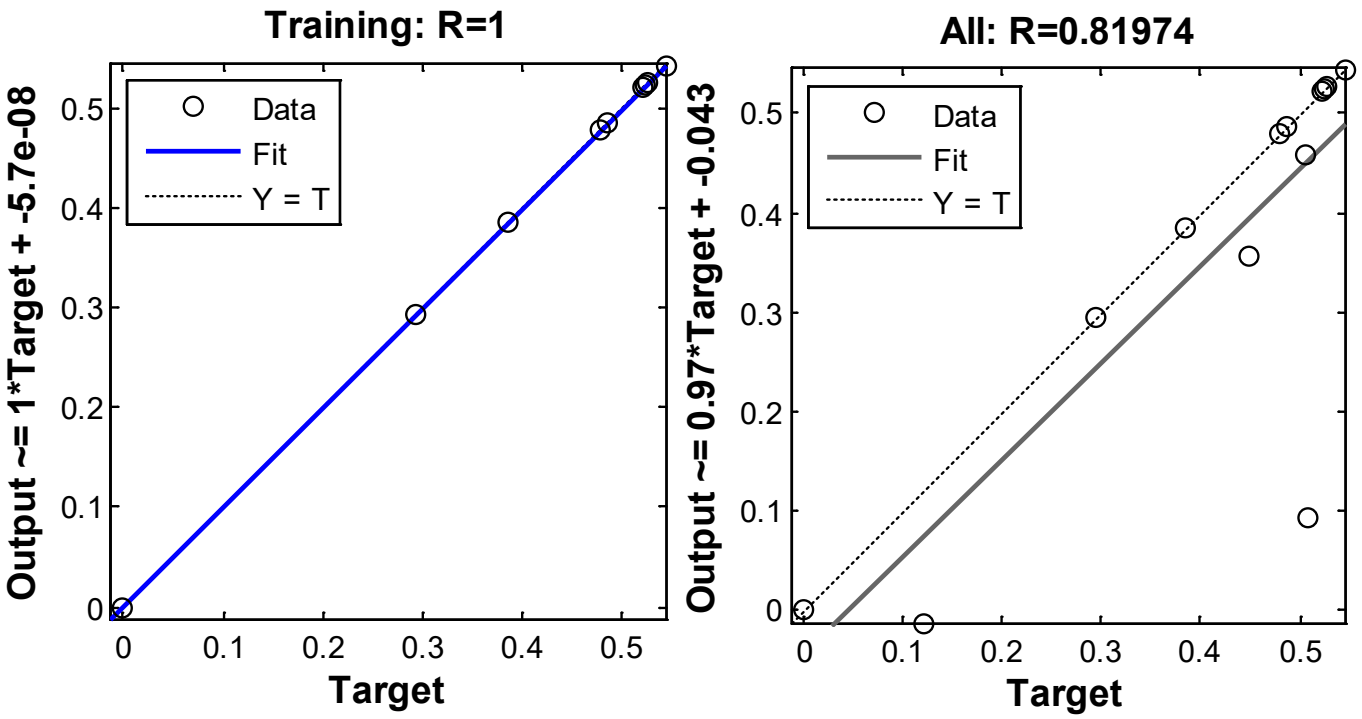

Figure 53: Regression analysis for shear stress surrogate model with the number of neurons set to 20

Finally, Figure 54 shows the target and output relationship when the number of neurons is 20. As can be seen, they are still apart from each other.

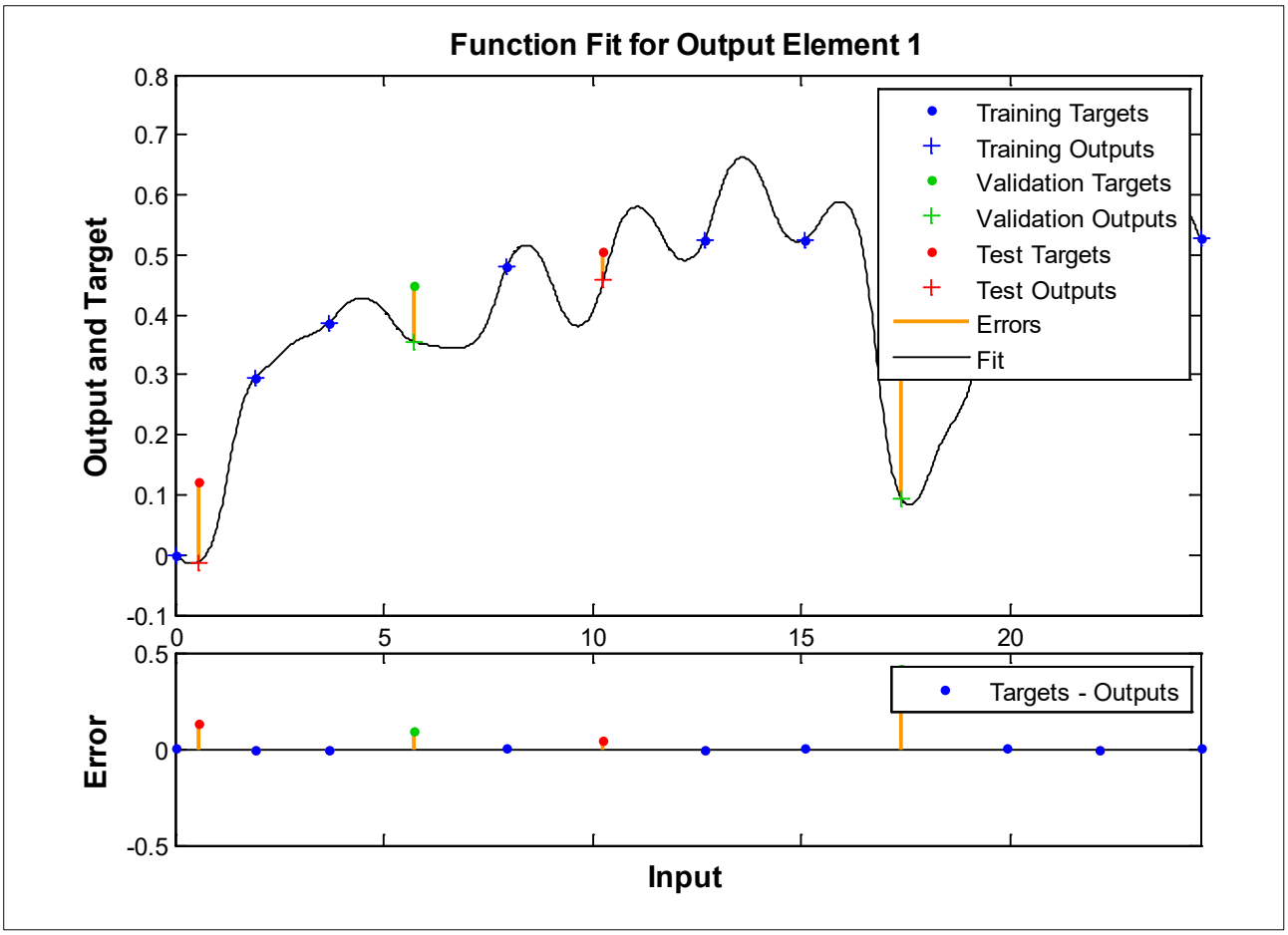

Figure 54: Comparison of target boundaries and surrogate model outputs (shear stress)

Neural Network with 25 Neurons

When the neuron count is increased to 25, the model does not exhibit improvement, with the MSE increasing to 0.098396 and the regression coefficient decreasing to 0.65754. This indicates that excessive model complexity leads to over-parameterisation and reduced predictive reliability. The mean squared error is 0.098396 as shown in figure 55.

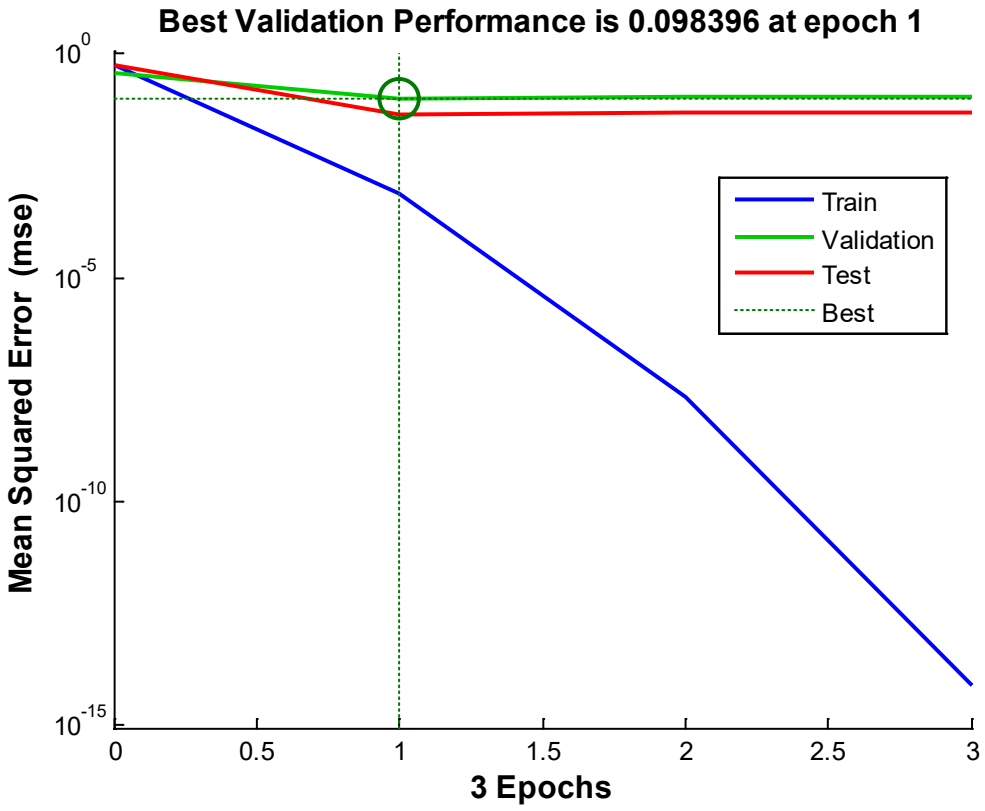

Figure 55: Performance of the trained surrogate model for shear stress prediction with the number of neurons set to 25

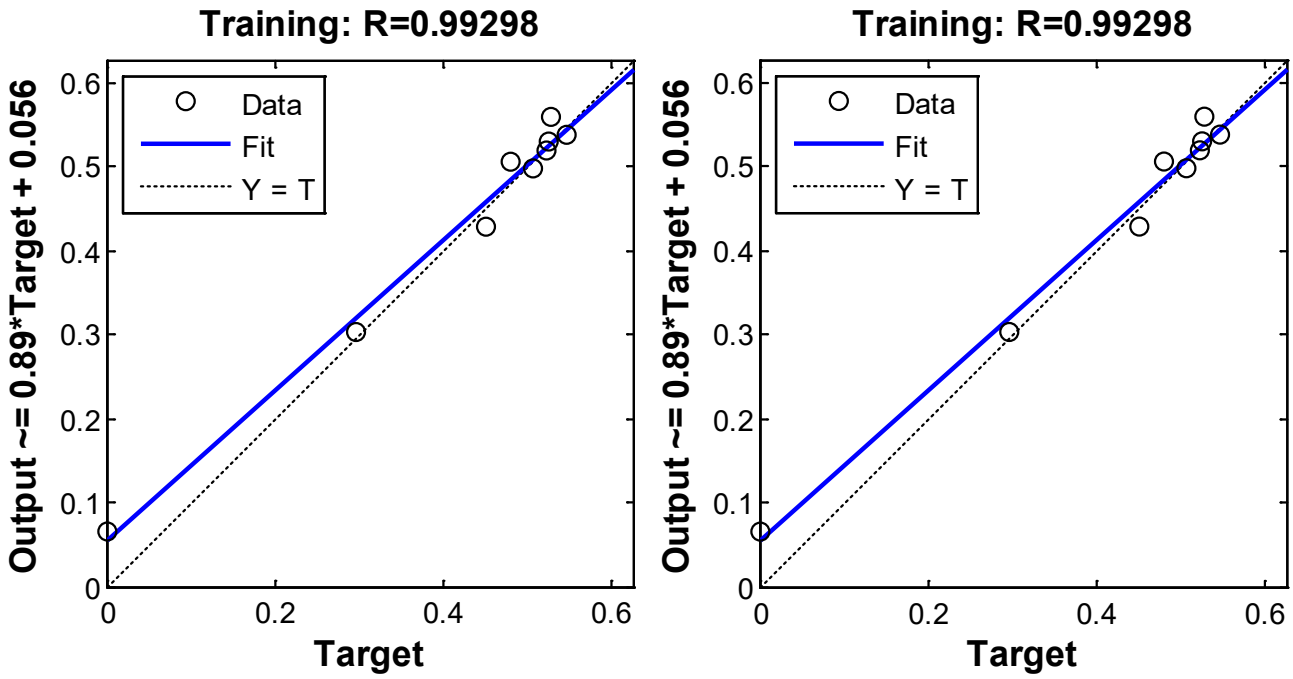

Figure 56: Regression analysis for shear stress surrogate model with the number of neurons set to 25

Figure 56 shows the regression line with a value of 0.65754. Also, Figure 57 presents the relationship between target and output variables to show the improvement in the performance of the surrogate model.

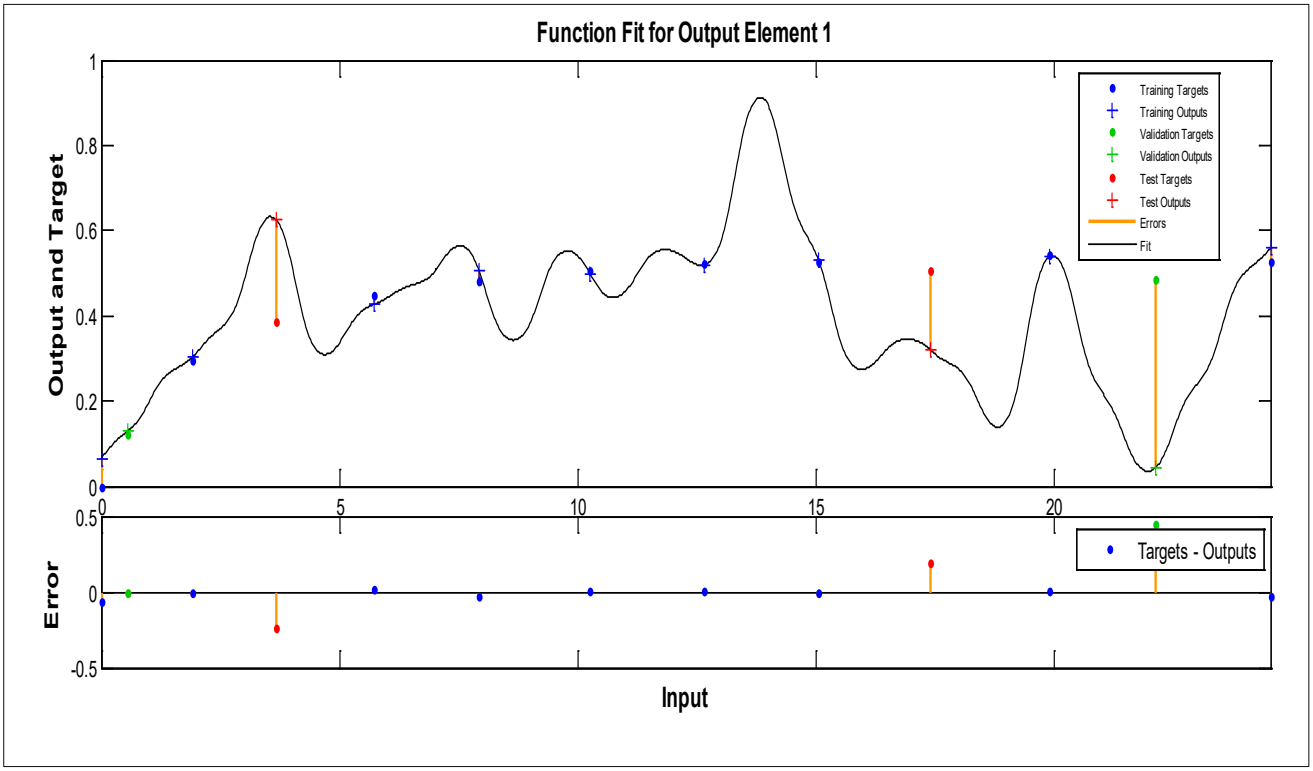

Figure 57: Comparison of target boundaries and surrogate model outputs (shear stress)

The results are summarised in Table 9. Like the vertical stress model, optimal performance is achieved at lower neuron counts, while intermediate and higher configurations generally result in reduced accuracy and regression performance.

Table 9: Comparison of the performance of the shear stress surrogate models

Number of neurons	Mean squared error mse	Regression R
5	0.0015	0.9917
10	0.0020	0.9493
15	0.0300	0.78931
20	0.0904	0.81974
25	0.0984	0.65754

The performance of the surrogate models developed by changing the number of neurons is compared in Table 9 for the shear stress analysis. It can be observed that changing the number of neurons can significantly change the performance of the surrogate model. Effectiveness decreases significantly when the number of neurons is changed from 10 to 15. There can be various reasons for this phenomenon. The neural network might get misled by an increasing number of neurons that connect the input and output. But when the neurons are again increased, it shows that the performance of the surrogate model is slightly improving, as can be seen in the case when the number of neurons is changed from 15 to 20. It can be due to the neural network, while training, can effectively understand the input-output behaviour, reducing errors.

It can be concluded that changes in parameters within the neural network process can also effectively alter the performance of the surrogate model. Therefore, the surrogate model needs to be trained as much as possible by feeding a large number of datasets to improve the input-output relationship function. This will lead to the efficient and accurate assessment of the structures.

Chapter 5.4: Laboratory setup for silo structures

The laboratory experiment was conducted in accordance with the safety and procedural requirements of Victoria University, following formal laboratory induction protocols. A cylindrical container was selected as the experimental prototype to simulate silo-like behaviour under controlled filling conditions, as introduced in Chapter 5.1.

The experimental setup is illustrated in Figure 58. The system consisted of an acrylic cylindrical tube, a base weighing scale, a load cell system, granular filling materials, a funnel, and a supporting steel frame with steel suspension elements. The cylindrical tube was suspended within the steel frame using steel strings, allowing load transfer to be measured both at the base and along the wall.

The acrylic tube had a height of 1000 mm, an external diameter of 109 mm, and an internal diameter of 103 mm. The expected filling height during testing was approximately 900 mm. The transparency of the acrylic material enabled visual observation of material filling behaviour and distribution patterns.

Figure 58: Cylinder used for the prototype

The base of the system consisted of a digital weighing scale capable of measuring up to 5200 g, as shown in Figure 59. This scale was used to measure the mass of the granular material transmitted directly to the base of the cylinder during filling. In addition, a digital force gauge (Model SHB-500) was installed at the top of the supporting frame and connected to the cylinder using steel strings, as shown in Figure

60. This load cell system was used to measure the force transferred to the cylinder walls due to lateral interaction with the filling material.

Figure 59: Base (weighing scale) to measure the mass

Figure 60: Load cell to capture the load transferred to the wall of the tube

The steel strings had a diameter of 1.5 mm, a breaking load capacity of 130 kg, and a recommended safe working load of 25 kg, ensuring safe operation throughout the experiments.

During testing, granular materials such as sand and grain were gradually introduced into the cylinder through a funnel. As the material level increased, load redistribution occurred between the base and the cylinder wall. The base scale recorded the vertical load contribution, while the load cell measured the lateral force transmitted to the walls.

The primary objective of the experiment was to quantify the development of vertical stress at the base and shear stress along the cylinder wall under different filling conditions. These measurements were subsequently used as input data for the development of neural network-based surrogate models.

Chapter 5.5: Laboratory testing implementation

The laboratory testing program was designed to investigate the behaviour of silo-like structures under different granular filling conditions. The experiments involved filling the cylindrical tube with various materials, including sand and grain, to evaluate the resulting vertical and lateral stress distributions.

The study considered multiple influencing parameters, including the total mass of filling material, moisture content, and frictional characteristics between the material and the internal wall surface. These parameters were varied systematically to generate a diverse dataset for surrogate model development.

The base scale measurements were used to determine the vertical load transferred through the material to the bottom of the cylinder, while the load cell readings represented the portion of load transferred laterally to the cylinder wall. These measurements were essential for estimating vertical stress and shear stress under different filling conditions.

Granular materials were selected for this study due to their ability to replicate complex bulk material behaviour, including particle interaction, frictional resistance, and flow characteristics. Unlike rigid structural materials such as reinforced concrete, granular materials allow repeated testing with minimal cost and time requirements, making them suitable for parametric studies.

Although granular materials do not replicate the constitutive behaviour of reinforced concrete, they provide a useful similarity for studying load redistribution procedures and wall–particle interaction effects within silo-like geometries.

Chapter 5.5.1: Defining layers for the testing

To capture variations in stress distribution with height, the filling height of the cylinder was discretised into multiple layers. Three different discretisation schemes were adopted: 10 layers (90 mm each), 20 layers (45 mm each), and 30 layers (30 mm each).

Each configuration was tested independently to investigate the influence of spatial resolution on stress estimation. For each layer configuration, experiments were repeated under varying material types and surface roughness conditions. These widened the range of data collected from the experiments required for the numerical simulation, required for the creation of the surrogate model.

Chapter 5.5.2: Required input data for the experiments

During each test, granular material was introduced incrementally into the cylinder through a funnel. Reading the load cell gauge would measure the mass spread onto the wall of the tube. The initial mass of the setup was determined by readings on the weighing scale (base). Mass spread on the base was determined by subtracting the reading on the load cell from the initial mass of the setup. Reading of the loads was necessary to estimate the vertical stress and the shear stress. Different readings were recorded for different layers. This resulted in a change of stresses for different levels of height.

Filling materials were different because they have their unique particle sizes, shapes, and distributions. Properties of fine sand would be different compared to those of granular sand. As such, changing the type of filling materials results in a change in the load spread in the structure. This also affects the stresses in the structure.

Similarly, when the moisture content of the filling materials is changed, the mass of the filling materials changes accordingly, which leads to a change in stresses. For example, the shear strength of the sand was influenced by the percentage of moisture content. The shear strength of fine sand would be reduced by an increment in moisture level, thereby diminishing cohesion. Pore water pressure increases in granular sand, which affects the effective stress.

To manage the scope of the study, the parameters that were studied are the type of filling material and the moisture content.

Chapter 5.5.3: Targeted output variables from the experiments

This sub-chapter discusses the output variables, which were derived from the laboratory experiments. These variables were used to construct a surrogate model to analyse the stress developed on the silo caused due to fillings. Vertical stresses developed on the base of the cylinder and shear stresses developed along the wall of the structure were assumed as the milestone for the reliability analysis of the structure.

The vertical stress acting at a point on the base below the surface level was developed due to the weight of the filling materials above that point. Since the weight of the filling materials were different at different heights, the vertical stress was different at various heights of the structure. Boussinesq's theory was used to compute the vertical stress beneath the centre of a uniformly loaded circular area at the ground surface. The formula for calculating vertical stress is as follows:

$$\sigma_z = q\left[1 - \frac{1}{\left[\left(\frac{R}{z}\right)^2 + 1\right]^{\frac{3}{2}}}\right] \quad (5.1)$$

The vertical stress created beneath the load is denoted by σ_z, whereas q represents the uniform pressure distribution over the surface area. Similarly, z is the total height of the load beneath the surface to the base, and R is the radius of the cylinder.

During the laboratory experiment, both vertical stresses would be examined to conduct the reliability analysis of the structure. Similarly, during the filling process in the cylinder, shear stress was also developed in the tube. It occurred along the wall of the tube. The maximum shear stress along the wall of the cylinder, τ max, was calculated by:

$$\tau_{max} = \frac{4}{3}\left[\frac{F}{\Pi R^2}\right] \quad (5.2)$$

F represents the force created due to the filling materials, and R denotes the radius of the cylinder. Also, the average shear stress, τ average, was calculated using the following formula:

$$\tau_{average} = \frac{F}{\Pi R^2} \quad (5.3)$$

However, for the purpose of the study, evaluating the maximum shear stress along the wall of the cylinder was considered the milestone of the laboratory experiment. Unlike vertical stress, shear stress is also affected by factors other than the weight of the filling materials distributed to the wall.

Chapter 5.5.4 Implementation of the laboratory procedures

The laboratory experiment was designed to investigate the influence of filling material properties and wall surface roughness on the shear stress developed along the wall of the cylindrical silo. Three granular materials—fine sand, river sand, and crusher dust—were selected as filling materials. To investigate the effect of wall friction, the internal surface of the acrylic tube was lined with three grades of sandpaper: P40, P60, and P80, representing different levels of surface roughness. The thickness of each deposited layer varied naturally during filling, as maintaining identical layer thicknesses is neither practical nor representative of actual silo filling operations.

Figures 61-64 illustrate the experimental setup and the granular materials used during the laboratory investigation.

Figure 61: Laboratory setup used for conducting the laboratory-based experiment

Figure 62: Fine sand used as the filling material in the experiment

Figure 63: Crusher dust used as the filling material in the experiment

Figure 64: River sand used as the filling material in the experiment

Loose grain materials were selected in place of solid structural materials for the laboratory experiments conducted for chapters 5 and 6 due to their ability to simulate specific, complex behaviours, facilitate rapid destructive testing, and significantly reduce experimental cost and turnaround time. Unlike reinforced concrete, which behaves as a relatively rigid and brittle composite, loose materials exhibit both solid-like and fluid-like responses. Sand or gravel possess high internal friction and pore structure.

Another key advantage is experimental efficiency. Granular materials can be easily reconfigured between tests, enabling multiple rapid iterations and parametric studies. In contrast, reinforced concrete specimens require substantial time and effort to fabricate and cannot be reused after failure. Furthermore, granular systems allow to create shear band formations and material flow, whereas failure in reinforced concrete is often sudden and brittle.

However, it is important to recognise that loose materials do not replicate the constitutive behaviour of reinforced concrete. Reinforced concrete response is governed by cracking, reinforcement interaction, and composite action, which are not captured in loose materials response. Therefore, the experiments are not intended to directly reproduce the structural response of reinforced concrete elements. Instead, it aims to investigate load redistribution and shear forces along the wall of the tube.

The laboratory testing was performed under three surface roughness conditions. In the first series of experiments, the internal surface of the tube was lined with P40 sandpaper, after which each of the three filling materials was tested independently. The entire procedure was then repeated using P60 and P80 sandpapers to examine the influence of wall roughness on stress development.

During each test, the filling material was introduced incrementally into the tube, and measurements were recorded at predetermined filling heights. At every measurement point, readings were obtained simultaneously from the digital weighing scale and the load cell.

To find the weight of each layer, the total weight of the preceding layer was subtracted from the weight of the previous layer. For example, to calculate the mass of the second layer, readings of 1st layer were recorded on the load cell as well as on the base weighing scale as M1 for the respective readings. When the material was filled up to the height of the 2nd layer, readings were recorded as M2, respectively. Since the base weighing scale provided the mass of the material above the base, M2–M1 readings from the base provide the mass of the 2nd layer spread to the base. This mass was used as the weight of the filling material directly above the base, and this was used to compute the vertical stress developed above the base by the filling material.

Similarly, there were also readings on the load cell. A load cell measures the weight of the material spread on the wall of the tube. Therefore, M2–M1 readings from the load cell would provide us with the mass of the 2nd layer spread to the wall. This mass was also converted to the weight for the computation of shear stress developed along the wall of the tube.

The same measurement procedure was followed for every filling layer, each filling material, and each wall roughness condition. Subsequently, a comprehensive experimental dataset was generated covering three filling materials and three surface roughness conditions. These datasets formed the basis for training, validating, and testing the neural network-based surrogate models presented in the following sections.

Chapter 5.6: Results and Analysis

The experimental data obtained from the laboratory testing were imported into the MATLAB environment to develop neural network-based surrogate models capable of predicting the shear stress developed along the internal wall of the cylindrical silo prototype. The objective of the surrogate model was to reproduce the stress behaviour of the physical experiments while significantly reducing the computational and experimental effort required for future analyses.

Based on the experimental procedures described in the previous sections, the primary variables influencing the shear stress response were identified as the filling height and the roughness of the internal wall surface, represented by the grit size of the sandpaper (expressed in microns). For each test, the load transferred to the wall was measured using the load cell, from which the corresponding shear stress was calculated. These experimentally obtained input-output datasets formed the training data for the neural networks.

Based on the experimental procedures described in the previous sections, the primary variables influencing the shear stress response were identified as the filling height and the roughness of the internal wall surface, represented by the grit size of the sandpaper (expressed in microns). For each test, the load transferred to the wall was measured using the load cell, from which the corresponding shear stress was calculated. These experimentally obtained input-output datasets formed the training data for the neural networks.

The neural network models were trained separately for each filling material—fine sand, river sand, and crusher dust. The input variables consisted of the filling height and

sandpaper grit size, while the output variable was the shear stress acting on the wall of the cylinder. Following training, the models were evaluated using regression analysis (R-value), mean squared error (MSE), and validation through comparison between experimentally measured stresses and surrogate model predictions.

Once an acceptable level of performance was achieved, the trained models were verified using independent datasets that were not used during the training process. The predicted outputs were compared with the experimental results, and an acceptable prediction range of ±10% was adopted by defining upper and lower target limits corresponding to 110% and 90% of the measured values, respectively.

The first surrogate model was developed using the experimental data obtained from tests conducted with fine sand. The experimental measurements are presented in Table 10, which includes the filling height, sandpaper grit size, load cell readings, calculated wall forces, average shear stresses, and shear stresses developed within individual layers.

Table 10: Experimental data obtained for fine sand

Height (mm)	micron	load cell reading (kg)	surface contact area (m^2)	Force on the wall (N)	average shear stress (N/m^2)	Force on the wall for each layer (N)	shear stress on each layer (Pa)
20	425	0.01	0.01	0.10	14.87	0.10	14.87
70	425	0.15	0.02	1.47	63.73	1.37	83.27
120	425	0.29	0.04	2.85	71.87	1.37	83.27
155	425	0.39	0.05	3.83	74.83	0.98	84.97
220	425	0.56	0.07	5.49	75.70	1.67	77.78
278	425	0.73	0.09	7.16	78.09	1.67	87.17
340	425	0.83	0.11	8.14	72.60	0.98	47.97
400	425	0.98	0.13	9.61	72.86	1.47	74.35
445	425	1.13	0.15	11.09	75.52	1.47	99.13

475	425	1.25	0.16	12.26	78.26	1.18	118.96
545	425	1.42	0.18	13.93	77.49	1.67	72.22
55	269	0.08	0.02	0.79	43.26	0.79	43.26
120	269	0.30	0.04	2.94	74.35	2.16	100.66
170	269	0.50	0.06	4.91	87.47	1.96	118.96
215	269	0.52	0.07	5.10	71.93	0.20	13.22
250	269	0.73	0.08	7.16	86.84	2.06	178.44
309	269	0.94	0.10	9.22	90.47	2.06	105.85
400	269	1.15	0.13	11.28	85.50	2.06	68.63
420	269	1.30	0.14	12.75	92.05	1.47	223.04
465	269	1.50	0.15	14.72	95.93	1.96	132.18
520	269	1.75	0.17	17.17	100.08	2.45	135.18
560	269	1.91	0.18	18.74	101.43	1.57	118.96
40	201	0.08	0.01	0.79	59.48	0.79	59.48
90	201	0.20	0.03	1.96	66.09	1.18	71.37
150	201	0.39	0.05	3.83	77.32	1.86	94.17
190	201	0.49	0.06	4.81	76.70	0.98	74.35
265	201	0.73	0.09	7.16	81.92	2.35	95.17
350	201	0.99	0.12	9.71	84.12	2.55	90.97
420	201	1.19	0.14	11.67	84.26	1.96	84.97
500	201	1.42	0.16	13.93	84.46	2.26	85.50
550	201	1.59	0.18	15.60	85.97	1.67	101.11
585	201	1.74	0.19	17.07	88.46	1.47	127.45

The collected data were used to train a feedforward neural network in MATLAB. The model learned the relationship between filling height, wall roughness, and the corresponding shear stress generated along the cylinder wall.

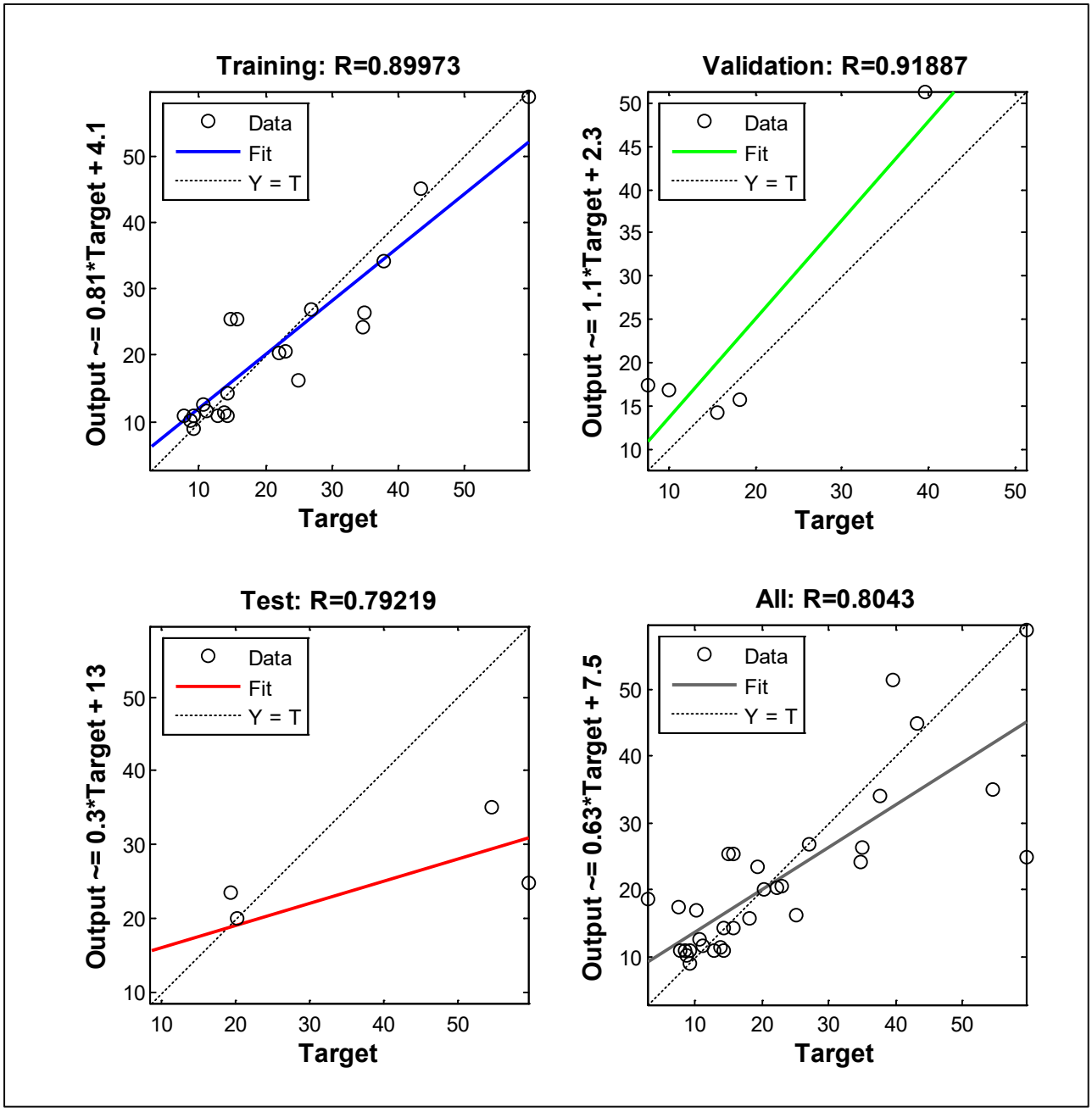

Figure 65: Regression plot of the neural network trained using fine sand data.

The regression analysis of the trained network is presented in Figure 65. After several iterations of training and parameter adjustment, the optimum network achieved a regression coefficient (R) of 0.8043, indicating a satisfactory correlation between the experimental data and the model predictions. The corresponding validation

performance curve is shown in Figure 66, with a mean squared error (MSE) of 57.7348.

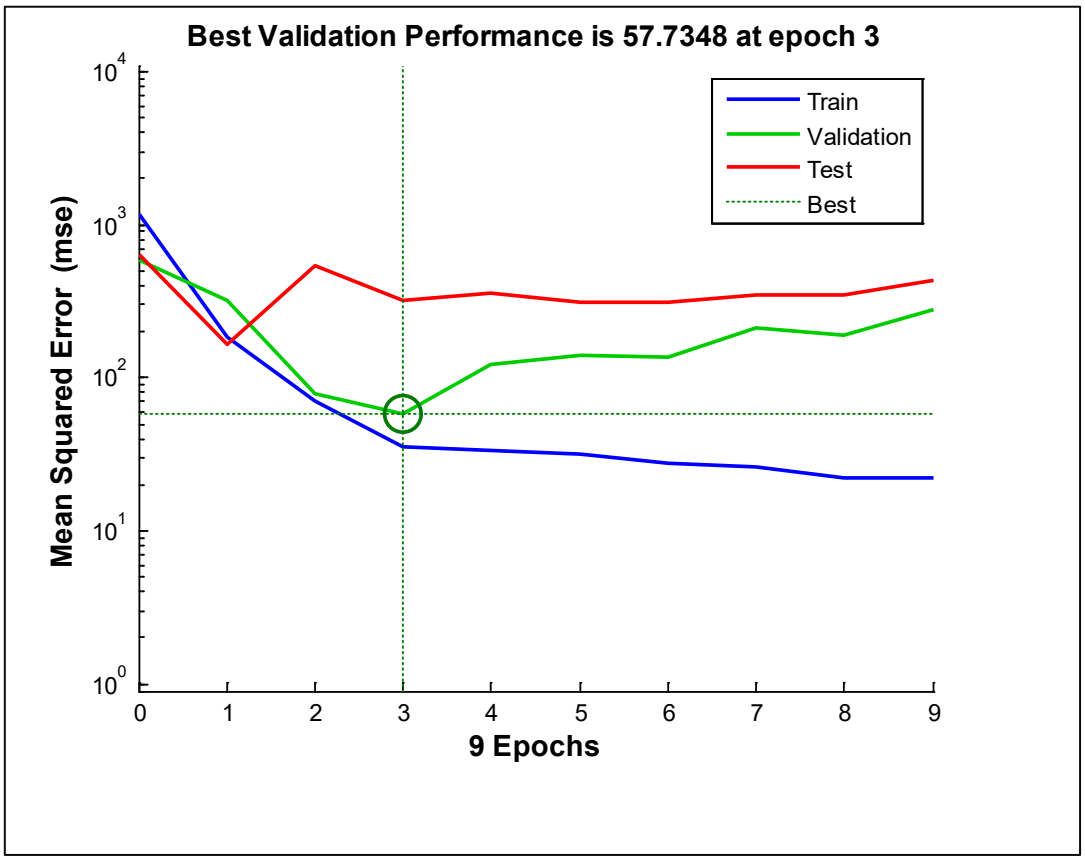

Figure 66: Validation performance of the trained neural network for fine sand

To verify the predictive capability of the surrogate model, an independent set of experimental measurements was compared with the outputs generated by the trained neural network using the same input parameters. For this purpose, initially a data set is generated from lab experiment. The shear stress data is used as the target. Secondly, using the height and the micron of the data from the data set, the shear stress is again generated using the trained surrogate model. This is assumed to be output data. The following table 11 show the data obtained through the lab-based experiment and the surrogate model for the same input factors.

Table 11: Comparison between laboratory measurements and surrogate model predictions for fine sand

Height (mm)	micron	shear stress in the layer obtained from lab (Pa)	shear stress in the layer obtained from surrogate model (Pa)
50	425	35.69	58.01
70	425	133.83	80.33
100	425	79.31	93.23
130	425	79.31	78.32
150	425	104.09	68.14
175	425	71.37	65.96
50	269	53.53	35.90
70	269	237.91	54.73
110	269	81.78	92.02
130	269	193.31	98.88
170	269	118.96	90.67
200	269	109.04	92.34
60	201	79.31	50.35
85	201	142.75	69.11
122	201	104.49	93.64
160	201	93.91	99.28
190	201	89.22	105.82
225	201	25.49	123.80

For model verification, the experimental values were treated as the target data, while the neural network predictions were considered the output data. Upper and lower acceptance limits corresponding to ±10% of the target values were established. The comparison between the target values, prediction limits, and surrogate model outputs is illustrated in Figure 67.

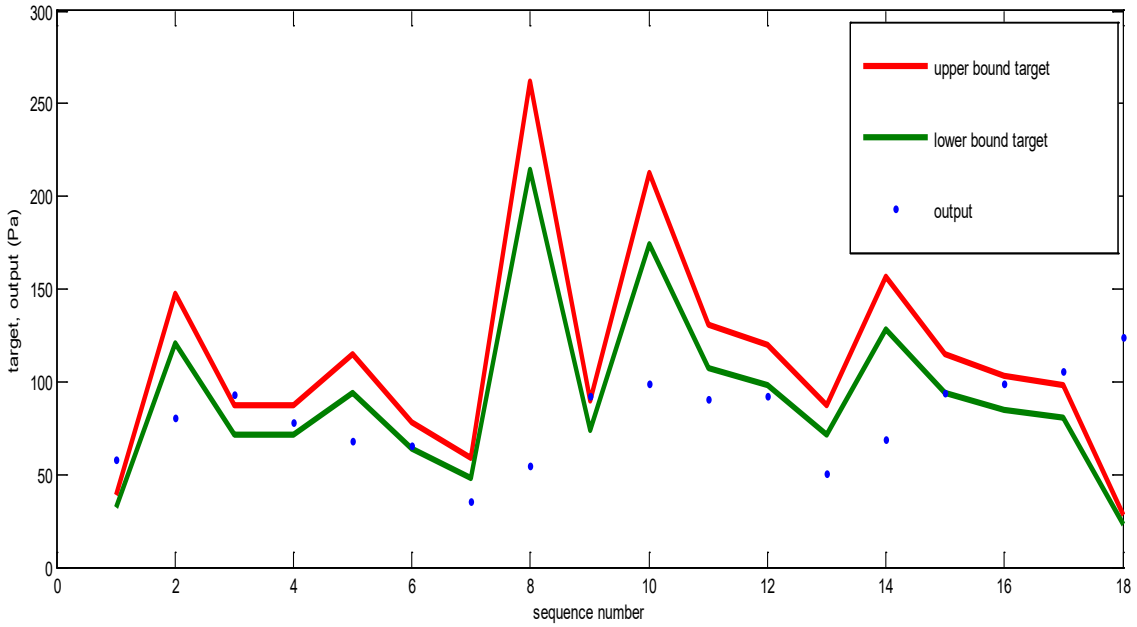

Figure 67: Comparison of the target and the output data from the lab and the surrogate model respectively

Most of the predicted shear stress values lie within or close to the predefined acceptance limits, demonstrating that the trained neural network successfully captured the overall relationship between filling height, wall roughness, and shear stress for fine sand. Although some deviations are observed, the results indicate that the surrogate model provides an acceptable approximation of the experimental behaviour.

The same modelling procedure was repeated using the experimental data obtained from the river sand tests. The laboratory measurements are summarised in Table 12.

Table 12 Experimental data obtained for river sand

Height (mm)	micron	load cell reading (kg)	surface contact area (m^2)	Force on the wall (N)	average shear stress (N/m^2)	force on the wall for each layer (N)	shear stress on each layer (N/m^2)
50	425	0.07	0.02	0.69	41.64	0.69	41.64
80	425	0.18	0.03	1.77	66.91	1.08	109.04
95	425	0.31	0.03	3.04	97.04	1.28	257.74
110	425	0.42	0.04	4.12	113.55	1.08	218.09
135	425	0.56	0.05	5.49	123.36	1.37	166.54
190	425	0.70	0.06	6.87	109.57	1.37	75.70
215	425	0.85	0.07	8.34	117.57	1.47	178.44
245	425	0.95	0.08	9.32	115.32	0.98	99.13
270	425	1.05	0.09	10.30	115.65	0.98	118.96
300	425	1.09	0.10	10.69	108.05	0.39	39.65
325	425	1.14	0.11	11.18	104.32	0.49	59.48
370	425	1.19	0.12	11.67	95.65	0.49	33.04
25	269	0.00	0.01	0.00	0.00	0.00	0.00
55	269	0.10	0.02	0.98	54.07	0.98	99.13
100	269	0.25	0.03	2.45	74.35	1.47	99.13
120	269	0.39	0.04	3.83	96.65	1.37	208.18
150	269	0.51	0.05	5.00	101.11	1.18	118.96
90	269	0.51	0.03	5.00	168.52	0.00	0.00
210	269	0.61	0.07	5.98	86.39	0.98	24.78
230	269	0.72	0.08	7.06	93.10	1.08	163.57
280	269	0.78	0.09	7.65	82.85	0.59	35.69
305	269	0.83	0.10	8.14	80.93	0.49	59.48
330	269	0.89	0.11	8.73	80.21	0.59	71.37

370	269	0.98	0.12	9.61	78.77	0.88	66.91
390	269	1.01	0.13	9.91	77.02	0.29	44.61
420	269	1.08	0.14	10.60	76.47	0.69	69.39
450	269	1.14	0.15	11.18	75.34	0.59	59.48
465	269	1.20	0.15	11.77	76.75	0.59	118.96
45	201	0.04	0.02	0.39	26.44	0.39	26.44
80	201	0.17	0.03	1.67	63.20	1.28	110.46
105	201	0.24	0.04	2.35	67.98	0.69	83.27
140	201	0.39	0.05	3.83	82.85	1.47	127.45
160	201	0.59	0.05	5.79	109.66	1.96	297.39
195	201	0.75	0.06	7.36	114.38	1.57	135.95
205	201	0.80	0.07	7.85	116.06	0.49	148.70
240	201	0.98	0.08	9.61	121.44	1.77	152.95
278	201	1.02	0.09	10.01	109.12	0.39	31.30
295	201	1.22	0.10	11.97	122.99	1.96	349.87
330	201	1.26	0.11	12.36	113.55	0.39	33.99
355	201	1.37	0.12	13.44	114.77	1.08	130.85

The experimental dataset was used to train a separate neural network surrogate model using the same input variables (filling height and sandpaper grit size/micron) and output variable (shear stress).

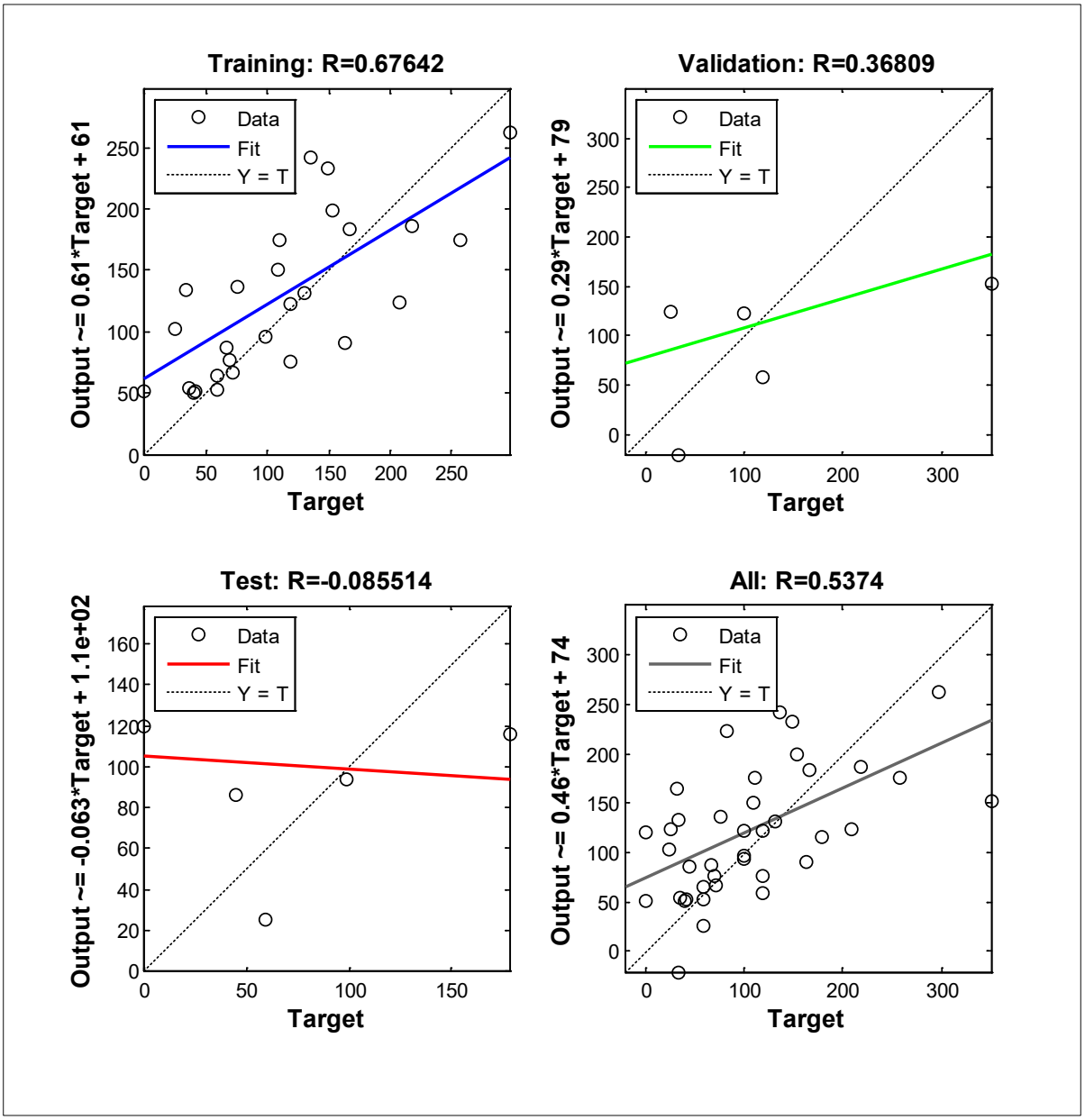

Figure 68: Regression plot of the neural network trained using river sand data

The regression performance of the trained model is presented in Figure 68. Following repeated training and optimisation, the final model achieved a regression coefficient of 0.5374. Although this value is lower than that obtained for fine sand, it still indicates

that the model captured the general trend of the experimental data. The corresponding validation performance is shown in Figure 69.

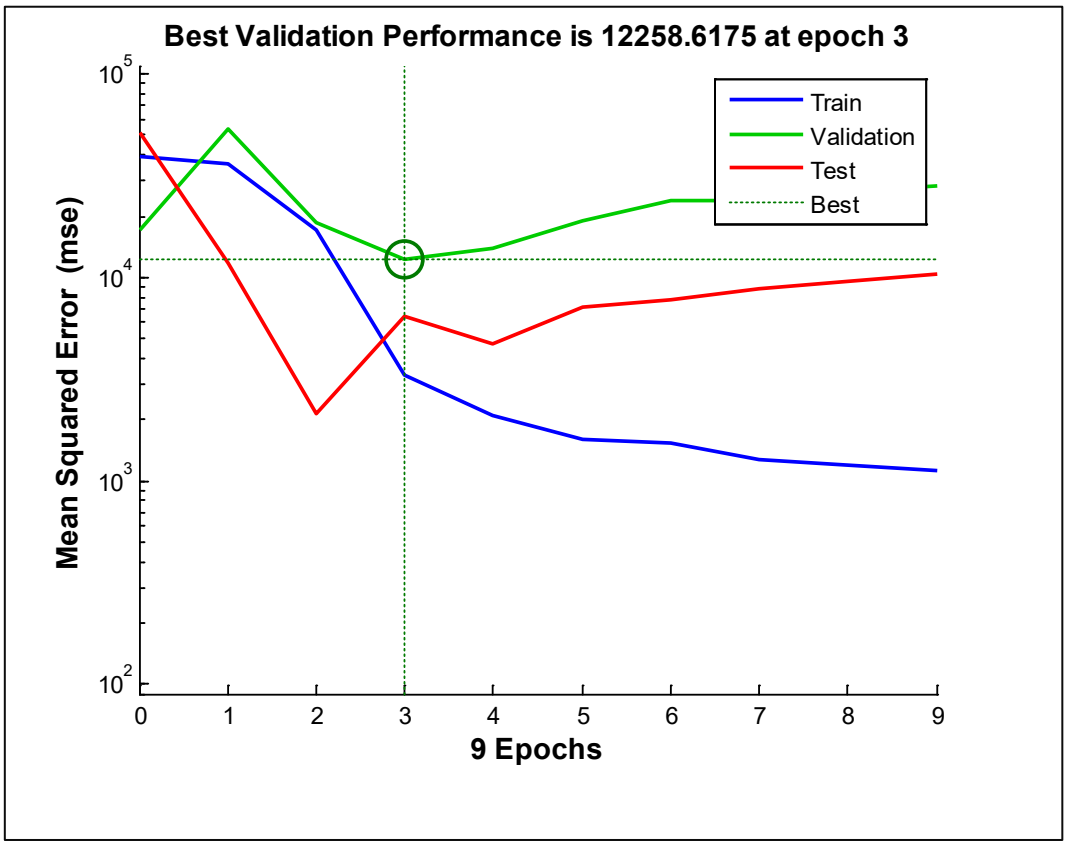

Figure 69: Validation performance curve for the river sand surrogate model

Model verification was carried out by comparing independent laboratory measurements with predictions generated by the trained surrogate model. The comparison is presented in Table 13.

Table 13: Comparison between laboratory measurements and surrogate model predictions for river sand

Height (mm)	micron	shear stress in the layer achieved from the experiment (Pa)	Shear stress in the layer obtained from MATLAB (Pa)
40	425	7.44	143.26
65	425	83.27	145.76
110	425	132.18	149.71
160	425	89.22	150.58

190	425	158.61	143.61
215	425	202.23	131.89
40	269	66.91	83.45
70	269	118.96	116.06
105	269	101.96	147.71
140	269	127.45	159.54
172	269	92.94	155.16
210	269	109.57	134.18
35	201	33.99	36.68
70	201	127.45	51.00
110	201	44.61	88.91
140	201	99.13	126.04
175	201	152.95	151.29
215	201	96.65	151.46

As in the previous case, upper and lower acceptance limits equal to ±10% of the experimental values were established. The comparison between the target values, acceptance limits, and predicted outputs is illustrated in Figure 70.

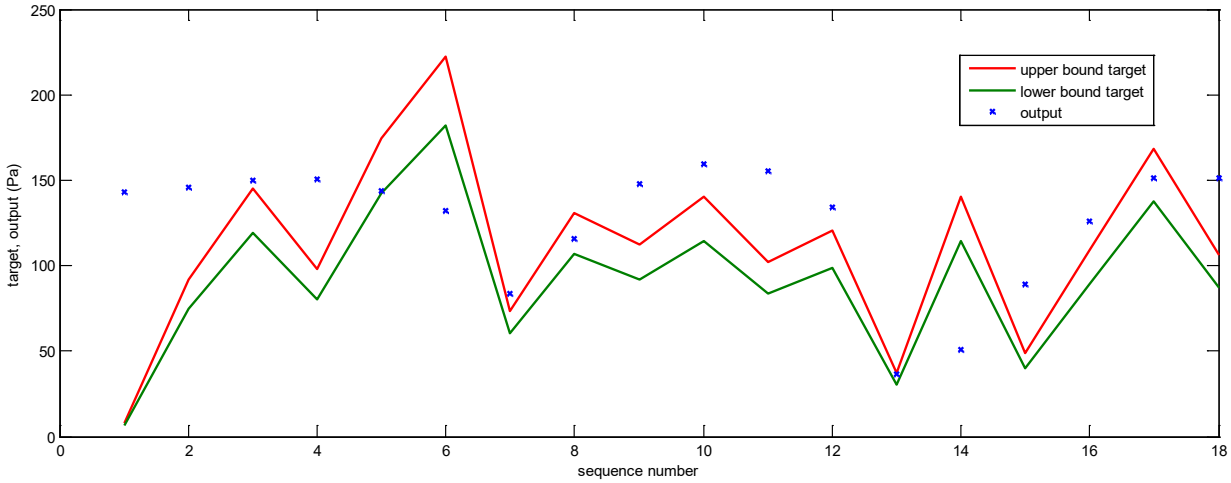

Figure 70: Figure representing the comparison of the output through lab-based experiment and the MATLAB surrogate model

Although the river sand model exhibits greater variability than the fine sand model, most predicted values remain reasonably close to the experimental results. The validation therefore confirms that the surrogate model can represent the overall stress behaviour of river sand under the tested laboratory conditions.

The final surrogate model was developed using the experimental data obtained from the crusher dust tests. The complete experimental dataset is presented in Table 14.

Table 14: Experimental data obtained for crusher dust

Height (mm)	micron	load cell reading (kg)	surface contact area (m^2)	Force on the wall (N)	average shear stress (N/m^2)	force on each layer (N)	shear stress on each layer (N/m^2)
20	425	0.07	0.01	0.69	104.09	0.69	104.09
60	425	0.18	0.02	1.77	89.22	1.08	81.78
100	425	0.28	0.03	2.75	83.27	0.98	74.35
130	425	0.40	0.04	3.92	91.51	1.18	118.96
160	425	0.55	0.05	5.40	102.23	1.47	148.70
200	425	0.69	0.07	6.77	102.60	1.37	104.09
232	425	0.86	0.08	8.44	110.24	1.67	157.99
271	425	1.03	0.09	10.10	113.03	1.67	129.63
298	425	1.16	0.10	11.38	115.76	1.28	143.19
340	425	1.31	0.11	12.85	114.58	1.47	106.21
364	425	1.46	0.12	14.32	119.28	1.47	185.87
410	425	1.58	0.14	15.50	114.61	1.18	77.58
20	269	0.00	0.01	0.00	0.00	0.00	0.00
50	269	0.07	0.02	0.69	41.64	0.69	69.39
75	269	0.17	0.02	1.67	67.41	0.98	118.96
130	269	0.29	0.04	2.85	66.34	1.18	64.89
140	269	0.41	0.05	4.02	87.09	1.18	356.87
175	269	0.58	0.06	5.69	98.56	1.67	144.45

192	269	0.73	0.06	7.16	113.07	1.47	262.41
228	269	0.89	0.08	8.73	116.09	1.57	132.18
270	269	1.06	0.09	10.40	116.75	1.67	120.37
300	269	1.17	0.10	11.48	115.98	1.08	109.04
330	269	1.29	0.11	12.66	116.25	1.18	118.96
360	269	1.45	0.12	14.23	119.78	1.57	158.61
20	201	0.01	0.01	0.10	14.87	0.10	14.87
60	201	0.06	0.02	0.59	29.74	0.49	37.17
95	201	0.16	0.03	1.57	50.09	0.98	84.97
125	201	0.27	0.04	2.65	64.24	1.08	109.04
140	201	0.40	0.05	3.92	84.97	1.28	257.74
165	201	0.60	0.05	5.89	108.14	1.96	237.91
190	201	0.80	0.06	7.85	125.22	1.96	237.91
250	201	1.03	0.08	10.10	122.53	2.26	114.00
265	201	1.26	0.09	12.36	141.40	2.26	456.00
300	201	1.47	0.10	14.42	145.72	2.06	178.44
325	201	1.71	0.11	16.78	156.47	2.35	285.50
365	201	1.97	0.12	19.33	160.51	2.55	193.31

Using these data, a neural network was trained with filling height and sandpaper grit size as input variables and wall shear stress as the output variable.

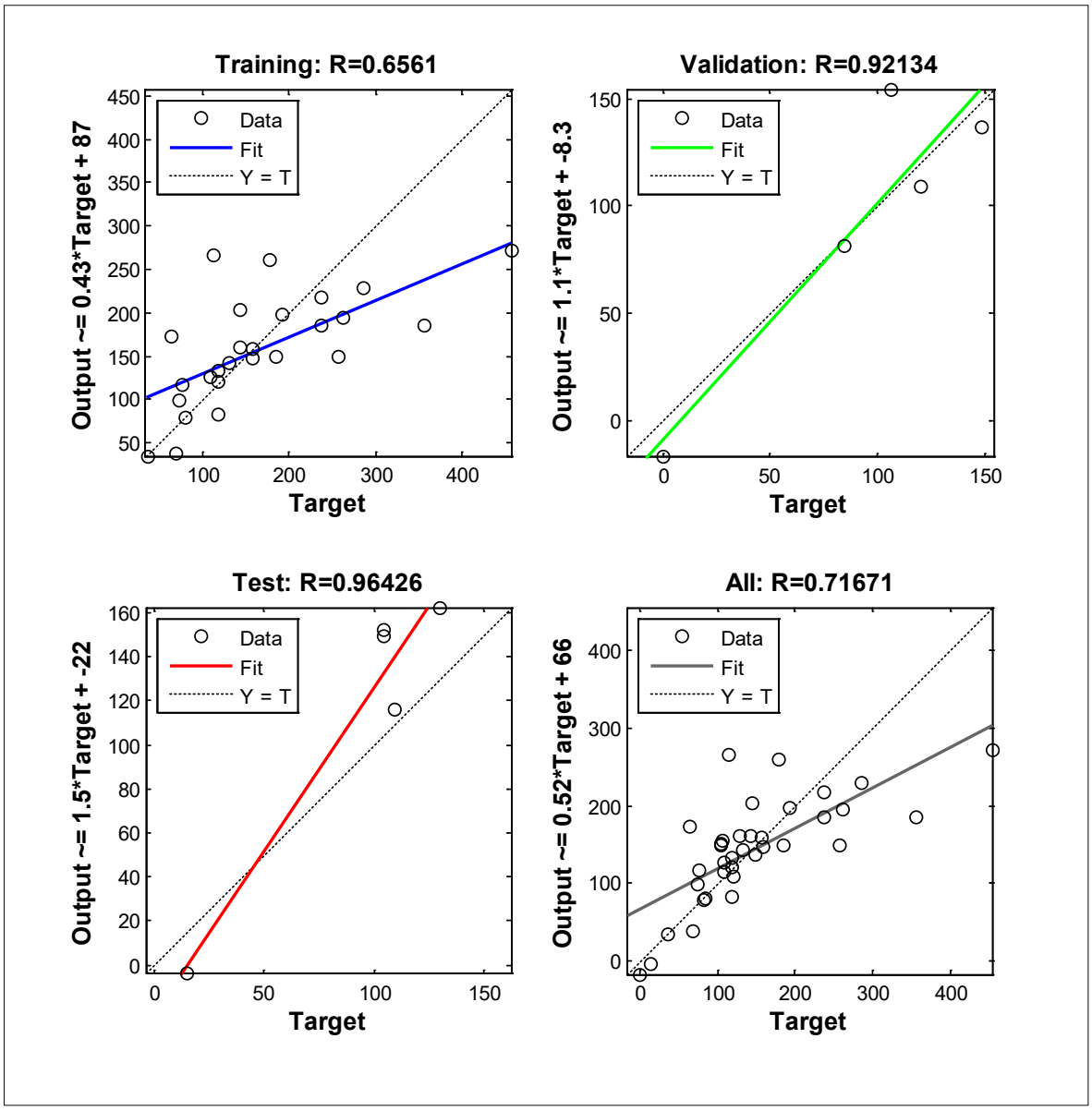

Figure 71: Regression plot of the neural network trained using crusher dust data

The regression performance of the trained network is presented in Figure 71. Following repeated optimisation, the final surrogate model achieved a regression coefficient of 0.7167 with a mean squared error of 573.9544. Although the prediction error is larger than that obtained for fine sand, the regression coefficient indicates that the model adequately represents the experimental response. The validation performance curve is shown in Figure 72.

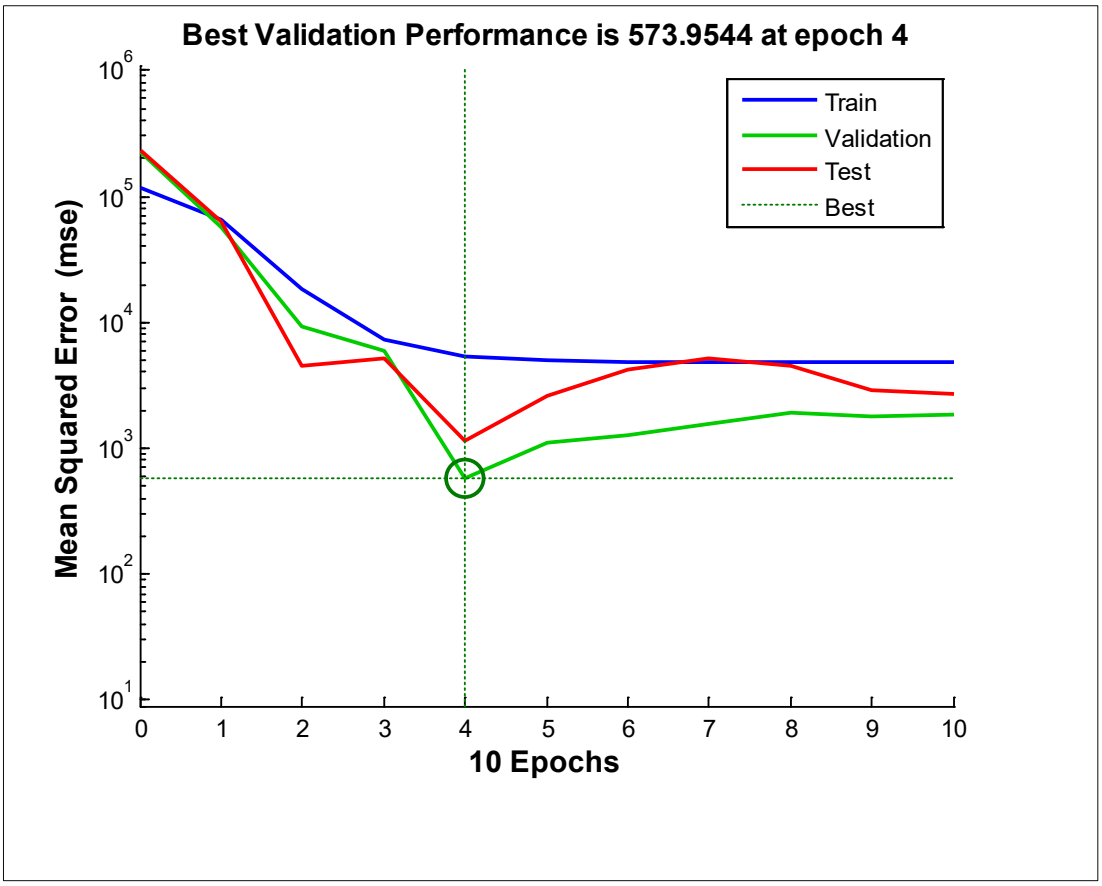

Figure 72: Validation performance curve for the crusher dust surrogate model

The predictive capability of the trained model was assessed by comparing the surrogate model outputs with an independent set of laboratory measurements, as presented in Table 15.

Table 15: Comparison between laboratory measurements and surrogate model predictions for crusher dust

Height (mm)	micron	shear stress in the layer achieved from the lab (Pa)	Shear stress in the layer obtained from MATLAB (Pa)
30	425	49.57	87.56
75	425	92.52	91.37
110	425	152.95	97.62
150	425	104.09	134.87
190	425	215.61	109.26
230	425	148.70	153.99

27	269	33.04	0.75
60	269	81.11	49.55
95	269	161.44	252.16
135	269	133.83	338.37
170	269	178.44	244.64
195	269	154.64	185.09
30	201	0.00	-1.01
65	201	67.98	54.07
100	201	110.46	100.51
130	201	148.70	209.29
160	201	109.04	262.84
190	201	128.87	261.84

The experimental values were again treated as the target data, while the neural network outputs represented the predicted values. Upper and lower acceptance limits of ±10% were defined, and the comparison is illustrated in Figure 73.

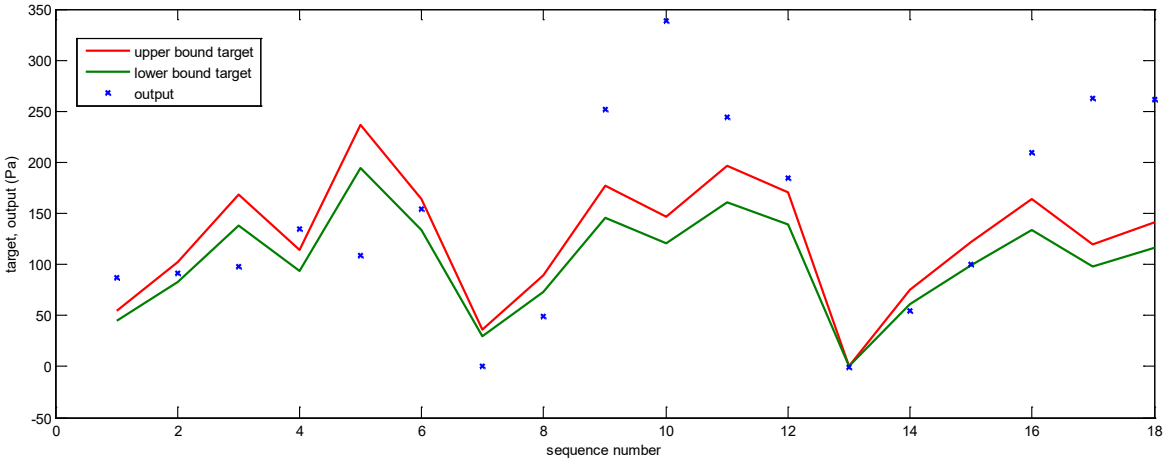

Figure 73: Comparison of the data (output and target data) for crusher dust

The above figure (73) reflects the output falls within the limits of the target data. The results indicate that the surrogate model captures the overall trend of the experimental data despite some local deviations. Most predictions remain within or close to the

predefined acceptance limits, confirming that the trained neural network provides a satisfactory representation of the laboratory behaviour.

The three neural network surrogate models developed in this study demonstrate that machine learning techniques can successfully approximate the shear stress behaviour of granular materials within a cylindrical silo under different wall roughness conditions. Separate models were developed for fine sand, river sand, and crusher dust because each material exhibits different particle characteristics and frictional behaviour, resulting in different stress distributions.

Among the three materials, the surrogate model for fine sand achieved the highest prediction accuracy with an R-value of 0.8043, followed by crusher dust (0.7167) and river sand (0.5374). The differences in performance are likely attributable to the inherent variability of the experimental data and the complexity of the interaction between particle properties and wall friction.

Model validation using independent datasets demonstrated that the predicted outputs generally remained within the adopted ±10% acceptance limits. Although individual prediction errors were observed, the surrogate models consistently reproduced the overall experimental trends and therefore provide a practical alternative to repeated laboratory testing.

Overall, the results confirm that neural network-based surrogate models can effectively predict shear stress development in cylindrical silo structures using a limited number of input variables. Once trained, these models provide rapid stress predictions with substantially lower computational and experimental effort than conventional analytical or numerical approaches. The validated surrogate models developed in this chapter are subsequently employed in Chapter 7 for structural safety and reliability assessment.

Chapter 6: Model surrogation for the safety assessment of backfilling mine stopes

Backfilling is an essential operation in underground mining, involving the refilling an excavated area with suitable filling material. It is necessary in construction to stabilize the soil around structures like foundations and trenches, improve ground stability, minimise surface subsidence, and facilitate the safe extraction of adjacent ore bodies. The mechanical behaviour of backfilled stopes is governed by several interacting factors, including the properties of the fill material, the geometry of the excavation, and the interaction between the backfill and the surrounding rock mass. Therefore, accurate prediction of stress development within backfilled stopes is critical for maintaining structural stability and ensuring safe mining operations.

Among the various mining methods employed worldwide, backfilled stopes are extensively used in Australia and other mining-intensive countries due to their ability to improve operational safety and maximise ore recovery. During the filling process, both vertical and shear stresses develop within the backfill mass. These stresses influence the stability of exposed cemented backfill faces, barricades, and surrounding rock structures. An inaccurate estimation of these stresses may result in structural instability or conservative designs that unnecessarily increase operational costs. Therefore, reliable prediction of stress distributions within backfilled stopes remains an important research problem in rock mechanics and mining engineering.

Traditionally, stress distributions in backfilled stopes have been evaluated using analytical solutions, laboratory experiments, and numerical modelling techniques such as the Discrete Element Method (DEM) and the Finite Element Method (FEM). Although these approaches provide detailed insight into the mechanical behaviour of backfilled systems, they are computationally demanding when repeated analyses are required for probabilistic reliability assessment. This limitation becomes particularly significant when Monte Carlo Simulation (MCS) is employed, where thousands or even millions of structural evaluations may be necessary to quantify uncertainty and estimate the probability of failure.

To address this limitation, this chapter investigates the application of surrogate modelling for the safety assessment of backfilled mine stopes. Like the surrogate models presented in Chapter 5, which were developed using laboratory experiment data for silo structures, the surrogate models presented herein are also trained using data obtained directly from laboratory experiments. The schematic testing setup shown in Figure 27 was adapted to simulate backfilled mine stopes. The experimental procedure was designed to reproduce the stress development occurring within backfilled stopes under controlled conditions while systematically varying the governing input parameters. The resulting experimental dataset was subsequently employed to develop artificial neural network-based surrogate models capable of rapidly predicting the corresponding stress responses.

The proposed surrogate modelling framework was implemented and trained within the MATLAB environment. Following model development, its predictive capability was evaluated through regression analysis, validation performance, and comparison with independent experimental observations. Furthermore, the predictions generated by the surrogate model were cross-validated against experimentally verified DEM-based numerical simulations to ensure consistency with established computational approaches. The principal objective of this chapter is to demonstrate that surrogate modelling provides an accurate and computationally efficient alternative for evaluating the safety performance of backfilled mine stopes, thereby enabling rapid probabilistic reliability assessment.

Chapter 6.1: Performance of backfilled mine stopes

The mechanical behaviour of backfilled mine stopes has been the subject of extensive investigation because of its direct influence on underground excavation stability and mine’s safety. Previous research has primarily focused on developing analytical formulations, numerical models, and laboratory investigations to improve the understanding of stress distributions and arching mechanisms within backfilled stopes.

Analytical approaches have sought to improve the prediction of vertical and shear stresses by extending classical formulations. For example, Kamash et al. (2022) proposed a modified analytical model based on Marston's equation that incorporates

an additional parameter representing the arching effect within inclined backfilled stopes. Their formulation demonstrated improved agreement with previously reported analytical and numerical solutions. Similarly, Li and Aubertin (2010) developed an analytical solution describing the nonlinear distribution of total and effective stresses in vertical backfilled stopes while accounting for positive pore water pressure, thereby providing a more realistic representation of stress development within cemented backfills.

Numerical modelling has also been extensively employed to investigate stress behaviour under conditions that cannot readily be represented analytically. Sobhi and Li (2017) conducted a numerical investigation of the stresses in backfilled stopes overlying a sill mat. Parameters such as mine depth and excavation of the underlying stope below the sill mat (horizontal pillar) not considered in the previous studies were considered in the experiment while performing the stress analysis. Liu et al. (2016, 2017, 2021) further demonstrated the importance of considering the mechanical interaction between the backfill and surrounding rock through interface elements and variable interface stiffness. Their studies showed that the backfill-rock interface significantly influences stress transfer and should therefore be incorporated into numerical analysis whenever realistic stress predictions are required.

Three-dimensional investigations have also highlighted the complexity of stress development within inclined stopes. Yan et al. (2019) developed a three-dimensional analytical solution to evaluate arching effects and demonstrated that two-dimensional plane-strain assumptions may overestimate the stresses acting on retaining barricades. Similarly, Falaknaz et al. (2015) investigated stress interactions between two adjacent backfilled stopes within an elasto-plastic rock mass, illustrating the influence of neighbouring excavations on the overall stress field. Rajeev et al. (2016) and Jahanbakhshzadeh et al. (2017) further proposed improved analytical formulations for predicting average vertical stresses while considering variations in stope geometry and wall inclination.

Collectively, these studies have substantially advanced the understanding of stress development within backfilled mine stopes. However, most existing approaches remain computationally intensive, particularly when applied within probabilistic

frameworks requiring repeated structural analyses. Although analytical and numerical methods can accurately estimate stress distributions, they are generally unsuitable for large-scale Monte Carlo simulations due to the considerable computational effort involved.

Furthermore, the application of machine learning-based surrogate modelling to backfilled mine stopes remains relatively unexplored. Existing studies have largely focused on improving analytical formulations or enhancing numerical simulation techniques rather than replacing these computationally expensive models with efficient data-driven alternatives. Thus, a significant research gap exists in the development of surrogate models capable of rapidly predicting stress responses while maintaining sufficient accuracy for reliability assessment.

The research presented in this chapter addresses this gap by developing artificial neural network-based surrogate models using experimentally generated datasets. By replacing repeated numerical or laboratory analyses with computationally efficient surrogate predictions, the proposed framework facilitates rapid Monte Carlo-based reliability assessment while substantially reducing computational cost. The methodology developed herein provides a practical foundation for uncertainty quantification and performance-based safety assessment of underground backfilled mining systems.

Chapter 6.2: Laboratory setup for backfilled mine stopes

This chapter describes the laboratory apparatus developed to generate the experimental data required for constructing the surrogate model for the safety assessment of backfilled mine stopes. The primary objective of the laboratory experiment was to quantify the shear stresses developed along the wall of a representative stope model under different filling conditions. The experimental observations were subsequently used to train and validate the artificial neural network-based surrogate model presented in this chapter.

To ensure that the experimental results realistically represented the physical behaviour of backfilled mine stopes, the laboratory apparatus was designed to

reproduce the principal stress transfer mechanisms occurring during the backfilling process. The experimental configuration, illustrated schematically in Figure 27 and shown in Figure 74, was adapted from the laboratory setup developed in Chapter 5 for silo structures. This approach ensured methodological consistency while allowing the proposed surrogate modelling framework to be evaluated across different engineering applications.

The experimental apparatus consisted of a cylindrical tube suspended from a rigid support frame positioned above a digital weighing scale. A load cell was attached to the external wall of the cylinder to measure the forces transmitted through wall friction during filling. Granular materials, namely coarse sand and crushed stone, were progressively introduced into the cylinder to simulate the backfilling process.

As the filling material accumulated, two stress components were generated within the system. The first was the vertical stress acting on the base of the cylinder, measured using the weighing scale. The second was the shear stress mobilised along the internal wall of the cylinder, measured using the load cell. In addition, the height of the fill was recorded throughout the experiment using a measuring tape. These measurements provided the information required to calculate the corresponding vertical and shear stresses, which subsequently formed the dataset used for surrogate model development.

Figure 74: Laboratory setup for the experimental simulation of backfilled mine stopes

Chapter 6.3: Laboratory testing implementation

This chapter presents the experimental methodology adopted to generate the dataset used for surrogate model development. The laboratory testing was designed to investigate the influence of material properties, filling height, and wall roughness on the development of stresses within the laboratory model. Emphasis was placed on

producing a sufficiently representative dataset for machine learning while maintaining consistency with the physical behaviour of backfilled mine stopes.

Chapter 6.3.1: Defining layers for the testing

The laboratory experiments required measurements to be taken at multiple elevations during the filling process. Previous investigations have commonly divided the fill height into equally spaced layers, allowing stress measurements to be obtained at predetermined intervals. The number of layers is typically selected according to the desired experimental resolution and the total filling height.

In the present study, however, the primary objective was the development of an accurate surrogate model rather than the detailed investigation of stress variation at uniformly spaced elevations. Therefore, the experimental procedure was designed to maximise the number of measurement points instead of maintaining equal layer thicknesses. Measurements were therefore recorded at selected fill heights that provided a broader distribution of stress observations across the complete filling process.

This approach increased the diversity of the training dataset and enabled the surrogate model to capture the nonlinear relationship between the governing input parameters and the corresponding stress response more effectively. The adoption of non-uniform measurement intervals therefore improved the overall representativeness of the experimental data while supporting the development of a robust machine learning model.

Chapter 6.3.2: Required input data for the experiments

The experimental process considered three principal input variables governing stress development within backfilled mine stopes:

- the type of filling material;
- the filling height; and
- the roughness of the confining surface.

These variables were selected because they represent the primary factors influencing stress transfer between the backfill material and the surrounding excavation walls. Two granular materials, namely coarse sand and crushed stone, were selected as representative backfill materials due to their widespread application in underground mining operations. The physical characteristics of these materials are shown in Figures 75 and 76.

The fill height was measured throughout each experiment using a measuring tape, while wall roughness was simulated by attaching commercial sandpaper to the internal surface of the cylindrical tube. Three surface roughness conditions were investigated using P40, P60 and P80 sandpapers. Among these, P40 possessed the greatest surface roughness, whereas P80 represented the smoothest surface. Varying the surface roughness enabled the influence of wall friction on stress development to be systematically evaluated.

Figure 75: Coarse sand used as the experimental backfill material

Figure 76: Crushed stone used as the experimental backfill material

Chapter 6.3.3: Targeted output variables from the experiments

This sub-chapter discusses the output variable, which was derived from the laboratory experiments. These variables were subsequently used to construct a surrogate model to evaluate the stress developed on the silo caused due to fillings. Vertical stresses developed on the base of the cylinder and shear stresses developed along the wall of the structure were assumed as the milestone for the reliability analysis of the structure. However, for the purpose of the study, evaluating the maximum shear stress along the wall of the cylinder was considered the milestone of the laboratory experiment. Unlike vertical stress, shear stress is also affected by factors other than the weight of the filling materials distributed to the wall.

During the laboratory experiment, both vertical stresses were examined to conduct the reliability analysis of the structure. Similarly, during the filling process in the cylinder, shear stress was also developed in the tube. It occurred along the wall of the tube. The maximum shear stress along the wall of the cylinder, τ max, was calculated by:

$$\tau_{max} = \frac{4}{3}\left[\frac{F}{\Pi R^2}\right] \quad (6.1)$$

F represents the force created due to the filling materials, and R denotes the radius of the cylinder. Also, the average shear stress, τ average, was calculated using the following formula:

$$\tau_{average} = \frac{F}{\Pi R^2} \quad (6.2)$$

Chapter 6.3.4 Implementation of the laboratory procedures

The laboratory experiment was conducted using two backfill materials (coarse sand and crushed stone) and three wall roughness conditions (P40, P60 and P80), resulting in six independent experimental configurations. The height of the layer of each fill may vary. It is not necessary to conduct the experiment based on the equal individual height, since the experiment is more focused on creating the surrogate model rather than wholly analysing the shear stresses for each individual layer.

The laboratory procedures were conducted for 3 different scenarios. In the first situation, the tube surface was internally covered with P40 sandpaper. Each material was filled into the tube.

To find the weight of each layer, the total weight of the preceding layer was subtracted from the weight of the previous layer. For example, to calculate the mass of the second layer, readings of the 1st layer were recorded on the load cell as well as on the base weighing scale as M1 for the respective readings. When the material was filled up to the height of the 2nd layer, readings were recorded as M2, respectively. Since the base weighing scale provided the mass of the material above the base, M2–M1 readings from the base provided the mass of the 2nd layer spread to the base. This mass was used as the weight of the filling material directly above the base, and this was used to compute the vertical stress developed above the base by the filling material.

Similarly, there were readings on the load cell. The load cell measures the weight of the material spread on the wall of the tube. Therefore, M2–M1 readings from the load cell provided the mass of the 2nd layer spread to the wall. This mass was also

converted to the weight for the computation of shear stress developed along the wall of the tube.

The process was repeated for the 2nd and 3rd situations, where the tube internal This procedure was repeated for each measurement level under all three surface roughness conditions. The complete experimental procedures therefore generated a comprehensive dataset covering a range of filling heights, material types, and wall friction conditions. The resulting database formed the foundation for training, validating, and evaluating the artificial neural network-based surrogate model developed in the subsequent sections.

Chapter 6.4: Results and Analysis

The experimental data obtained from the laboratory were fed back into the MATLAB software for the development of neural network-based surrogate models. The objective of the surrogate modelling process was to establish a computationally efficient representation of the stress behaviour observed during the laboratory experiments while maintaining an acceptable level of prediction accuracy. Based on the experimental process, the principal variables influencing the stress response were identified as the load recorded by the wall-mounted load cell and the surface roughness represented by the sandpaper grade. Therefore, these variables were adopted as the primary inputs for the surrogate model.

The experimental investigation focused on modelling the shear stress developed along the wall of the cylindrical apparatus during the filling process. For each experimental configuration, the recorded input variables and the corresponding shear stress values were compiled into a training dataset. These datasets were subsequently used to train feedforward neural network models in MATLAB. The training process was repeated iteratively by adjusting the network parameters until satisfactory convergence between the predicted and measured responses was achieved.

Following model development, the predictive capability of each surrogate model was evaluated using multiple validation techniques, including regression analysis, mean squared error (MSE), validation performance curves, and comparisons between

predicted outputs and experimentally measured target values. These corresponding validation approaches provided an assessment of both the learning capacity and the generalisation performance of the developed models.

Table 16 presents the experimental data collected during the filling of coarse sand under different wall roughness conditions. The dataset includes the filling height, surface roughness, load cell readings, calculated forces, and the corresponding average and layer-wise shear stresses. These measurements formed the training dataset for the neural network surrogate model.

Table 16: Experimental data obtained for coarse sand

Height (mm)	micron	load cell reading (kg)	surface contact area (m^2)	Force on the wall (N)	average shear stress (N/m^2)	force on each layer (N)	shear stress on each layer (N/m^2)
25	425	0.00	0.01	0.00	0.00	0.00	0.00
50	425	0.07	0.02	0.69	41.64	0.69	83.27
85	425	0.24	0.03	2.35	83.97	1.67	144.45
110	425	0.35	0.04	3.43	94.63	1.08	130.85
140	425	0.44	0.05	4.32	93.47	0.88	89.22
185	425	0.53	0.06	5.20	85.20	0.88	59.48
220	425	0.66	0.07	6.48	89.22	1.28	110.46
240	425	0.75	0.08	7.36	92.94	0.88	133.83
280	425	0.87	0.09	8.54	92.40	1.18	89.22
315	425	0.96	0.10	9.42	90.63	0.88	76.47
350	425	1.08	0.12	10.60	91.77	1.18	101.96
370	425	1.21	0.12	11.87	97.26	1.28	193.31
30	269	0.00	0.01	0.00	0.00	0.00	0.00
55	269	0.11	0.02	1.08	59.48	1.08	130.85
100	269	0.33	0.03	3.24	98.14	2.16	145.39
125	269	0.51	0.04	5.00	121.34	1.77	214.12
155	269	0.63	0.05	6.18	120.88	1.18	118.96

185	269	0.85	0.06	8.34	136.64	2.16	218.09
230	269	1.01	0.08	9.91	130.59	1.57	105.74
255	269	1.15	0.08	11.28	134.12	1.37	166.54
305	269	1.24	0.10	12.16	120.91	0.88	53.53
335	269	1.34	0.11	13.15	118.96	0.98	99.13
380	269	1.41	0.13	13.83	110.35	0.69	46.26
395	269	1.48	0.13	14.52	111.43	0.69	138.78
20	201	0.02	0.01	0.20	29.74	0.20	29.74
40	201	0.09	0.01	0.88	66.91	0.69	104.09
80	201	0.20	0.03	1.96	74.35	1.08	81.78
100	201	0.37	0.03	3.63	110.04	1.67	252.78
120	201	0.54	0.04	5.30	133.83	1.67	252.78
160	201	0.64	0.05	6.28	118.96	0.98	74.35
200	201	0.69	0.07	6.77	102.60	0.49	37.17
225	201	0.77	0.07	7.55	101.77	0.79	95.17
240	201	0.95	0.08	9.32	117.72	1.77	356.87
290	201	1.03	0.10	10.10	105.63	0.79	47.58
315	201	1.13	0.10	11.09	106.68	0.98	118.96
360	201	1.18	0.12	11.58	97.48	0.49	33.04

These data were fed into MATLAB to create a trained neural network based surrogate model. After retraining the surrogate model repeatedly, the trained surrogate model was created. Figure 77 shows the efficacy of the trained surrogate model for the analysis of the shear stress along the wall while filling coarse sand.

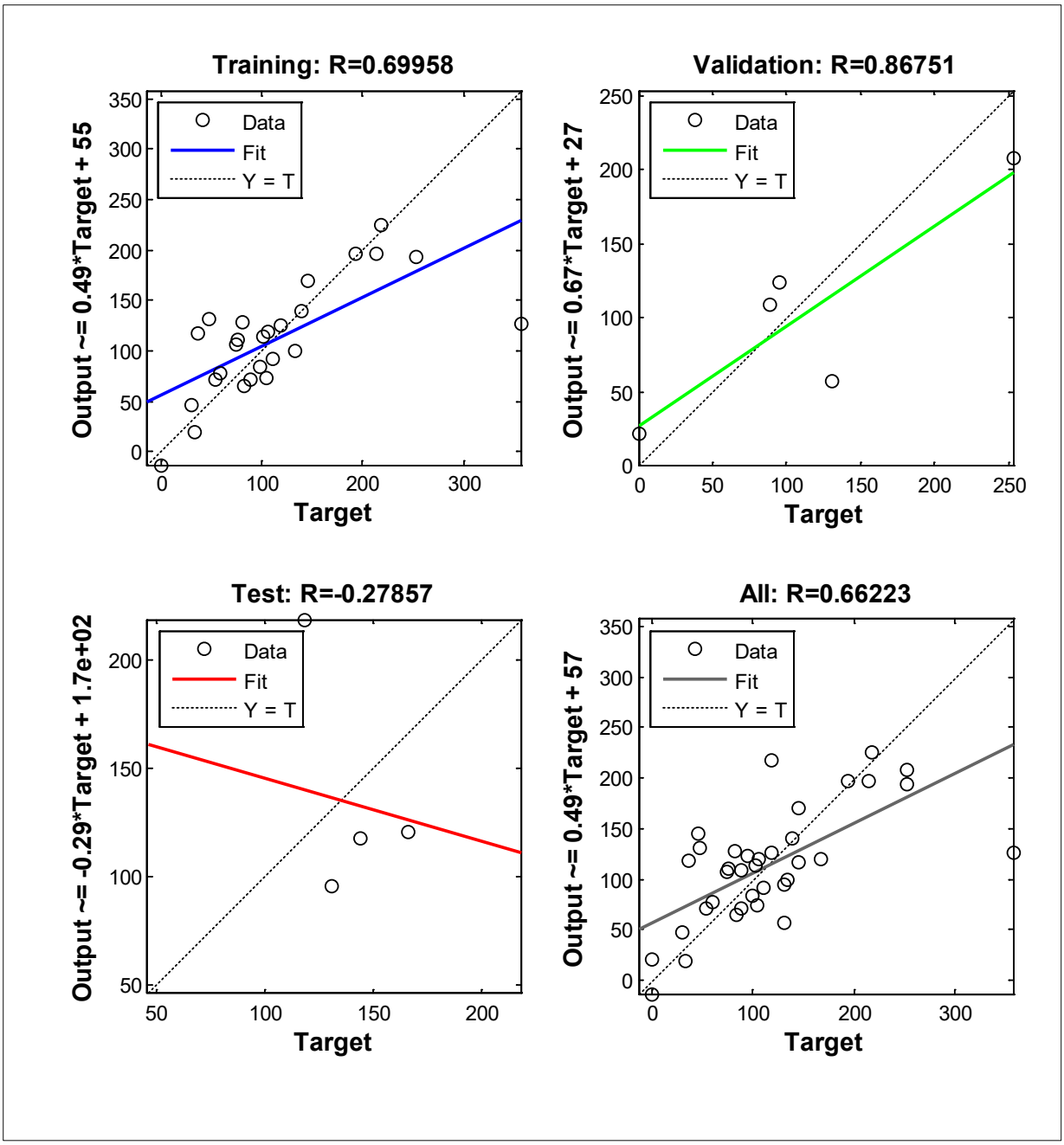

Figure 77: Regression plot of the neural network trained using coarse sand data

After repeated training iterations, the neural network achieved a regression coefficient (R) of 0.6623, as illustrated in Figure 77. Although this regression value is lower than those typically associated with highly accurate prediction models, it represents the highest level of performance obtained using the available experimental dataset. The corresponding validation performance curve is presented in Figure 78, where the mean squared error indicates the prediction error during the training process.

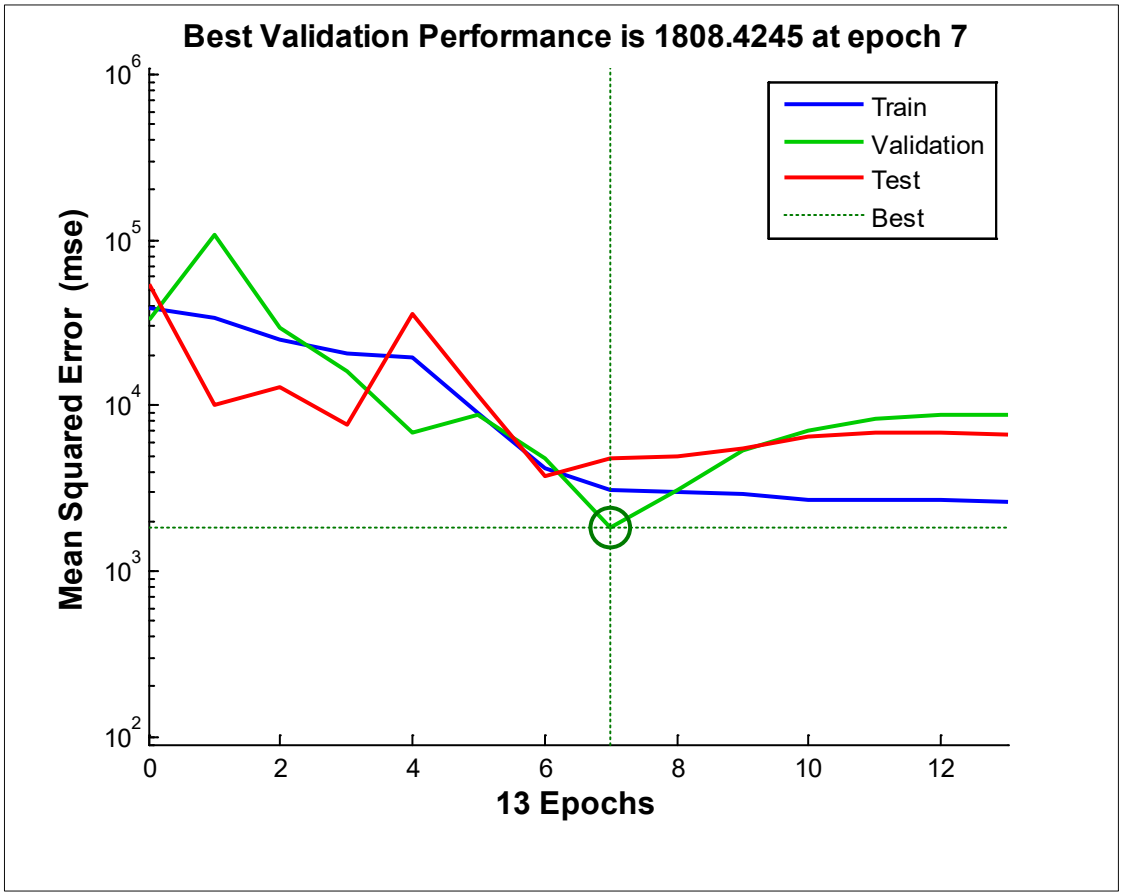

Figure 78: Validation performance of the trained neural network for coarse sand

The relatively modest regression coefficient can primarily be attributed to the limited size of the experimental dataset and the inherent variability associated with laboratory measurements. Unlike numerical simulations, laboratory experiments are influenced by unavoidable uncertainties arising from material heterogeneity, measurement precision, and experimental handling. Therefore, some deviation between the predicted and measured responses is expected.

To further evaluate the predictive capability of the surrogate model, an independent verification exercise was undertaken. New input combinations were introduced into both the laboratory experiment and the trained neural network model, and the corresponding shear stress values were compared. The results are summarised in Table 17.

Table 17: Comparison between laboratory measurements and surrogate model predictions for coarse sand

Height (mm)	micron	shear stress in the layer obtained from the lab (Pa)	shear stress in the layer obtained from the surrogate model (Pa)
90	425	56.17	146.10
130	425	96.65	51.72
150	425	208.18	49.12
200	425	89.22	91.22
250	425	59.48	122.84
280	425	138.78	101.77
40	269	29.74	89.35
80	269	96.65	168.93
120	269	22.30	227.41
160	269	89.22	169.61
200	269	118.96	191.14
240	269	89.22	154.53
38	201	31.30	85.52
90	201	97.23	162.47
120	201	178.44	197.82
165	201	138.78	80.19
185	201	148.70	43.27
255	201	63.73	509.04

For verification purposes, the experimentally measured values were treated as the target outputs, whereas the predictions generated by the surrogate model represented the model outputs. To assess prediction accuracy, upper and lower acceptance limits were established at ±10% of the target values. Figure 79 compares the surrogate model predictions with these acceptance boundaries.

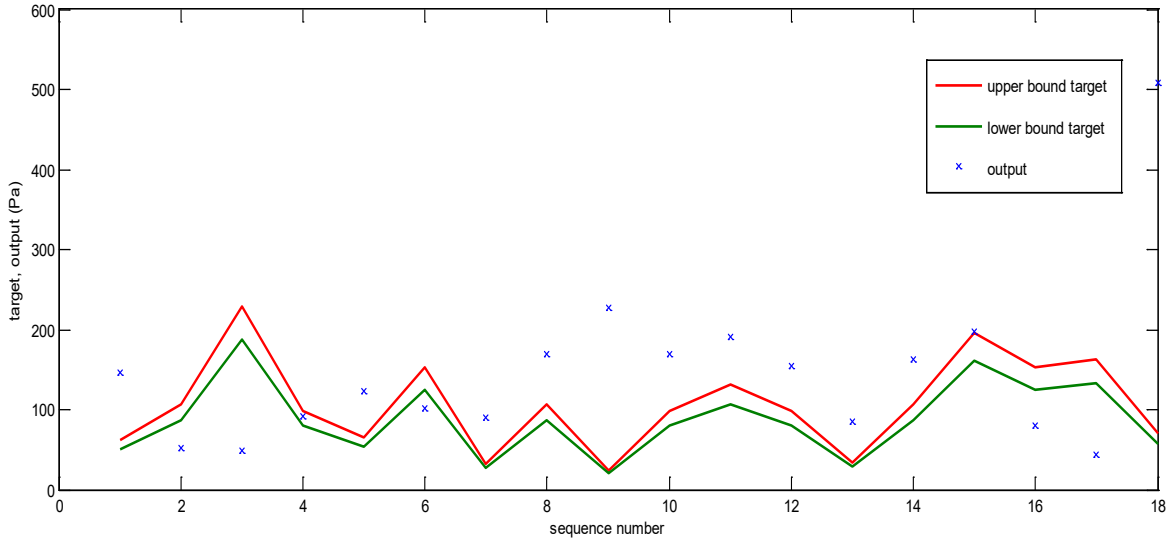

Figure 79: Comparison of the target and the output from the lab data and the surrogate model respectively for coarse sand

The above table 17 and the above figure 79 presents the effectiveness of the trained surrogate model by comparing the data achieved from the lab and the surrogate model itself, respectively. The figure shows although several predictions deviate from the experimentally measured values, most of the predicted responses follow the overall trend of the experimental data and remain within or close to the predefined acceptance limits. These results demonstrate that the surrogate model can understand the relationship between the input variables and the resulting shear stress despite the limited amount of training data.

A second surrogate model was developed using the experimental data obtained during the filling of stone. The complete experimental dataset is presented in Table 18. As with the coarse sand model, the measured variables included filling height, wall roughness, load cell readings, applied forces and calculated shear stresses.

Table 18: Experimental data obtained for stone

Height (mm)	micron	load cell reading (kg)	surface contact area (m^2)	Force on the wall (N)	Average shear stress (N/m^2)	force on each layer (N)	shear stress on each layer (N/m^2)
60	425	0.00	0.02	0.00	0.00	0.00	0.00
100	425	0.07	0.03	0.69	20.82	0.69	52.04
160	425	0.19	0.05	1.86	35.32	1.18	59.48
210	425	0.28	0.07	2.75	39.65	0.88	53.53
265	425	0.42	0.09	4.12	47.13	1.37	75.70
320	425	0.56	0.11	5.49	52.04	1.37	75.70
395	425	0.71	0.13	6.97	53.46	1.47	59.48
440	425	0.83	0.15	8.14	56.10	1.18	79.31
492	425	0.95	0.16	9.32	57.42	1.18	68.63
545	425	1.01	0.18	9.91	55.11	0.59	33.67
80	269	0.09	0.03	0.88	33.46	0.88	33.46
150	269	0.23	0.05	2.26	45.60	1.37	59.48
220	269	0.36	0.07	3.53	48.66	1.28	55.23
285	269	0.50	0.09	4.91	52.17	1.37	64.05
340	269	0.62	0.11	6.08	54.23	1.18	64.89
390	269	0.73	0.13	7.16	55.67	1.08	65.43
450	269	0.84	0.15	8.24	55.51	1.08	54.52
490	269	0.97	0.16	9.52	58.87	1.28	96.65
535	269	1.05	0.18	10.30	58.37	0.79	52.87
590	269	1.20	0.19	11.77	60.49	1.47	81.11
105	269	0.09	0.03	0.88	25.49	0.88	25.49
165	269	0.21	0.05	2.06	37.85	1.18	59.48
220	269	0.32	0.07	3.14	43.26	1.08	59.48
280	269	0.44	0.09	4.32	46.73	1.18	59.48
315	269	0.54	0.10	5.30	50.98	0.98	84.97
380	269	0.58	0.13	5.69	45.39	0.39	18.30

455	269	0.70	0.15	6.87	45.75	1.18	47.58
485	269	0.75	0.16	7.36	45.99	0.49	49.57
542	269	0.90	0.18	8.83	49.38	1.47	78.26
595	269	1.02	0.20	10.01	50.98	1.18	67.33
60	201	0.02	0.02	0.20	9.91	0.20	9.91
125	201	0.10	0.04	0.98	23.79	0.79	36.60
180	201	0.20	0.06	1.96	33.04	0.98	54.07
235	201	0.35	0.08	3.43	44.29	1.47	81.11
295	201	0.45	0.10	4.42	45.37	0.98	49.57
360	201	0.61	0.12	5.98	50.39	1.57	73.20
418	201	0.71	0.14	6.97	50.51	0.98	51.28
485	201	0.86	0.16	8.44	52.73	1.47	66.58
545	201	1.04	0.18	10.20	56.75	1.77	89.22
595	201	1.19	0.20	11.67	59.48	1.47	89.22

The training procedure was repeated until the optimal neural network configuration was obtained. The resulting surrogate model achieved a regression coefficient of 0.7764, indicating a stronger correlation between the predicted and measured responses than that obtained for coarse sand. The corresponding mean squared error was 197.0373, as shown in Figure 80, while the regression analysis is presented in Figure 81.

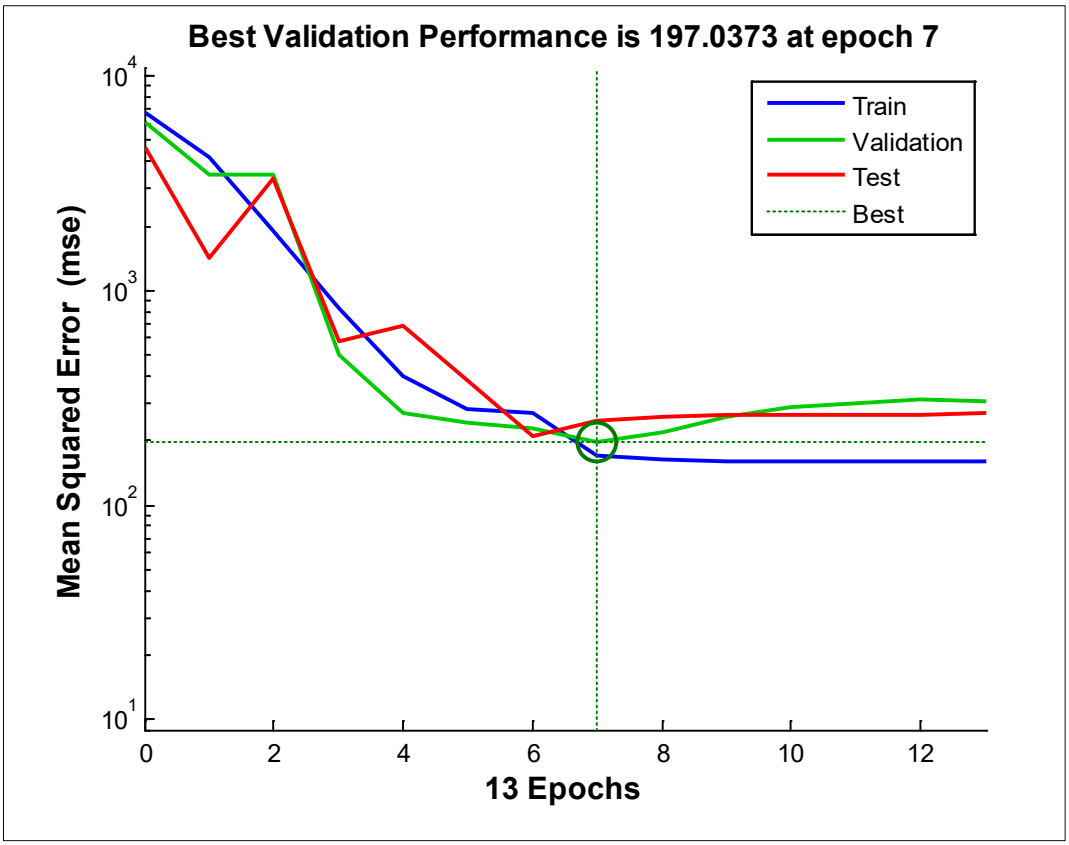

Figure 80: Validation performance of the trained neural network for stone

The higher regression coefficient suggests that the stone dataset exhibited a more consistent relationship between the selected input variables and the resulting shear stress. Thus, the neural network was able to learn the underlying input-output mapping more effectively.

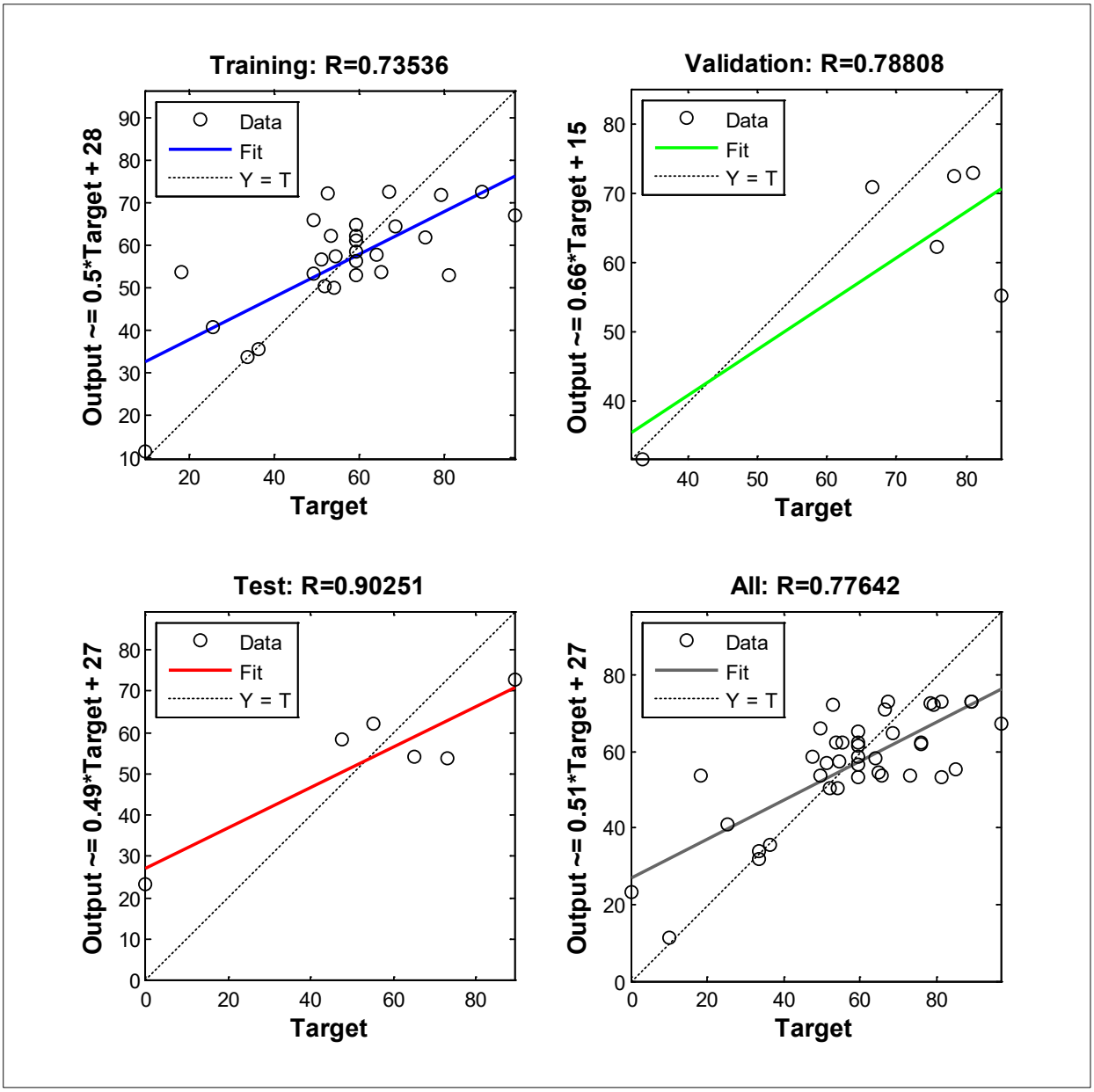

Figure 81: Regression plot of the neural network trained using stone data

The predictive capability of the stone surrogate model was verified using an independent dataset generated through both laboratory testing and surrogate model prediction. Table 19 presents the comparison between the experimentally measured shear stresses and those predicted by the trained neural network.

Table 19: Comparison between laboratory measurements and surrogate model predictions for stone

Height (mm)	micron	shear stress in the layer achieved through the lab (Pa)	Shear stress in the layer obtained from MATLAB (Pa)
65	425	36.60	7.41
120	425	81.11	68.46
180	425	84.26	66.27
240	425	79.31	48.52
290	425	89.22	52.78
350	425	84.26	58.15
70	269	0.00	-5.40
120	269	47.58	38.47
175	269	86.51	56.74
250	269	63.44	63.21
310	269	79.31	72.62
375	269	73.20	46.64
65	201	0.00	11.29
135	201	46.73	40.59
210	201	59.48	51.08
282	201	57.83	52.55
330	201	68.15	53.27
390	201	69.39	55.36

As in the previous verification process, upper and lower tolerance limits corresponding to ±10% of the target values were established. Figure 82 illustrates the comparison between the experimental measurements and the surrogate model predictions. Most of the predicted values lie within or close to the prescribed tolerance limits, indicating that the surrogate model provides an acceptable representation of the experimental behaviour. These results confirm that the neural network successfully captures the dominant trends governing shear stress development for the stone backfill material.

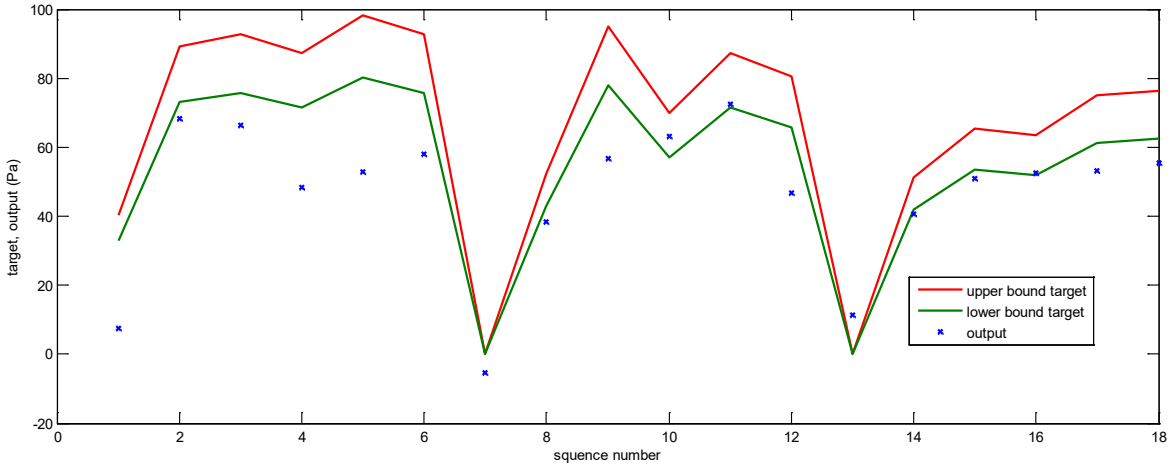

Figure 82: Comparison of the output and the target data for stone

The results demonstrate that neural network-based surrogate models can successfully approximate the stress behaviour observed in laboratory simulations of backfilled mine stopes. Although the prediction accuracy is not perfect, the developed models reproduce the general relationship between the governing input variables and the resulting shear stress with satisfactory accuracy for engineering reliability applications.

It should be recognised that the experimental datasets used for model training are relatively small. This limitation arises from the labour-intensive nature of the experimental procedure, where each individual test required approximately five minutes to complete. Generating substantially larger datasets would therefore require a significant investment in laboratory time and resources, making such an approach impractical within the scope of this research.

Despite this limitation, the available datasets are sufficient to demonstrate the feasibility of the proposed surrogate modelling framework. The principal objective of this research is not to develop a universally applicable predictive model, but rather to investigate the capability of surrogate models to replace computationally intensive stress evaluation procedures within Monte Carlo-based structural reliability analysis. From this perspective, the developed models successfully demonstrate the proof-of-concept by providing rapid stress predictions while preserving the essential characteristics of the experimental behaviour.

Several measures were implemented during model development to maximise reliability despite the limited amount of training data. These included repeated network training, appropriate selection of input variables, independent verification using unseen datasets, and continuous monitoring of regression performance and prediction error to minimise overfitting. The verification results indicate that the surrogate models adequately capture the dominant trends present in the experimental observations.

It is acknowledged that expanding the experimental database would likely improve both the prediction accuracy and the generalisation capability of the surrogate models. Future research should therefore investigate the integration of larger laboratory datasets with high-fidelity numerical simulations, such as discrete element method (DEM) analysis, to generate more comprehensive training datasets. Such an approach has the potential to improve surrogate model robustness while retaining the significant computational advantages demonstrated in this study.

Overall, the results presented in this chapter demonstrate that neural network-based surrogate modelling provides an effective and computationally efficient alternative for predicting shear stress in backfilled mine stopes. The developed models significantly reduce the computational effort required for repeated stress evaluations and therefore provide a practical framework for large-scale reliability assessment using Monte Carlo simulation.

Chapter 7: Application of surrogate model to structural safety assessment

The preceding chapters demonstrated the development and validation of neural network-based surrogate models for a range of civil engineering applications, including structures subjected to wind loading, seismic actions, storage silos, and backfilled-mine stopes. In conventional structural reliability analysis, these systems are typically assessed using Monte Carlo simulation (MCS)-based approaches combined with numerical modelling or laboratory experimentation. While such methods provide reliable estimates of structural performance and failure probability, they often require a large number of simulations, resulting in substantial computational costs and time-consuming analysis.

The surrogate models developed in Chapters 3–6 were designed to address this limitation by replacing computationally intensive numerical or experimental simulations with efficient data-driven approximations. The results presented in the previous chapters demonstrated that the developed surrogate models can accurately reproduce the responses of the original high-fidelity models while significantly reducing computational effort.

This chapter investigates the practical application of the developed surrogate models within a structural safety assessment framework. Rather than focusing on model development, the chapter evaluates how the trained surrogate models can be integrated into reliability analysis procedures to estimate the probability of structural failure under specified performance criteria. The objective is to demonstrate the effectiveness of surrogate modelling as a computational tool for large-scale Monte Carlo simulations and to illustrate its potential application in real-world engineering practice.

The chapter is divided into two main sections. Section 7.2 examines the application of surrogate models developed from numerical simulations, specifically those associated with structures subjected to wind and seismic loads. Section 7.3 investigates the application of surrogate models developed from laboratory-based experiments involving silo structures and backfilled mine stopes. In each case, the developed

surrogate models are employed within a Monte Carlo simulation framework to estimate structural reliability and assess computational efficiency.

Chapter 7.1: Applications of constructed surrogate model in relation to data collected from numerical studies (wind load and seismic actions)

The surrogate models presented in Chapters 3 and 4 were developed using datasets generated through numerical simulations. For wind-induced loading, structural response data were generated using MATLAB-based numerical analysis, while seismic response data were obtained through nonlinear structural analysis conducted in ETABS. These datasets were subsequently used to train neural network-based surrogate models capable of predicting structural responses with high accuracy.

To demonstrate the practical applicability of the developed framework, the surrogate models were incorporated into Monte Carlo simulation procedures for structural safety assessment. Since both chapters employed similar numerical modelling approaches, the seismic surrogate model developed in Chapter 4 was selected as a representative example.

Six neural network surrogate models were originally developed by varying the concrete strength and analysing both horizontal and vertical displacement responses of a three-storey building subjected to earthquake loading. Among these models, the best-performing horizontal displacement model and the best-performing vertical displacement model, selected based on regression performance, were adopted for reliability assessment.

To evaluate the application of the surrogate model for predicting horizontal displacement, the model developed using a mean Young's Modulus of 30 GPa was selected. Monte Carlo simulations were performed in MATLAB to estimate the probability of structural failure. Initially, 10,000 simulations were conducted using a constant displacement limit of 75 mm. The number of simulation rounds was subsequently increased while maintaining the same displacement limit. The corresponding computational times are presented in Table 20.

Table 20: Simulation time spent for analysing the probability of failure of the structure in relation to horizontal displacement

Number of rounds of simulation	Time spent on the simulation (s)
10000	26.70
20000	55.30
50000	239.98
70000	319.70
100000	487.30

The estimated probability of failure was zero for all simulation cases (10,000, 20,000, 50,000, 70,000, and 100,000 simulations). As expected, the computational time increased with the number of simulation rounds, reaching a maximum of 487.30 seconds for 100,000 simulations.

Although the horizontal displacement limit of 75 mm may appear relatively large compared with typical serviceability limits, it was selected based on the response of a simplified three-storey building model subjected to the El Centro earthquake record in ETABS. This model was used to generate the dataset required for training the surrogate model. Since the objective of this research is to improve the safety assessment of structural systems, the selected displacement threshold is appropriate for demonstrating the capability of the proposed approach. The surrogate model enables up to 20,000 Monte Carlo simulations to be completed in less than one minute, while 100,000 simulations require only approximately eight minutes, demonstrating a significant improvement in computational efficiency.

Similarly, the surrogate model was evaluated for predicting vertical displacement using the same mean Young's Modulus value of 30 GPa. Monte Carlo simulations were again performed in MATLAB with varying numbers of simulation rounds while maintaining a constant vertical displacement limit of 20 mm. The computational times are summarised in Table 21.

Table 21: Simulation time spent for analysing the probability of failure of the structure in relation to vertical displacement

Number of rounds of simulation	Time spent for the simulation (s)
10000	35.90
20000	97.20
50000	191.20
70000	366.60
100000	1199.95

As shown in Table 21, the computational time for 10,000 simulations remained below one minute, whereas 100,000 simulations required 1,199.95 seconds. Like the horizontal displacement analysis, the estimated probability of failure was zero for all simulation cases. These results demonstrate that the surrogate model based on the neural network substantially reduces computational time while maintaining the ability to efficiently evaluate the structural probability of failure. Therefore, the proposed approach provides an effective and computationally efficient framework for assessing structural safety performance under uncertainty.

The trained surrogate models were integrated into Monte Carlo simulations to estimate the probability of failure based on predefined displacement thresholds. The results demonstrated that thousands of simulations could be completed within a relatively short period. Even when the number of simulation runs was increased to 100,000, the total computational time remained within practical limits. This highlights the capability of surrogate models to significantly accelerate reliability analysis while preserving the ability to evaluate structural performance under uncertain loading conditions.

For both horizontal and vertical displacement criteria, the calculated probabilities of failure remained negligible within the selected threshold limits. More importantly, the analysis confirmed that the surrogate models enabled rapid execution of large-scale

simulations that would otherwise require substantial computational resources if performed using the original numerical models.

Chapter 7.2: Applications of constructed surrogate model in relation to experimental studies (silo structures and backfilled mine stopes)

Like the application presented in Section 7.1, this section evaluates the applicability of the surrogate models developed in Chapters 5 and 6 for the probabilistic safety assessment of laboratory-based structural systems representing silo structures and backfilled mine stopes. The objective is to demonstrate the capability of the proposed surrogate modelling framework to perform efficient reliability analysis by replacing computationally intensive numerical simulations with trained neural network models.

Since the surrogate models developed in Chapters 5 and 6 were constructed using similar experimental methodologies, only the silo structure was selected as the representative case study for the probabilistic analysis. Monte Carlo Simulation (MCS) was implemented in MATLAB to estimate the probability of failure based on the responses predicted by the trained surrogate models. The analyses were performed for three different granular fill materials, namely fine sand, river sand, and crusher dust. Separate neural network surrogate models were developed for each fill material while accounting for the influence of wall surface roughness. The performance of these surrogate models was subsequently evaluated in terms of their computational efficiency and their ability to estimate the probability of structural failure.

The surrogate model developed for the fine sand condition was first evaluated. Monte Carlo simulations were performed using a constant pressure limit state of 155 Pa while progressively increasing the number of simulation samples from 10,000 to 40,000. The corresponding computational times are summarised in Table 22.

Table 22: Simulation time spent for analysing the probability of failure of silo in relation to fine sand

Number of simulations	Time spent on the simulation (s)
10000	32.50
20000	119.97
30000	138.90
35000	160.30
40000	174.40

As expected, the computational time increased with the number of Monte Carlo samples, reaching a maximum of 174.40 s for 40,000 simulations. The estimated probability of failure remained relatively stable throughout the analysis, varying only between 0.0044 and 0.0055. Specifically, probabilities of failure of 0.0044, 0.0055, 0.0045, 0.0045 and 0.0045 were obtained for 10,000, 20,000, 30,000, 35,000 and 40,000 simulations, respectively. The limited variation in the estimated probability of failure indicates that the surrogate model provides stable and consistent reliability estimates even when the number of Monte Carlo samples is varied.

The applicability of the surrogate model was subsequently assessed for the river sand condition. A constant pressure limit state of 250 Pa was adopted, and Monte Carlo simulations were performed using sample sizes ranging from 10,000 to 30,000. The computational times are presented in Table 23.

Table 23: Simulation time spent for analysing the probability of failure of silo in relation to river sand

Number of simulations	Time spent on the simulation (s)
10000	46.40
15000	53.00
20000	72.20
25000	99.90
30000	133.80

The results indicate a gradual increase in computational time with increasing sample size, with the maximum computational time remaining below three minutes for 30,000 simulations. The estimated probabilities of failure were 0.0637, 0.0635, 0.0640, 0.0649 and 0.0651 for 10,000, 15,000, 20,000, 25,000 and 30,000 simulations, respectively. The close agreement among these estimates suggests that the probability of failure converges rapidly, demonstrating that reliable results can be obtained without requiring an excessively large number of Monte Carlo simulations.

Finally, the surrogate model developed for the crusher dust condition was evaluated using a constant pressure limit state of 320 Pa. Monte Carlo simulations were performed using 10,000, 20,000 and 30,000 samples. The corresponding computational times are presented in Table 24.

Table 24: Simulation time spent for analysing the probability of failure of silo in relation to crusher dust

Number of simulations	Time spent on the simulation (s)
10000	32.80
20000	91.80
30000	97.10

The computational time increased from 32.80 s for 10,000 simulations to 97.10 s for 30,000 simulations. The corresponding probabilities of failure were estimated as 0.0107, 0.0124 and 0.0116, respectively. Like the previous cases, only minor variations were observed as the number of Monte Carlo samples increased, indicating that the surrogate model provides consistent probability estimates while significantly reducing computational cost.

Overall, the analyses conducted for the three fill materials demonstrate that the proposed neural network-based surrogate models are capable of efficiently estimating structural reliability with relatively low computational effort. Even for tens of thousands

of Monte Carlo simulations, the required computational time remained within a few minutes, making the proposed framework suitable for applications involving repeated probabilistic evaluations.

The reduction in computational time is particularly important when analysing more complex structural systems or when uncertainty quantification requires a large number of model evaluations. In such applications, direct numerical simulations can become computationally expensive, whereas the surrogate models developed in this research provide rapid predictions without compromising the consistency of the probability of failure estimates.

Although the present study focuses on silo structures as a representative laboratory-based case study, the proposed surrogate modelling framework is readily transferable to other structural systems. It should be recognised, however, that the quantity and quality of training data required to develop an accurate surrogate model depend on the complexity of the structural response and the associated uncertainty. So, the proposed framework incorporates an independent verification stage, in which a portion of the available dataset is reserved exclusively for model validation and is not used during the training process. This verification strategy, described in Chapters 3–6, ensures that the predictive capability and generalisation performance of the surrogate models are rigorously evaluated before they are employed for reliability assessment.

Chapter 7 presents the practical application of previously developed surrogate models for assessing the structural safety and reliability of different systems, including buildings, silo structures, and backfilled mine stopes. The main goal is to show how surrogate models can significantly reduce the computational time required compared to traditional Monte Carlo simulation methods.

For numerical studies (wind and seismic loads), surrogate models developed in earlier chapters were applied to a 3-storey building subjected to earthquake loading. By running thousands of simulations in MATLAB, the surrogate models were used to estimate the probability of failure based on displacement limits. Results show that even large numbers of simulations (up to 100,000 runs) can be completed in minutes, demonstrating a major improvement in efficiency compared to conventional methods.

For experimental studies (silos and backfilled mine stopes), surrogate models trained on laboratory data were used to analyse different fill materials and conditions. Simulations showed how the models could quickly estimate failure probabilities for silo structures and mine stopes under different materials (e.g., sand, river sand, crusher dust) while maintaining reasonable accuracy. Across all cases, the probability of failure values was generally consistent, and the computation time remained low even for large simulation runs.

Overall, the chapter concludes that surrogate models are effective, fast, and scalable tools for structural safety assessment, enabling reliable Monte Carlo-based analysis with greatly reduced computational cost, though proper validation and verification remain essential for different structural systems.

The innovative part of the project is to use surrogate models effectively for the assessment of safety performance of civil structures. Lab-based experiments in the research were conducted as a part of Monte Carlo simulation methods. Monte Carlo simulation methods include conducting 1 experiment to evaluate the assessment of civil structures. Use of Monte Carlo simulation method is used as 1 step in reliability analysis. These steps need to be conducted thousands of times, which can realistically be time consuming to get optimal result. This chapter demonstrates the application of surrogate model and shows how it can be applied to Monte Carlo simulation-based analysis. The research proposed to shorten time in Monte Carlo simulation. This chapter presents the overall process of use of surrogate models on reliability analysis of civil structures.

Chapter 8: Summary, Conclusion, Recommendations for future work

Chapter 8.1: Summary and Conclusion

Structural reliability analysis is a necessary tool required for the effective quantitative safety assessment in civil engineering. Traditional reliability analysis methods often depend on Monte Carlo simulation, numerical modelling, and experimental testing procedures, which can be computationally intensive and time-consuming. This research proposed, developed, and validated neural network-based surrogate models as efficient alternatives to selected computationally expensive components within conventional structural safety assessment frameworks.

The primary objective of this study was to investigate the applicability of surrogate modelling techniques for improving the computational efficiency of reliability analysis while maintaining acceptable levels of accuracy. To achieve this objective, a series of numerical and experimental studies were conducted involving different civil engineering structures and loading conditions.

In Chapter 3, a neural network-based surrogate model was developed for the fragility analysis of a two-storey nonlinear frame structure subjected to wind loading. A simple two-storey building was used as the case study. The surrogate model was trained using datasets generated from a conventional time-marching numerical simulation procedure. The results demonstrated that the surrogate model was capable of accurately reproducing the structural response while significantly reducing computational time. In the case study considered, simulation times were reduced from several hours to only a few seconds, illustrating the significant efficiency gains achievable through model surrogation.

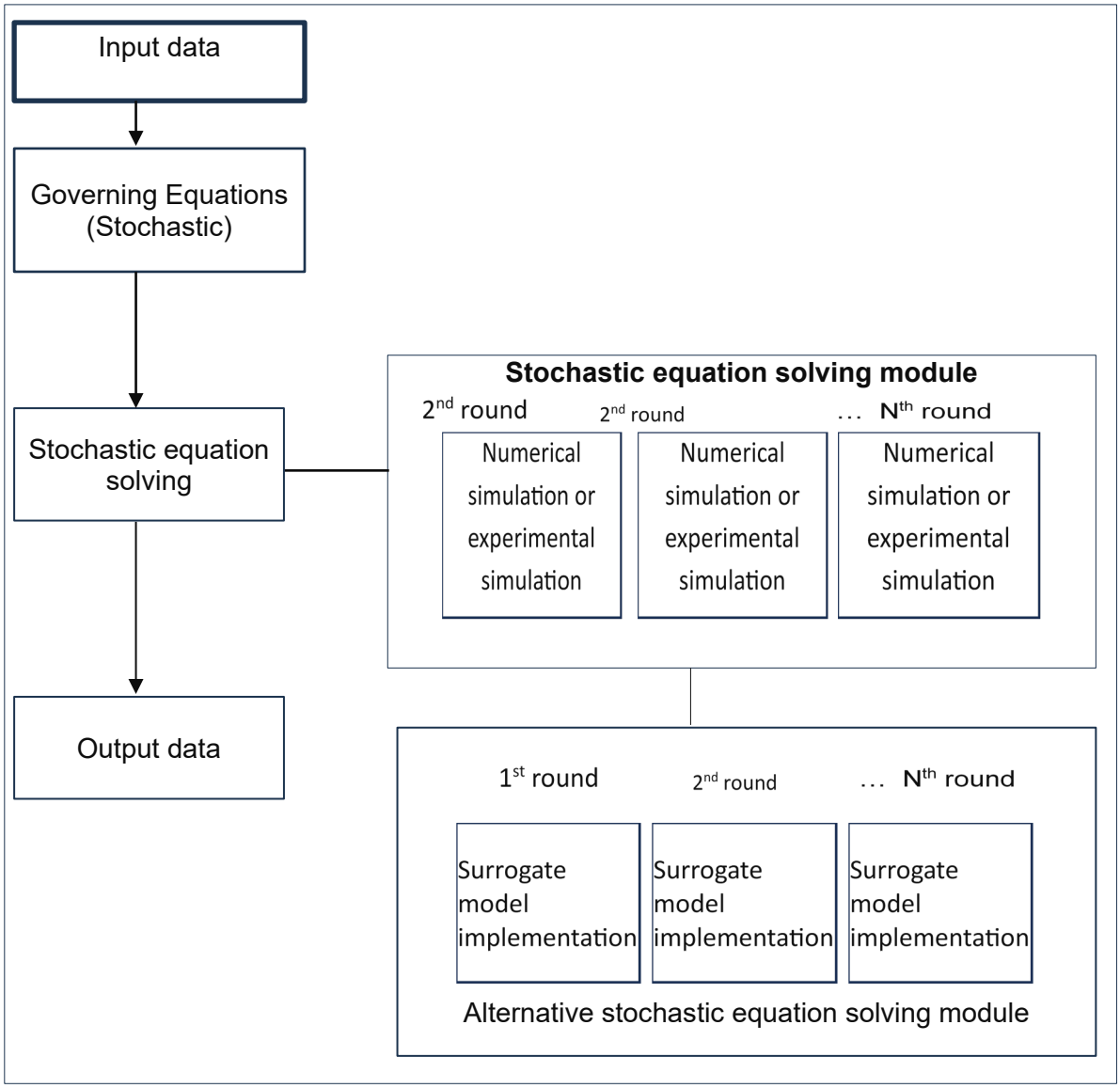

Figure 83: A general framework of model surrogation for other application purposes

A key finding from Chapter 3 was that the surrogate model construction process depended primarily on the relationship between input and output variables rather than on the internal computational procedures of the original simulation model. The input variables consisted of excitation forces and storey stiffness values, while the output variable was the inter-storey displacement response used for fragility assessment. This observation provided the foundation for extending the surrogate modelling

framework to other numerical and experimental applications investigated throughout the remainder of the thesis.

The general framework developed in this research demonstrates that surrogate modelling can be applied to replace computationally demanding components in both numerical and laboratory-based simulations. While the initial application focused on a specific time-marching algorithm, the broader concept is applicable to a wide range of structural engineering problems where repeated simulations are required for probabilistic safety assessment.

To validate the generality of the proposed framework, three additional studies were conducted. Chapter 4 extended the surrogate modelling approach to the fragility assessment of structures subjected to seismic actions. Chapters 5 and 6 investigated surrogate model development based on laboratory experiments involving silos and backfilled mine stopes, respectively. Despite the differences in structural systems and loading conditions, they shared a commonality: there was at least one time-consuming component in the process of solving the respective stochastic governing equations when their safety performance is to be quantified probabilistically. Essentially, making these time-consuming components less time-consuming motivates the model surrogation and demonstrates its benefit or even necessity.

In Chapter 4, the proposed methodology was applied to a three-storey building subjected to earthquake loading. Structural responses were obtained using industry-standard design software, and fragility assessment was conducted using horizontal and vertical displacement responses. Multiple neural network surrogate models were developed by varying the mean value of the concrete Young's modulus. Separate models were trained for horizontal and vertical displacement predictions, and their performance was evaluated through regression analysis. The results demonstrated that the surrogate models could accurately reproduce the structural responses obtained from nonlinear numerical simulations while significantly reducing computational effort.

Chapter 5 focused on the development of surrogate models for the safety assessment of silo structures. An initial pilot study was conducted using experimental data obtained

from previous research Widisinghe (2014) to investigate the relationship between filling height and stress development within silo systems. The study also examined the influence of neural network architecture through a parametric investigation of the number of hidden neurons. Subsequently, laboratory experiments were performed using a purpose-built silo prototype. The effects of filling height, wall roughness, and filling material properties on stress development were investigated, and the resulting datasets were used to train neural network surrogate models. The developed models accurately predicted stress responses while providing substantial computational savings compared with repeated experimental evaluations.

In Chapter 6, the surrogate modelling framework was further extended to the safety assessment of backfilled mine stopes. Experimental procedures like those employed for silo structures were adopted, with modifications reflecting the characteristics of mine backfill systems. Variations in filling materials, fill height, and wall roughness were considered to generate representative datasets for surrogate model development. The resulting neural network models demonstrated strong predictive capabilities and confirmed the versatility of the proposed surrogate modelling framework across different engineering applications.

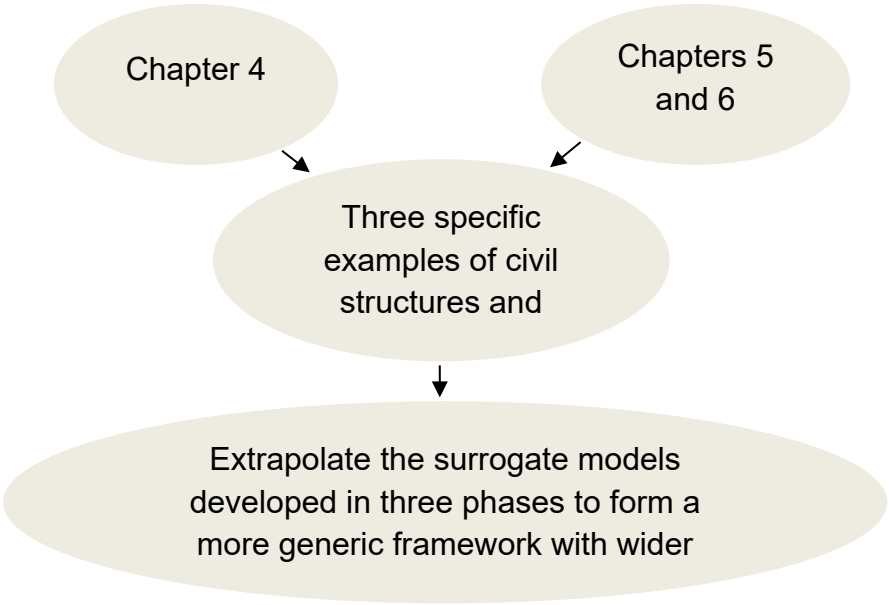

Figure 84: Relationship between chapters 4, 5 and 6

As shown in the above Figure 84, the distinct civil structures and systems involved in chapters 4, 5 and 6 share a commonality: there is at least one time-consuming component in the process of solving the respective stochastic governing equations when their safety performance is to be quantified probabilistically. Safety assessment of these structures contains time-consuming module method. The aim is to shorten the time period of a simulation to improve the computational efficiency.

The practical applicability of the developed surrogate models was investigated in Chapter 7. The surrogate models were integrated into Monte Carlo simulation-based reliability analyses to estimate probabilities of failure for representative structural systems. Results demonstrated that large numbers of simulations could be performed rapidly while maintaining reliable estimates of structural performance. Significant reductions in computational time were achieved compared with traditional numerical and experimental simulation approaches. These findings confirm that surrogate modelling can effectively improve the practicality of probabilistic safety assessments involving large-scale simulation studies.

The collective findings of this thesis demonstrate that neural network-based surrogate models provide an effective means of enhancing the efficiency of structural reliability analysis. By replacing selected time-consuming numerical or experimental procedures, the developed models enable rapid probabilistic assessment while maintaining acceptable levels of predictive accuracy. The proposed framework therefore contributes both methodological and practical advances to the field of structural safety assessment.

Several limitations were encountered during this research. The numerical studies were restricted to selected wind loading and seismic scenarios, with seismic analysis based primarily on a specific earthquake record. Similarly, the laboratory investigations were constrained by the dimensions of the experimental apparatus and the range of wall roughness conditions that could be practically implemented. While these limitations did not affect the successful completion of the research objectives, they indicate opportunities for further development and broader application of the proposed framework.

Overall, this research has demonstrated that surrogate modelling represents a viable and effective approach for improving the efficiency of Monte Carlo simulation-based reliability assessment. The developed framework provides a foundation for future studies seeking to integrate advanced machine learning techniques into structural safety assessment and reliability analysis procedures.

Chapter 8.2 Recommendations for future works

Based on the findings of this study, the following recommendations are proposed for future research:

1. The surrogate modelling framework developed in this thesis should be extended to establish a more generalised reliability assessment framework applicable to a broader range of civil engineering structures and systems.

2. Additional numerical studies should be conducted using loading conditions other than wind and seismic actions, including blast loads, impact loads, fatigue loading, and climate-related hazards.

3. Future seismic studies should incorporate earthquake records from multiple geographical regions to improve the generality and effectiveness of the developed surrogate models. In addition to the El Centro earthquake record used in this study, a wider range of ground motions with varying amplitudes, frequency characteristics, and durations should be considered to develop more representative seismic surrogate models.

4. Laboratory investigations should incorporate realistic concrete wall surfaces instead of sandpaper-based roughness conditions to better replicate full-scale engineering structures. Larger experimental prototypes should be developed to investigate scale effects and improve the representativeness of laboratory observations. Additional material characteristics, including moisture content, particle shape, density, and internal friction properties, should be incorporated into future experimental studies to create more comprehensive surrogate models.

5. Advanced machine learning techniques, including deep neural networks, ensemble learning methods, and hybrid surrogate modelling approaches, should be investigated to further improve prediction accuracy and computational efficiency. Future studies should present detailed comparisons between surrogate model predictions and independent reliability analyses to provide additional validation of estimated failure probabilities.

6. The integration of surrogate models into real-time structural health monitoring and digital twin frameworks represents a promising research direction with significant practical implications for infrastructure management and decision-making.

The continued development of surrogate modelling techniques has the potential to transform structural reliability assessment by enabling rapid, accurate, and computationally efficient probabilistic analysis for increasingly complex engineering systems.

References

E. Agarwal, E. Pain, T. Mukhopadhyay, S. Metya and S. Sarkar, “Efficient computational system reliability analysis of reinforced soil-retaining structures under seismic conditions including the effect of simulated noise,” Engineering with Computers, vol. 38, no. Suppl 2, p. 901–923, 2022.

C. Apostolopoulos, A. Drakakaki and M. Basdeki, “Seismic assessment of RC column nder seismic loads,” International Journal of Structural Integrity, vol. 10, no. 1, pp. 41-54, 2019.

Standards Australia 1996, Loads on bulk solids containers, AS 3774-1996, Standards Australia, NSW.

L. R. Barroso, S. . E. Breneman and H. A. Sith, “Performance Evaluation of Controlled Steel Frames under Multilevel Seismic Loads,” JOURNAL OF STRUCTURAL ENGINEERING, vol. 128, no. 11, pp. 1368-1378, 2002.

K. Benyahi, Y. Bouafia, S. Barboura and M. S. Kachi , “Nonlinear analysis and reliability of metallic truss structures,” Frontiers of Structural and Civil Engineering, vol. 12, no. 4, p. 577–593, 2018.

S.-E. Cho, “Fragility Analysis for Water-Retaining Structures Resting on Spatially Random Soil,” Water, vol. 15, p. Article 4165, 2023.

T.-A. Chou, . S. H. Lee, . C. Chang and T. H.-K. Kang, “Reinforced Concrete Coupling Beams with Different Layouts under Seismic and Wind Loads,” ACI Structural Journal, pp. 120-S73, 2023.

American Concrete Institute 2016, Design Specification for Concrete Silos and Stacking Tubes for Storing Granular Materials and Commentary, ACI 313: 2016, American Concrete Institute, MI.

A. Dhar and B. Datta, “Saltwater intrusion management of coastal aquifers. I: linked simulation-optimization,” Journal of Hydrologic Engineering, vol. 14, pp. 1263-1272, 2009.

J. E. El-ghareeb, H. E. Abd-EL-Mottaleb, E. A. Elshamy and M. Emara, “Seismically resistant progressive collapse behavior of infilled frame structures under seismic loads and column loss: A numerical investigation,” Structures, vol. 66, 2024.

B. R. Ellingwood and K. Kinali, “Quantifying and communicating uncertainty in seismic risk assessment,” Structural Safety, vol. 31, no. 2, pp. 179-187, 2009.

B. Erdil, F. Korkut, M. Aydin and N. Yaltay, “Structural Performance of Masonry Buildings Under Harsh Climate and Seismic Loads,” Iranian Journal of Science and Technology, vol. 46, pp. 4031-4049, 2022.

S.-E. Fang, J.-L. Zheng and S.-R. Wang, “Hybrid reliability analysis of structures using fuzzy Bayesian interval estimation,” Engineering Structures, vol. 307, p. Article 117915, 2024.

Y. Fang, X. Li, L. Gao, R. Gu, W. Luo and Z. Yan, “The experiment and analysis of the stress dip underneath the granular Silo,” Granular Matter, vol. Article 54, p. 24, 2022.

M. Z. Fank, J. W. B. d. Nascimento, D. L. Cardoso, A. S. Meira and F. L. Willrich, “VERTICAL PRESSURES AND COMPRESSIVE FRICTION FORCE IN A LARGE SILO,” Engenharia Agrícola, vol. 38, no. 4, pp. 498-503, 2018.

E. Gavanski and G. A. Kopp, “Fragility assessment of roof-to-wall connection failures for wood-frame houses in high winds,” ASCE-ASME Journal of Risk and Uncertainty in Engineering Systems. Part A – Civil Engineering, vol. 3, no. 4, 04017013, 2017.

S. Ghosh, A. Roy and S. Chakraborty, “Kriging Metamodeling-Based Monte Carlo Simulation for Improved Seismic Fragility Analysis of Structures,” Journal of Earthquake Engineering, vol. 25, no. 7, pp. 1316-1336, 2019.

J. Ginger, D. Henderson, M. Humphreys, C. Konthesingha and M. G. Stewart, “Wind Loads on the Frames of Industrial Buildings,” Australian Journal of Structural Engineering, vol. 16, no. 2, pp. 169-178, 2015.

Z. Gökalp, “Finite Element Analysis for Displacements and Stresses Developed over Horizontally Corrugated Steel Silo Wall Panels,” Journal of Tekirdag Agricultural Faculty, vol. 7, no. 3, pp. 119-127, 2010.

J. S. Goode and J. W. van de Lindt, “Reliability-based design of medium mast lighting structural supports,” Structural and Infrastructure Engineering, vol. 9, no. 6, pp. 594-600, 2013.

M. Gordini, M. R. Habibi, M. H. Tavana, M. TahamouliRoudsar and M. Amiri, “Reliability Analysis of Space Structures Using Monte-Carlo Simulation Method,” Structures, vol. 14, pp. 209-219, 2018.

S. S. Kar and L. B. Roy, “Probabilistic Based Reliability Slope Stability Analysis Using FOSM, FORM, and MCS,” Engineering, Technology & Applied Science Research, vol. 12, no. 2, pp. 8236-8240, 2022.

H. Kibar, T. Öztürk and K. E. Temizel, “Effective engineering properties in the design of storage structures of postharvest dry bean grain,” Acta Scientiarum , vol. 36, no. 2, pp. 147-158, 2014.

S. D. Koduru and T. Haukaas, “Feasibility of FORM in finite element reliability analysis,” Structural Safety, vol. 32, no. 2, pp. 145-153, 2010.

D. U. Kumar and V. M. Reddy, “Analysis and design of reinforced concrete silo by conventional method,” in E3S Web of Conferences 391, 01200 , 2023.

K. KWON, . H. C. CHOI, . K. JI, Y. CHOI and J. S. KONG, “FRAGILITY ASSESSMENT OF INSTALLATION DEFECTS IN INDUSTRIAL STANDING SEAM

METAL ROOF SUBJECTED TO WIND LOADS," JOURNAL of CIVIL ENGINEERING and MANAGEMENT, vol. 30, no. 5, p. 437–451, 2024.

A. Lal and B. Datta, "Development and Implementation of Support Vector Machine Regression Surrogate Models for Predicting Groundwater Pumping-Induced Saltwater Intrusion into Coastal Aquifers," Water Resources Management, vol. 32, pp. 2405-2419, 2018.

Li Li & Michel Aubertin (2010) An analytical solution for the nonlinear distribution of effective and total stresses in vertical backfilled stopes, Geomechanics and Geoengineering, 5:4, 237-245, DOI: 10.1080/17486025.2010.497871

Z. Li, Z. Xu, G. Huang and Z. Liu, "Wind-Induced Dynamic Response of Inter-Story Isolated Tall Buildings with Friction Pendulum Bearing Based on an Enhanced Simplified Model," Buildings, vol. 14, p. Article 1568, 2024.

Guangsheng Liu, Li Li, Xiaocong Yang & Lijie Guo (2016) A numerical analysis of the stress distribution in backfilled stopes considering nonplanar interfaces between the backfill and rock walls, International Journal of Geotechnical Engineering, 10:3, 271-282, DOI: 10.1080/19386362.2015.1132123

B. R. Magar, Assessing the safety performance of civil structures under elevated temperature, Melbourne: Victoria University, 2019.

N. Makhinko, "Stress-strain state of the storage silos under the action of the asymmetric load," in MATEC Web of Conferences 230, 02018, 2018.

M. Moghaddasi, M. Cubrinovski , J. G. Chase , S. Pampanin and A. Carr, "Effects of soil–foundation–structure interaction on seismic structural response via robust Monte Carlo simulation," Engineering Structures, vol. 33, pp. 1338-1347, 2011.

D. Mohammed and S. Al-Zaidee , "Deflection Reliability Analysis for Composite Steel Bridges," Engineering, Technology & Applied Science Research, vol. 12, no. 5, pp. 9155-9159, 2022.

N. Mostaghel and R. A. Byrd, "Analytical Description of Mutlidegree Bilinear Hysteretic System," Journal of Engineering Mechanics, vol. 126, no. 6, pp. 588-598, 2000.

T.-H. Nguyen, V.-D. Le, X.-H. Vu and D.-K. Nguyen, Engineering, Technology & Applied Science Research, vol. 12, no. 6, pp. 9766-9770, 2022.

T.-T. Nguyen, . M.-H. Ha, T.-P. Nguyen and . V.-H. Dang, “Seismic reliability analysis of building structures using subset simulation coupled with deep learning-based surrogate model,” Advances in Structural Engineering, vol. 25, no. I I, p. 2301–2318, 2022.

P. Ni, Z. Yuan, Q. Han, X. Du and J. Fu , “Reliability assessment of civil structures with incomplete probability distribution information,” Probabilistic Engineering Mechanics, vol. 2023, p. Article 103541, 2023.

S. L. Pantaleev, S.-A. Papanicolopulos and J. Y. Ooi, “Finite element analysis of stresses in a flexible bulk solid container,” Advances in Structural Engineering, vol. 21, no. 16, pp. 2518-2533, 2018.

F. Rashidiyan, S. . R. Mirghaderi and S. Mohebbi, “Seismic behaviour of the non-straight steel beams in the structural plans,” International Journal of Structural Integrity, vol. 15, no. 2, pp. 221-245, 2024.

A. Roy , S. Chakraborty and S. Adhikari, “Seismic reliability analysis of nonlinear structures by active learning-based adaptive sparse Bayesian regressions,” International Journal of Non-Linear Mechanics, vol. 165, p. Article 104817, 2024.

National Statement on Ethical Conduct in Human Research. The National Health and Medical Research Council, the Australian Research Council and Universities Australia. Commonwealth of Australia, Canberra, 2007 (updated 2018).

H. Sabermahany and R. Attarnejad, “Seismic performance of buildings supported by a shallow doubly-curved shell raft foundation,” Structures, vol. 36, pp. 619-634, 2022.

O. B. Sadan, L. Petrini and G. M. Calvi, “Direct displacement-based seismic assessment procedure for multi-span reinforced concrete bridges with single-column piers,” Earthquake Engineering & Structural Dynamics, vol. 42, no. 7, pp. 1031-1051, 2013

A. M. Salman and Y. Li, “Multihazard risk assessment of electric power systems,” Journal of Structural Engineering, vol. 143, no. 3, 04016198, 2017.

M. Shen and G. Deodatis, “Variability response functions for statically indeterminate structures,” Probabilistic Engineering Mechanics, vol. 70, p. Article 103361, 2022.

K. Shi, . Q. Guo and A. E. Jeffers, “Stochastic Analysis of Structures in Fire by Monte Carlo Simulation,” Journal of Structural Fire Engineering , vol. 4, no. 1, pp. 37- 46, 2013.

N. Sivakugan, S. Widisinghe and V. Z. Wang, "Vertical Stress Determination withing Backfilled Mine Stopes," International Journal of Geomechanics, vol. 14, no. 5, pp. 06014011-1-5, 2014.

K. Song, Y. Zhang, X. Yu and B. Song, "A New Sequential Surrogate Method for Reliability Analysis and Its Applications in Engineering," IEEE Access, vol. 7, pp. 60555-60571, 2019.

L. Song , Y. Yu, J. Yu, S. Wu, J. Ma and Z. Jin, “An Innovative Method for Wind Load Estimation in High-Rise Buildings Based on Green’s Function,” Mathematics, vol. 12, p. Article 1747, 2024.

J. Sreekanth and B. Datta, "Multi-objective management of saltwater intrusion in coastal aquifers using genetic programming and modular neural network based surrogate models," Journal of Hydrology, vol. 393, pp. 245-256, 2010.

M. G. Stewart, P. C. Ryan, D. J. Henderson and J. D. Ginger, “Fragility analysis of roof damage to industrial buildings subject to extreme wind loading in non-cyclonic regions,” Engineering Structures, vol. 128, pp. 333-343, 2016.

B. Sudret, G. Defaux and M. Pendola, “Time-variant finite element reliability analysis - application to the durability of cooling towers,” Structural Safety, vol. 27, no. 2, pp. 93-112, 2005.

M. S. Sufyan, P. Samui and S. S. Mishra, “Reliability analysis of portal frame subjected to varied lateral loads using machine learning,” Asian Journal of Civil Engineering, vol. 25, p. 2045–2058, 2024.

J. Szafran, K. Juszczyk and M. Kaminski, “Experiment-based reliability analysis of structural joints in a steel lattice tower,” Journal of Constructional Steel Research, vol. 154, pp. 278-292, 2019.

L.-W. Tsai and A. Alipour, “Structural health monitoring and fatigue life reliability assessment of a flexible structure in extreme wind,” Journal of Civil Structural Health Monitoring, vol. 13, p. 677–691, 2023.

Victoria University, "HEALTH AND SAFETY - CONFINED SPACES PROCEDURE," Victoria University Policy Library, [Online]. Available: https://policy.vu.edu.au/document/view.php?id=332&version=2. 2019b [Accessed 23 October 2019].

Victoria University, "HEALTH AND SAFETY - CHEMICAL MANAGEMENT PROCEDURE," Victoria University Policy Library, [Online]. Available: https://policy.vu.edu.au/document/view.php?id=378&version=1. 2019a [Accessed 23 October 2019].

V. Z. Wang and J. D. Ginger, "Maximum a posteriori estimation based wind fragility analysis with applications to existing linear or hysteretic shear frames," Structural Engineering and Mechanics, vol. 50, no. 5, pp. 653-664, 2014.

V. Z. Wang, T. Pease and S. Robinson, "Statistical Damage Prognosis for In-Service Civil Structures against Hazards: Formulations and Applications," Journal of Engineering Mechanics, vol. 142, no. 3, 04015090, 2016.

Y. Wang, G. Yuan, Z. Huang, J. Lyv, Z.-Q. Li and T.-y. Wang, "Experimental study on the fire behaviour of reinforced concrete slabs under combined uni-axial in-plane and out-of-plane loads," Engineering Structures, vol. 128, pp. 316-332, 2016.

U. . W. Woju, S. . T. Tadesse and A. . E. Onse, “Time-dependent reliability of structures under consideration of epistemic uncertainty,” Life Cycle Reliability and Safety Engineering, vol. 12, p. 247–258, 2023.

K. Wu, Y. Zhao, J. Zhai, J. Yue and Q. Liang, “Experimental study on seismic damage of SRC-RC vertical hybrid structure,” Structures, vol. 70, 2024.

X. Wu, X. Peng, W. Chen and W. Zhang, "A developed surrogate-based optimization framework combining HDMR-based modeling technique and TLBO algorithm for high-dimensional engineering problems," Structural and Multidisciplinary Optimization, vol. 60, pp. 663-680, 2019.

Q. Xu, C. Han, Y. C. Wang, X. Li, L. Chen and Q. Liu, "Experimental and numerical investigations of fire resistance of continuous high strength steel reinforced concrete T-beams," Fire Safety Journal, vol. 78, pp. 142-154, 2015.

Baoxu Yan, Wancheng Zhu, Chen Hou & Kai Guan (2019) A three dimensional analytical solution to the arching effect in inclined backfilled stopes, Geomechanics and Geoengineering, 14:2, 136-147, DOI: 10.1080/17486025.2019.1574031

C. Yang, X. Xu, Z. Le, F. Zong, L. Tong and M. Chen, “Three-dimensional creep calculation model for reliability analysis of concrete-filled steel tubular (CFST) structure,” Construction and Building Materials, vol. 414, p. Article 134923, 2024.

Y. YOO, . Z. SHAHID, . R. CHEN, M. KOLIOU, A. MULIANA and . N. KALANTAR, “Structural performance of flexible freeform panels subjected to wind loads,” Frontiers of Structural and Civil Engineering, vol. 18, pp. 851-869, 2024.

X. Yu, . A. Raees, H. Ghaednia, J. Heydariha, S. Das and S. Xie, “Behavior of a Large Steel Field Silo Structure Subject to Grain Loading,” Journal of Performance of Constructed Facilities, vol. 31, no. 5, p. Article 04017038 , 2017.

S. Zhao, C. Zhang, X. Dai and Z. Yan, “Review of Wind-Induced Effects Estimation through Nonlinear Analysis of Tall Buildings, High-Rise Structures, Flexible Bridges and Transmission Lines,” Buildings, vol. 13, p. Article 2033, 2023.